SILICA SOURCE-DEPENDENT SYNTHESIS OF FERRIERITE: APPLICATION IN Cu^{2+} REMOVAL FROM WASTEWATER

by

COLLET MASWANGANYI

DISSERTATION

Submitted in fulfilment of the requirements for the degree of

Master of Science

in

Chemistry

in the

Faculty of Science and Agriculture

(School of Physical and Mineral Sciences)

at the

University of Limpopo

Supervisor: Prof. MP Mokhonoana

2015

DECLARATION

I declare that the dissertation hereby submitted to the University of Limpopo, for the degree of Master of Science in Chemistry has not previously been submitted by me for a degree at this or any other university; that it is my work in design and in execution, and that all material contained herein has been duly acknowledged.

_____ _____

Maswanganyi, C (Mr) Date

ACKNOWLEDGEMENTS

I wish to express my deepest gratitude to my supervisor Prof. Malose Peter Mokhonoana for his outstanding guidance, support and encouragement throughout this study. His understanding and supervision is very much appreciated.

I would like to thank my wife, my three daughters for support and encouragement and for having faith in me.

I am very grateful for the technical assistance provided by Witwatersrand University for the XRD and NH_3-TPD analyses. I would also like to thank Dr. Phokoane Betty Ramatsetse from University of Pretoria for SEM analyses.

My special thanks go to Mr Muluvhu Brian Muluvhu, Ms Winnie Monama, Mr Khutso Mokami and Mr Nyiko Maurice Chauke for their IT expertise.

I would like to thank NRF and University of Limpopo for financial support. I would also like to express my gratitude to all my colleagues of the Department of Chemistry.

ABBREVIATIONS

AAS	Atomic absorption spectrometry
BET	Brunauer-Emmett-Teller
bmp	1-Benzyl-1-methylpyrrolidinium cation
CEPT	Chemical-enhanced primary treatment
EDA	Ethylenediamine
ETBE	Ethyl t*ert*-butyl ether
FCC	Fluid catalytic cracking
FTIR	Fourier transform infrared spectroscopy
MCL	Metal contaminant levels
MR	Membered ring
MTBE	Methyl *tert*-butyl ether
NH_3-TPD	Temperature-programmed desorption of ammonia
Qui	Quinuclidinium
SBU(s)	Secondary building unit(s)
SDA(s)	Structure-directing agent(s)
SEM	Scanning electron microscopy
TAME	*tert*-Amyl methyl ether
TCD	Thermal conductivity detector
TEA	Triethylamine
TEOS	Tetraethyl orthosilicate
TMA	Tetramethylammonium

VPT	Vapour-phase transport
XRD	X-ray diffraction
WHO	World Health Organization

ABSTRACT

This dissertation investigated the properties of ferrierite synthesised using different SiO_2 sources under identical conditions. The SiO_2 sources used were TEOS, water-glass, Aerosil 200 and Ludox LS-30. The synthesis procedure comprised preparation of a gel with molar composition:

$$20\ Na_2O : Al_2O_3 : 37\ \text{pyrrolidine} : 66{:}5\ SiO_2 : 6{:}3\ H_2SO_4 : 1460\ H_2O.$$

This was followed by hydrothermal treatment at 160 ^oC in a stainless steel autoclave for 72 h. The solid products were characterised by XRD, SEM, NH_3-TPD and BET techniques.

The ferrierite prepared using sodium silicate was more crystalline than ferrierite zeolites synthesised using Ludox LS-30, Aerosil 200 and tetraethyl orthosilicate as SiO_2 sources. An amorphous phase was produced when ferrierite was synthesised using unhydrolysed TEOS as a sole SiO_2 source. The physicochemical properties of the materials were not only affected by the nature of the SiO_2 source, but also some synthesis manipulations such as acid-hydrolysis and water-glass addition when TEOS was used as a primary silica source. There were improvements in the materials produced when the TEOS was pre-hydrolysed with HCl and also mixed with water-glass in equal proportions.

The SEM images of ferrierite materials synthesised using water-glass and Ludox LS-30 were uniform. The water-glass-based materials were thin sheets, flake-like images and Ludox LS-30-based produced thin-plate-like morphologies. The micrograph of ferrierite synthesised using TEOS as the SiO_2 source showed hexagonal-type morphology and aggregates of smaller particles. There were two types of shapes in the ferrierite synthesised using Aerosil 200 as the silica source, namely, octagonal prismatic and hexagonal type morphologies. An equimolar mixture of TEOS and water-glass showed octagonal prismatic shape with triangular faces along certain edges of the material. The NH_3-TPD acid site distribution profiles showed two peaks of weak acid strength at low temperatures (≤ 350 ^oC) for the representative H-ferrierite investigated. The ferrierite materials synthesised using unhydrolysed TEOS and Ludox LS-30 as SiO_2 sources, showed NH_3 desorption

peaks at higher temperatures (≥ 350 ^{o}C). These peaks correspond to ammonia eluted from strong acid sites.

The BET surface area of ferrierite synthesised using water-glass was high, while the material synthesised using unhydrolysed TEOS had the lowest surface area. Novel crystal shapes, comprising octagonal prisms with additional triangular phases, were observed in ferrierite samples prepared by the use of TEOS/water-glass mixture as silica source.

The zeolitic materials prepared in this study were tested for the efficiency in the removal of Cu^{2+} from simulated wastewater, using a batch method. The effects of initial pH, initial concentration, contact time and adsorbent dose on Cu^{2+} adsorption were studied. All the materials showed maximum metal uptake efficiency at pH 5, and this pH was fixed in further studies involving other variables. It was observed that the metal uptake from aqueous solution increased with contact time and adsorbent dose. The Na-form of ferrierite synthesised using water-glass was the poorest Cu^{2+} adsorbent with respect to the four variables investigated (pH, contact time, adsorbent dose and initial metal ion concentration).

KEY CONCEPTS

Acidity, Adsorption, Ferrierite, Morphology, Silica source.

TABLE OF CONTENTS

LIST OF FIGURES

LIST OF TABLES

CHAPTER ONE

INTRODUCTION AND BACKGROUND OF THE STUDY

1.1 General introduction

The world is facing a water crisis due to the lack of clean drinking water. With the fast development of various industries, a large quantity of wastewater is produced from industrial processes and discharged into soil and water systems. Wastewater usually contains many pollutants such as cationic and anionic ions, oil and organics, which have toxic effects on ecosystems [1]. Removal of these contaminants requires cost-effective technologies, a variety of which have been developed in the past decades. Currently adsorption is believed to be a simple and effective technique for wastewater treatment. Its success depends largely on the development of efficient adsorbents. The demand for environmentally-friendly and more efficient technologies has enhanced interest in the use and development of porous solids. Activated carbon, clay minerals, biomaterials, zeolites and some industrial wastes have been widely used as adsorbents [2]. Zeolites are less expensive than commercial adsorbents like activated carbon, have high surface areas, offer unique reaction and adsorption selectivity [3].

1.2 Definition and structural properties of zeolites

The name ‘’zeolite’’ was introduced by the Swedish mineralogist, A. F. Cronstedt, in 1756 to describe stilbite, the first mineral zeolite to be identified. He found that stilbite lost water rapidly on heating and thus seemed to boil. The word zeolite comes from the Greek words *zeo* (to boil) and *lithos* (stone) [4]. A zeolite is a crystalline substance with a structure characterised by a framework of linked tetrahedra, each consisting of four oxygen (O) atoms surrounding a cation [5]. This framework contains open cavities in the form of channels and cages, which are usually occupied by water molecules and extra-framework cations that are commonly exchangeable [6, 7]. The channels allow the passage of guest species. In the

hydrated phases, dehydration occurs at temperatures mostly below about 400 ^{o}C and is largely reversible. The framework may be interrupted by hydroxyl and fluoride groups. These occupy a tetrahedron apex that is not shared with adjacent tetrahedra [8, 9]. Nearly all zeolites found in nature are aluminosilicates, but other compositions including silicates, aluminophosphates, silicoaluminophosphates and titanosilicates have been synthesised [10 - 12].

The structural formula of a zeolite is based on the crystallographic unit cell:

$$M_{x/n}[(AlO_2)_x(SiO_2)_y].wH_2O,$$

where M is an alkali or alkaline earth cation, n is the valence of the cation, w is the number of water molecules per unit cell, x and y are the total number of tetrahedra per unit cell, and the ratio y/x usually takes values from 1 to 5, though for high silica zeolites, y/x can range from 10 to 100 [13].

The structure of zeolites can be represented simply by a network of tetrahedral frameworks having four-coordinated T-atoms (T representing Si and Al atoms) with bridging O atoms. The tetrahedron $TO_{4/2}$ is known as the primary building unit [14]. The description and classification of the topology of zeolites is based on the concept of larger units, known as secondary building units (SBUs). These can consist, for example, of simple rings and prisms of various sizes, which are assembled from the primary building units, the AlO_4 and SiO_4 tetrahedra, as depicted in Figure 1.1. The SBUs can be used to completely build all known zeolite frameworks [15].

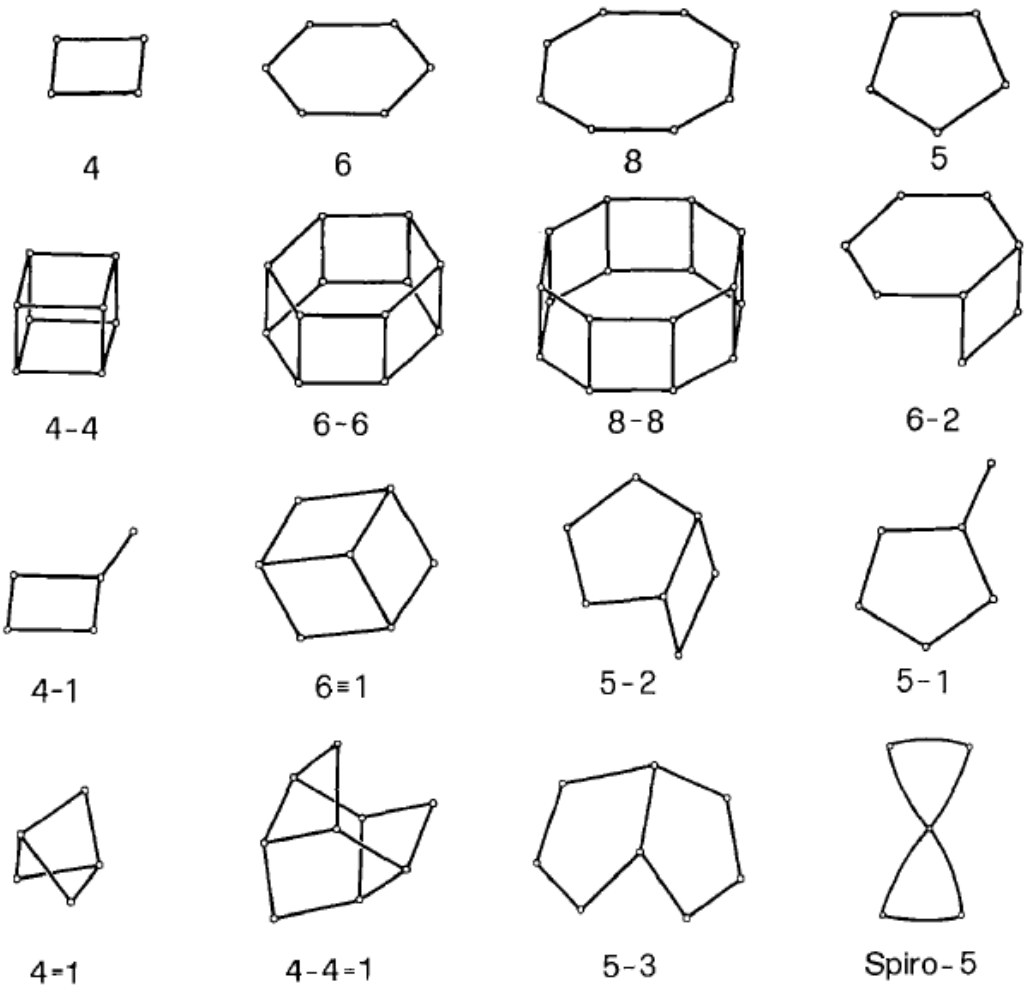

Figure 1.1 SBU of the zeolite structures. The dots represent the T atoms whereas the lines summarise the T-O-T bonds. Oxygen atoms are omitted for clarity [15].

Silicon atoms generally prefer to form bonds with four neighbouring atoms (e.g. O) in a tetrahedral geometry. If a SiO_4 entity could be isolated, its charge would be 4- since silicon has an oxidation state of 4+ and each oxygen anion carries a 2- charge. However, a SiO_4 unit in a framework is neutral since each O atom bridges two T atoms and shares electron density with each of them as shown in Figure 1.1 [16]. Thus, a defect-free pure silica (SiO_2) framework will not contain any charge. If Al is tetrahedrally-coordinated to four O atoms in a framework, it carries a 3+ charge. When tetrahedra containing Si and Al are connected to form an aluminosilicate framework, there is a negative charge associated with each Al atom, which is counter-balanced by a cation (M^+ in Figure 1.2) to give electrical neutrality. Typical cations are alkali metal ions, e.g., Na^+, K^+, alkaline earth metal ions, e.g., Ca^{2+}, Ba^{2+}, and the proton, H^+ [17, 18].

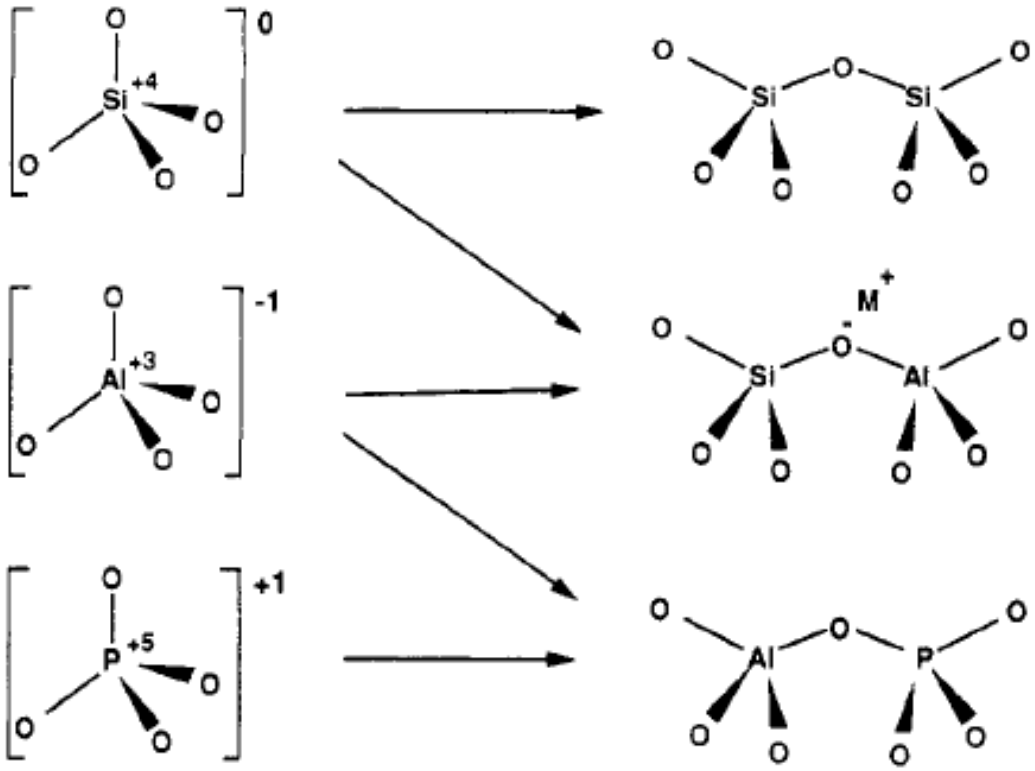

Figure 1.2 TO_2 in zeolites and aluminophosphates [17].

Zeolites have characteristic features [8] developed to varying degrees, such as:

(i) Reversible low-temperature dehydration,

(ii) Ability of the dehydrated forms to reversibly absorb other molecules,

(iii) More or less easy low temperature exchange of extra-framework cations, and

(iv) Lack of a clear-cut structurally controlled constraints on end-member compositions in terms of Si : Al ratios of the framework.

In some cases, the observed extra-framework compositions may be artefacts of cation-exchange resulting from human activities in the laboratory or elsewhere [8, 9].

1.3 Applications of zeolites

Zeolites have been phenomenally successful in a wide range of non-catalytic and catalytic applications. Key areas include adsorptive separation of hydrocarbons, purification of gases and liquids, and catalytic cracking of long-chain hydrocarbons to form more valuable short-chain homologues [19]. Applications of natural zeolites have disadvantages such as: variable composition, low purity and often poorer separation performance compared to synthetic zeolites [20]. Synthetic zeolites come in a wide range of pore sizes [21], topologies, as well as thermal, chemical and mechanical stabilities [22]. They are also widely used in agriculture and form part of building materials [23, 24].

1.3.1 Non-catalytic applications of zeolites

Along with silica gels, alumina, activated carbons, carbon-molecular sieves, and organic resins, zeolites are important industrial adsorbents with a wide range of uses [25, 26]. Natural and synthetic zeolites have been used as adsorbents, ion exchangers, etc. [27]. Compared with above-mentioned adsorbents, zeolites have the advantage of high thermal stability, non-flammability, and, depending on the Si/Al ratio, they have hydrophobic character. In addition to these properties, regeneration is possible by treating the zeolite at elevated temperatures [20]. Their diversity is also due to their microporous structure, high adsorption capacity, and they are highly selective, so that substances may be separated and purified. Separation processes are the biggest application, particularly for gas-gas and gas-vapour separation processes. Kusakabe *et al*. [24] studied the permeation of several gases through a Y-type zeolite membrane. The selective adsorption of CO_2 by a Y-type zeolite membrane makes it an excellent gas-gas separation adsorbent in the natural gas industry. Modifying the hydration degree of the zeolite has shown a strong influence on the permeability of water vapours and every type of gas [28, 29].

Zeolites have found application as water softeners in detergency, where their relatively lower cost makes them attractive ion exchangers, or in the removal and storage of radionuclides [30]. Zeolites have also been applied in the removal of ammonia from drinking water and municipal wastewater to a safe level [31], removal of heavy metal ions in wastewater [32], and the removal of radioactive fission

products, such as caesium and strontium ions during wastewater treatment [33]. In chemical industries zeolites are used as adsorbents in the separation of azeotropic solutions [32 - 37].

There are three major factors that influence the adsorption behaviour of zeolites [38, 39]:

(i) *Pore size*: The regular pores of zeolites allow separation of substances of different molecular dimensions. This selectivity can be influenced through post-synthesis treatment of zeolites. For instance, the apparent pore size of zeolite NaA can be varied by exchanging its counter ions: replacement of Na^+ by Ca^{2+} increases the apparent pore size, whereas replacement of Na^+ by K^+ narrows it,

(ii) *Adsorption kinetics*: Differences in the rate of diffusion of two or more co-adsorbed molecules into the zeolite pores, and

(iii) *The Al content*: In Al-rich zeolites, where the negative framework charge is balanced by cations, electrostatic interactions favour adsorption of substances with a large dipole moment, or quadrupole moment. In contrast, increasing Si content leads to an increasingly hydrophobic character and the adsorption is governed by van der Waals forces.

The application of zeolites in this dissertation is the removal of Cu^{2+} ions from metal-polluted wastewater. This application relies on the factors listed above.

1.3.2 Catalytic applications of zeolites

Since its first industrial application in the early 1970s, catalysis on zeolites continues to be a promising field of research [38]. The advantages of microporous crystalline materials over more conventional solid catalysts are recognised by an ever-increasing number of scientists. Among these advantages are [38, 40]:

(i) The strictly regular pore size and pore architecture,

(ii) Pore widths of molecular dimensions, which enable shape- or size-selective catalysis,

(iii) Surface acidity, with the possibility to tune the nature (Brønsted versus Lewis acidity), density, strength (or strength distribution) and location

(e. g., inside the pores or at the external surface) of the acid sites within certain ranges,

(iv) The high thermal stability,

(v) The possibility to regenerate deactivated catalysts, and

(vi) The capability of zeolites to act as hosts for a variety of guest species with catalytically attractive properties, such as transition metal ions, small metal clusters or highly selective transition metal complexes or chelates [40].

The oil refining industry is presently facing a number of major challenges. Among these are the environmental laws relating to both the quality of the fuels that are produced, as well as the operation of the refineries [34]. It is also necessary to produce sufficient gasoline and, at the same time, products, such as light alkenes, to serve as feedstocks for the petrochemical industry [41]. Light alkenes are used as raw materials for the production of polyethylene, polypropylene, styrene, cumene, phenol, methyl-*tert*-butyl ether and alkylated gasoline [42]. Catalytic cracking is a key process in producing the classical building blocks of the petrochemical industry, *viz*. light alkenes and aromatics. These alkenes are converted into higher-value products, via:

(i) Alkylation of aromatics,

(ii) Aromatisation of alkanes/alkenes,

(iii) Skeletal isomerisation of *n*-butene,

(iv) Oligomerisation of alkenes, and

(v) Isomerisation of long-chain alkanes.

Taking into account the actual state-of-the-art, it seems that the easiest solution for increasing the production of olefins by fluid catalytic cracking (FCC) is the use of zeolites [34 - 36, 43], as zeolites exhibit a property called shape selectivity, which is discussed in Section 1.3.3 below.

1.3.3 Shape-selectivity in zeolites

Shape-selective catalysis is a term normally used to describe reactions that take place over various pore molecular sieves. First proposed by Weisz and Frilette in 1960, the concept of shape-selective catalysis has been the basis for at least 10 commercial zeolite-catalysed processes, including: distillate dewaxing, lube dewaxing, xylene isomerisation, toluene disproportionation, ethylbenzene synthesis, methanol to gasoline conversion, and *para*-ethyltoluene synthesis [39, 44].

Shape-selective catalysis on confined reaction sites of zeolites is a promising way for the highly selective synthesis of the smallest target isomers [45]. Shape- and size-selectivity are a vital consideration for many industrial catalytic processes. It is typically attained by utilising catalysts of a nanoporous nature. Selectivity can be based on the shape/size of the reactant, the product or the intermediate, resulting in reactant shape-selectivity, product shape-selectivity and restricted-transition-state shape selectivity. In order to provide such shape/size selective behaviour, the catalyst must have uniform pores of molecular dimensions [46]. These are shown in Figure 1.3.

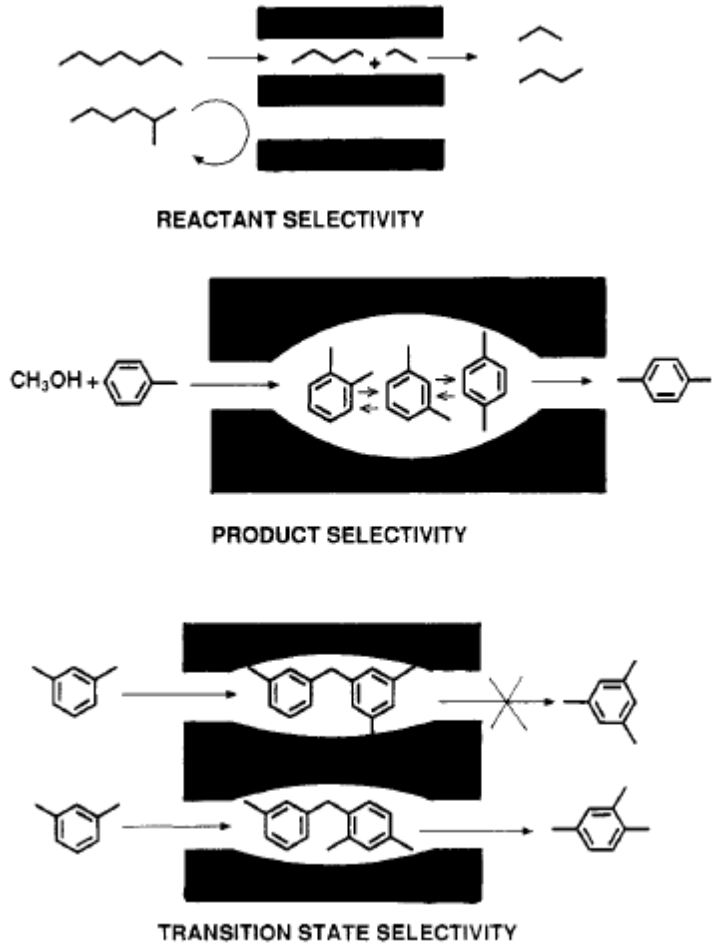

Figure 1.3 Schematic representation of the type of shape-selectivities exhibited by zeolites [17, 38].

In reactant shape-selectivity, there are at least two reactants with differences in their molecular dimensions. If the diffusion of the bulkier reactant molecules inside the pores is hindered, the less bulky molecules will react preferentially. The extreme case is a complete size exclusion of one reactant. In product shape selectivity, at least two products with differences in their molecular dimensions may form in parallel or consecutive reactions. If the diffusion of the bulkier product molecules inside the pores is hindered, equilibrium will be shifted to the less bulky molecules, which will be formed preferentially. The extreme case is a complete suppression of the formation of the bulkier molecules. Lastly, in restricted-transition-state shape-selectivity, neither the reactant nor the product molecules experience a hindered diffusion. However, out of at least two (parallel or consecutive) reactions, one proceeds via a bulky transition state or intermediate, which cannot be accommodated inside the zeolite pores. The chances for achieving restricted-

transition-state shape-selectivity in a suitably selected zeolite are usually very good, when the same reactant can undergo a monomolecular and a bimolecular reaction [17, 38, 45, 47 - 49].

1.4 Zeolite synthesis

Conventional zeolite synthesis involves the hydrothermal crystallisation of aluminosilicate gels or solutions in a basic environment. The crystallisation is carried out in a closed hydrothermal system at elevated temperature, autogenous pressure and varying time. The type of zeolite produced is affected by the following factors:

(i) *Composition of the reaction mixture (SiO_2/Al_2O_3 ratio; OH^-; inorganic cations)*: Increasing the Si/Al ratio strongly affects the physical properties of the zeolites. The pH modifies the nucleation time by influencing the transport of silicates from the solid phase into the solution. Inorganic cations balance the framework charge and affect the crystal purity and product yield. Besides acting as counter ions to balance the zeolite framework charge, the type of inorganic cations present often appear to be the dominant factors determining which structure is obtained. The inorganic cations may also influence the pathway of the crystallisation process and the morphology of the crystallised zeolite(s), either by favouring nucleation of new crystals, or by selectively enhancing the crystal growth in a given direction [50]. Hence, it is possible to control the pathway of zeolite crystallisation, including structural and particulate properties of the crystallised zeolite, by controlled addition of different cations into the reaction mixture [51],

(ii) *Nature of reactants and their pre-treatments*: The zeolite synthesis is carried out with inorganic as well as organic precursors. The inorganic precursors yield more hydroxylated surfaces, whereas the organic precursors easily incorporate the metals into the network,

(iii) *Temperature*: The rate of crystallisation is directly proportional to temperature, while the rate of nucleation is inversely proportional to temperature,

(iv) *Reaction time*: Crystallisation time must be adjusted to minimise the production of the other phases while also minimising the time needed to obtain the desired crystalline phase,

(v) *The pH of the reaction mixture*: The process of zeolitisation is carried out in alkaline medium (pH > 10). As the pH increases, the ability of the silicate to condense decreases, and there is a decrease in the amount of $Si\text{-}O^-$ species relative to Si-OH. The anionic form is necessary in order for the initial nucleophilic attack to take place. In contrast, the condensation rate of $[Al(OH)_4]^-$ remains constant and so Al-rich zeolites crystallise preferentially at high pH, and vice versa [52],

(vi) *Other factors*: The synthesis can be carried out in a continuous or semi-continuous mode, which enhances the capacity, making it more cost effective for industrial applications [53 - 56]. The semi-continuous mode allows for pulse-renewal of the synthesis solution in an autoclave at periodic intervals by the action of a set of electro-pneumatic valves. Layer formation can be controlled by adjusting the gel renewal rate (i.e. the rate at which fresh gel is introduced into and used gel removed out of the autoclave) [57]. The semi-continuous mode has disadvantages, such as large-scale implementation, and the periodic pulse-renewal of the gel in the lumen of the support, which might sweep away the zeolite seeds and remove the amorphous gel layer covering the support surface during the synthesis. To overcome the above-stated limitations, an alternative method for gel renewal focuses on using a flow system where the gel is continuously circulated in the lumen of the tubes. The process is called continuous mode synthesis [58 - 60]. The process of synthesising zeolites also depends on a wide range of experimental parameters such as concentrations and degree of supersaturation, the source of framework materials, solvent, gel dissolution rate, ageing and addition of seed crystals [52].

Seeding (addition of seed crystals) is a powerful technique for controlling zeolite synthesis pathways, and hence is frequently used in studies of the kinetics and the mechanisms of zeolite crystallisation [61]. Crystals of the desired structure are normally used as seeds that will be, at least partially, dissolved generating the nuclei

[62]. The advantages of seeding are: (i) shortening the induction period, and (ii) increasing the crystallisation rate. The latter is due to the increased surface area available for crystal growth in the presence of the seed [56, 63, 64]. A variety of seeding techniques exists, including rubbing zeolite crystals over the outer side of a tubular support (or over the inner side by brushing) laser ablation, cross-flow filtration of a suspension of crystals, and spin coating or dip coating of a colloidal mixture of nanocrystals [60].

1.5 Research background

Heavy metals such as cadmium, zinc, copper, nickel, lead, mercury and chromium are often detected in industrial wastewaters. They originate from metal plating, mining activities, smelting, battery manufacturing, tanneries, petroleum refining, paint manufacturing, pesticides, pigment manufacturing, printing, photographic industries, etc. These toxic metals must be effectively removed from wastewaters. If the wastewaters were discharged directly into natural waters, they will constitute a great risk for the aquatic ecosystem. Also, the direct discharge into the sewerage system may negatively affect the subsequent biological wastewater treatment [65]. Precipitation, reverse osmosis, cementation, electro-coagulation, electro-winning and ion exchange are widely used methods for the removal of heavy metals from water [66, 67]. These methods suffer from drawbacks, such as high capital costs, high operational costs and the problem of residual metal sludge disposal. Ion exchange is feasible when an exchanger has a high selectivity for the metal to be removed and when the concentrations of competing ions are low [68]. In light of the above, some adsorption materials have emerged as economic and environmentally-friendly options. Adsorption is also effective in removing heavy metals from aqueous solutions [69 - 71]. Activated carbon, chitosan, zeolites, clays, etc., have been widely used as adsorbents for heavy metal ions [43, 44, 64, 72]. Copper is a micronutrient, but excessive intake by man leads to diseases such as, liver damage, Wilson disease, insomnia [73]. As Cu^{2+} is a highly toxic element in water, its removal from wastewater is crucial. In this study, the use of ferrierite is investigated in laboratory-scale experiments for the adsorption of copper ions from simulated wastewater.

1.6 Aim

The aim of this research is to investigate the influence of the SiO_2 precursor on the structural properties of ferrierite and its Cu^{2+} uptake efficiency from aqueous systems.

1.7 Objectives

The objectives of this study are to:

(i) synthesise a series of ferrierite-type zeolites under identical conditions using different SiO_2 precursors,

(ii) characterise the resulting materials using physicochemical techniques including XRD, SEM, NH_3-TPD and BET surface area measurements, and

(iii) investigate the Cu^{2+} uptake efficiency of these materials from simulated wastewater.

1.8 Scope of the dissertation

Chapter 1 presents a brief overview over aspects of the proposed study. These include the environmental impact of heavy metals, water treatment technology, and zeolites. Chapter 2 is a literature survey of ferrierite zeolite science and the use of other materials in the treatment of wastewater effluents. Experimental work is reported in Chapter 3. The experimental work includes the synthesis of ferrierites characterisation of ferrierites by X-ray diffraction (XRD), scanning electron microscopy (SEM), Brunauer-Emmett-Teller (BET) surface area measurements, and temperature-programmed desorption of ammonia (NH_3-TPD). The final part of the experimental work is the testing of the toxic metal adsorption capabilities of the synthesised ferrierites from wastewater. The adsorption of Cu^{2+} is performed under variation of the following parameters: pH of the solution, contact time, zeolite dose and initial concentration of simulated wastewater. Quantitative analysis of the Cu^{2+} ions was performed using atomic absorption spectrometry (AAS). Ferrierite characterisation and Cu^{2+} adsorption results are presented in Chapter 4. Summary, conclusions and recommendations are presented in Chapter 5.

1.8 References

[1] E. Alvarez-Ayuso, A. Garcia-Sanchez, X. Querol, Purification of metal electroplating waste waters using zeolites, Water Research 37 (2003) 4855 – 4862.

[2] S. Wang, Y. Peng, Natural zeolites as effective adsorbents in water and wastewater treatment, Chemical Engineering Journal 156 (2010) 11 – 24.

[3] Y. Tao, H. Kanoh, L. Abrams, K. Kaneko, Mesopore-modified zeolites: Preparation, characterization, and applications, Chemical Reviews 106 (2006) 896 – 910.

[4] E. Izci, A. Izci, Dielectric behaviour of the catalyst zeolite NaY, Turkish Journal of Chemistry 31 (2007) 523 – 530.

[5] S. Yang, M. Lach-hab, I.I. Vaisman, E. Blaisten-Barojasa, X. Li, V.L. Karen, Framework-type determination for zeolite structures in the inorganic crystal structure database, Journal of Physical and Chemical Reference Data 39 (2010) 1 – 45.

[6] H. Ghobarkar, O. Schaf, Y. Massiani, P. Knauth, The reconstruction of natural zeolites: A new approach to announce old materials by their synthesis, Springer Publishers, Netherlands (2003) 3.

[7] C. Rosales-Landeros, C.E. Barrera-Díaz, B. Bilyeu, V.V. Guerrero, F.U. Nunez, A review on Cr(VI) adsorption using inorganic materials, American Journal of Analytical Chemistry 4 (2013) 8 – 16.

[8] D.S. Coombs, A. Alberti, T. Armbruster, G. Artioli, C. Colella, E. Galli, J.D. Grice, F. Liebau, J.A. Mandarino, H. Minato, E.H. Nickel, E. Passaglia, D.R. Peacor, S. Quarteiri, R. Rinaldi, M. Ross, R.A. Sheppard, E. Tillmanns, G. Vezzalini, Recommended nomenclature for zeolite minerals: Report of the subcommittee on zeolites of the international mineralogical association, commission on new minerals and mineral names, The Canadian Mineralogist 35 (1997) 1571 – 1606.

[9] D.S. Coombs, A. Alberti, T. Armbruster, G. Artioli, C. Colella, E. Galli, J.D. Grice, F. Liebau, J.A. Mandarino, H. Minato, E.H. Nickel, E. Passaglia, D.R. Peacor, S. Quarteiri, R. Rinaldi, M. Ross, R.A. Sheppard, E. Tillmanns, G. Vezzalini, Recommended nomenclature for zeolite minerals: Report of the subcommittee on

zeolites of the international mineralogical association, commission on new minerals and mineral names, Mineralogical Magazine 62 (1998) 533 – 571.

[10] W. Loewenstein, The distribution of aluminium in the tetrahedra of silicates and aluminates, American Mineralogist 39 (1954) 92 – 96.

[11] H. Choo, S.B. Hong, L. Kevan, Comparative ESR and catalytic studies of ethylene dimerization on Pd(II)-exchanged clinoptilolite, mordenite, ferrierite and SUZ-4, Journal of Physical Chemistry B 105 (2001) 7730 – 7738.

[12] S. Zhen, K. Seff, Structures of organic sorption complexes of zeolites; Microporous and Mesoporous Materials 39 (2000) 1 – 18.

[13] R. Anuwattana, P. Khummongkol, Conventional hydrothermal synthesis of Na-A zeolite from cupola slag and aluminium sludge, Journal of Hazardous Materials, 166 (2009) 227 – 232.

[14] J.A. Boscoboinik, X. Yu, B. Yang, S. Shaikhutdinov, H. Freund, Building blocks of zeolites on an aluminosilicate ultra-thin film, Microporous and Mesoporous Materials 165 (2013) 158 – 162.

[15] V.J. Inglezakis, A.A. Zorpas, Natural zeolites structure porosity, Handbook of Natural Zeolites (2012) 133 – 146.

[16] M.M. Helmkamp, M.E. Davis, Synthesis of porous silicates, Annual Reviews of Material Science 25 (1995) 161 – 192.

[17] M.E. Davis, Zeolites and molecular sieves: Not just ordinary catalysts, Industrial & Engineering Chemistry Research 30 (1991) 1675 – 1683.

[18] M.E. Davis, R.F. Lobo, Zeolite and Molecular Sieve Synthesis, Chemistry of Materials 4 (1992) 756 – 768.

[19] X. Xian, G. Liu, X. Zhang, L. Wang, Z. Mi, Catalytic cracking of n-dodecane over HZSM-5 zeolite under supercritical conditions: Experiments and kinetics, Chemistry Engineering Science. 65 (2010) 5588 – 5604.

[20] M.W. Ackley, S.U. Rege, H. Saxena, Application of natural zeolites in the purification and separation of gases, Microporous and Mesoporous Materials 61 (2003) 25 – 42.

[21] A. Al-Haddad, E. Chmielewska, S. Al-Radwan, A brief comparable lab examination for oil refinery wastewater treatment using the zeolitic and carbonaceous adsorbents, Petrol & Coal 49 (2007) 21 – 26.

[22] F. Pechar, D. Rykl, Study of the thermal stability of the natural zeolite heulandite, Chemical Papers 39 (1985) 369 – 377.

[23] D. Bhattacharya, M. Chatterjee, S. Sivasanker, Studies on the cracking of *n*-hexane over H-ZSM-48, Reaction Kinetics and Catalysis Letters 60 (1997) 395 – 403.

[24] K. Kusakabe, T. Kuroda, A. Murata, S. Morooka, Formation of a Y-type zeolite membrane on a porous α-alumina tube for gas separation, Industrial & Engineering Chemistry Research 36 (1997) 649 – 655.

[25] V.D. Santo, F. Liguori, C. Pirovano, M. Guidotti, Design and use of nanostructured single-site heterogeneous catalysts for the selective transformation of fine chemicals, Molecules 15 (2010) 3829 – 3856.

[26] S. Deng, Sorbent technology, Encyclopedia of Chemical Processing and Design (2006) 2825 – 2845.

[27] D. Mravec, J. Hudec, I. Janotka, Some possibilities of catalytic and noncatalytic utilization of zeolites, Chemical Papers 59 (2005) 62 – 69.

[28] K.I. Okamoto, H. Kita, K. Horii, K.T. Kondo, Zeolite NaA membrane: Preparation, single-gas permeation, and pervaporation and vapour permeation of water/organic liquid mixtures, Industrial & Engineering Chemistry Research 40 (2001) 163 – 175.

[29] H. Ghobarkar, O. Schaf, U. Guth, Zeolites: From kitchen to space, Progress in Solid State Chemistry 27 (1999) 29 – 73.

[30] R.P. Townsend, Ion exchange in zeolites: Some recent developments in theory and practice, Pure & Applied Chemistry, 58 (1986) 1359 – 1366.

[31] M. Li, X. Zhu, F. Zhu, G. Ren, G. Cao, L. Song, Application of modified zeolite for ammonium removal from drinking water, Desalination 271 (2011) 295 – 300.

[32] T.S. Jamil, H.S. Ibrahim, I.H.A. El-Maksoud, S.T. El-Wakeel, Application of zeolite prepared from Egyptian kaolin for removal of heavy metals: 1. Optimum conditions. Desalination 258 (2010) 34 – 40.

[33] Z. Adamczyk, B. Bialecka, Hydrothermal Synthesis of Zeolites from Polish Coal Fly Ash, Polish Journal of Environmental Studies 14 (2005) 713 – 719.

[34] J.E. Naber, K.P. de Jong, W.H.J. Stork, H.P.C.E. Kuipers, M.F.M. Post, Industrial applications of zeolites, Studies in Surface Science and Catalysis 84 (1994) 2197 – 2219.

[35] G. Bellussi, P. Pollesel, Industrial applications of zeolite catalysts: Production and uses of light olefins, Studies in Surface Science and Catalysis 158 (2005) 1201 – 1212.

[36] I.E. Maxwell, W.H.J. Stork, Hydrocarbon processing with zeolites, Studies in Surface Science and Catalysis 137 (2001) 747 – 819.

[37] R.T. Yang, Adsorbents: Fundamentals and applications; John Wiley & Sons: Hoboken, New Jersey (2003) 3.

[38] J. Weitkamp, Zeolites and catalysis, Solid State Ionics 131 (2000) 175 – 188.

[39] E.M. Flanigen, Molecular sieve zeolite technology: The first twenty-five years, Pure and Applied Chemistry 52 (1980) 2191 – 2211.

[40] M.I.P. da Silva, F.L. da Silva, C.A. Tellez S, FT-infrared band analysis and temperature programmed desorption for the Y, L and ferrierite zeolites, Spectrochimica Acta 58 (2002) 3159 – 3166.

[41] B. Yilmaz, N. Trukhan, U. Müller, Industrial outlook on zeolites and metal organic frameworks, Chinese Journal of Catalysis 33 (2012) 3 – 10.

[42] D. Mier, A.T. Aguayo, A.G. Gayubo, M. Olazar, J. Bilbao, Synergies in the production of olefins by combined cracking of *n*-butane and methanol on a HZSM-5 zeolite catalyst, Chemical Engineering Journal 160 (2010) 760 – 769.

[43] P.N. Dave, N. Subrahmanyam, S. Sharma, Kinetics and thermodynamics of copper ions removal from aqueous solution by use of activated charcoal, Indian Journal of Chemical Technology 16 (2009) 234 – 239.

[44] J. Weitkamp, New directions in zeolite catalysis, Catalysis and Adsorption by Zeolites (1991) 21 – 46.

[45] Y. Sugi, Shape-selective alkylation of naphthalene over zeolites: Steric interaction or reagents with zeolites, Journal of the Chinese Chemical Society 57 (2010) 1 – 13.

[46] B. Yilmaz, U. Muller, Catalytic applications of zeolites in chemical industry, Topics in Catalysis 52 (2009) 888 – 895.

[47] C.P. Canlas, J. Lu, N.A. Ray, N.A. Grosso-Giordano, S. Lee, J.W. Elam, R.E. Winans, R.P. Van Duyne, P.C. Stair, J.M. Notestein, Shape-selective sieving layers on an oxide catalyst surface, Nature Chemistry 4 (2012) 1030 – 1036.

[48] C. Song, Recent advances in shape-selectivity catalysis over zeolites for synthesis of speciality chemicals, Studies in Surface Science and Catalysis 113 (1998) 163 – 186.

[49] Y. Sugi, K. Komura, J.H. Kim, Shape-selective catalysis over zeolite. An attempt in the alkylation of biphenyl, The Korean Journal of Chemical Engineering 17 (2006) 235 – 242.

[50] A. Cizmek, B. Subotica, D. Kralj, V. Babic-Ivancic, A. Tonejc, The influence of gel properties on the kinetics of crystallization and particulate properties of MFI-type zeolites. I. The influence of time and temperature of gel ageing on the particulate properties of silicalite-1 microcrystals, Microporous Materials 12 (1997) 267 – 280.

[51] S. Bosnar, T. Antonic-Jelic, J. Bronic, I. Krznaric, B. Subotic, Influence of anions on the kinetics of zeolite A crystallization: A population balance analysis, Journal of Crystal Growth 267 (2004) 270 – 282.

[52] J.W. Steed, J.L. Atwood, Supramolecular Chemistry, 22nd Edition, John Wiley and Sons (2009) 543.

[53] G.E. Christidis, H. Papantoni, Synthesis of FAU Type Zeolite Y from Natural raw materials: Hydrothermal SiO_2-sinter and perlite glass, The Open Mineralogy Journal 2 (2008) 1 – 5.

[54] M.C. Dalconi, G. Cruciani, A. Alberti, P. Ciambelli, M.T. Rapacciuolo, Ni^{2+} ion sites in hydrated and dehydrated forms of Ni-exchanged zeolite ferrierite, Microporous and Mesoporous Materials 39 (2000) 423 – 430.

[55] M.C. Dalconi, A. Alberti , G. Cruciani, P. Ciambelli, E. Fonda, Siting and coordination of cobalt in ferrierite: XRD and EXAFS studies at different Co loadings, Microporous and Mesoporous Materials 62 (2003) 191 – 200.

[56] J. Bronić, B. Subolić, M. Škreblin, Investigation of the influence of seeding on the crystallization of zeolite A in the membrane-type reactor, Microporous and Mesoporous Materials 28 (1999) 73 – 82.

[57] M. Pera-Titus, M. Bausach, J. Llorens, F. Cunill, Preparation of inner-side tubular zeolite NaA membranes in a continuous flow system, Separation and Purification Technology 59 (2008) 141 – 150.

[58] M. Pera-Titus, J. Llorens, F. Cunill, R. Mallada, J. Santamaria, Preparation of zeolite NaA membranes on the inner side of tubular supports by means of a controlled seeding technique, Catalysis Today 104 (2005) 281 – 287.

[59] H. Richter, I. Voight, P. Fischer, P. Puhlfurb, Preparation of zeolite membranes on the inner surface of ceramic tubes and capillaries, Separation and Purification Technology 32 (2003) 133 – 138.

[60] S. Aguado, J. Gascón, J.C. Jansen, F. Kapteijn, Continuous synthesis of NaA zeolite membranes, Microporous and Mesoporous Materials 120 (2009) 170 – 176.

[61] K. Suzuki, T. Hayakawa, The effects of seeding in the synthesis of zeolite ZSM-48 in the presence of tetramethylammonium ion, Microporous and Mesoporous Materials 77 (2005) 131 – 137.

[62] U. Dıaz, V. Fornes, A. Corma, On the mechanism of zeolite growing: Crystallization by seeding with delayered zeolites, Microporous and Mesoporous Materials 90 (2006) 73 – 80.

[63] C.S. Cundy, P.A. Cox, The hydrothermal synthesis of zeolites: Precursors, intermediates and reaction mechanism, Microporous and Mesoporous Materials 82 (2005) 1 – 78.

[64] M. Balintova, M. Holub, E. Singovszka, Study of iron, copper and zinc removal from acidic solutions by sorption, Chemical Engineering Transactions 28 (2012) 175 – 180.

[65] W.S. Wan Ngah, M.A.K.M. Hanafiah, Removal of heavy metal ions from wastewater by chemically modified plant wastes as adsorbents: A review, Bioresource Technology 99 (2008) 3935 – 3948.

[66] S.S. Ahluwalia, D. Goyal, Microbial and plant derived biomass for removal of heavy metals from wastewater, Bioresource Technology 98 (2007) 2243 – 2257.

[67] Y. Sağ, T. Kutsal, Biosorption of heavy metals by *Zooglodea ramigera*: Use of adsorption isotherms and a comparison of biosorption characteristic, The Chermcal Engineering Journal 60 (1995) 181 – 188.

[68] B. Silva, H. Figueiredo, I.C. Neves, T. Tavares, The role of pH on Cr(VI) reduction and removal by *Arthrobacter viscosus,* International Journal of Chemical and Biological Engineering 2 (2009) 100 – 103.

[69] S.S.R. Putluru, A. Riisager, R. Fehrmann, Alkali resistant Cu/zeolite deNO_x catalysts for flue gas cleaning in biomass fired applications, Applied Catalysis B: Environmental 101 (2011) 183 – 188.

[70] Y. Sag, T. Kutsal, Recent trends in the biosorption of heavy metals: A Review, Biotechnology and Bioprocess Engineering 6 (2001) 376 – 385.

[71] M.H. Al-Qunaibit, W.K. Mekhemer, A.A. Zaghloul, The adsorption of Cu(II) ions on bentonite: A kinetic study, Journal of Colloid and Interface Science 283 (2005) 316 – 321.

[72] M.A. Ulibarri, I. Pavlovic, C. Barriga, M.C. Hermosin, J. Cornejo, Adsorption of anionic species on hydrotalcite-like compounds: Effect of interlayer anion and crystallinity, Applied Clay Science 18 (2001) 17 − 27.

[73] M.A. Barakat, New trends in removing heavy metals from industrial wastewater, Arabian Journal of Chemistry 4 (2011) 361 – 377.

CHAPTER TWO

LITERATURE REVIEW

2.1 Occurrence of ferrierite

Natural ferrierite belongs to the mordenite group of zeolites and can be found, although rare, as small crystalline incrustations in volcanic rocks, or as extensive sedimentary deposits [1]. Naturally occurring ferrierite was first described by Graham [2]. This followed the examination of specimens collected by W.F. Ferrier of the Canadian Geological Survey in a railway cutting on the north Shore of Kamloops Lake in British Columbia [2]. Since its discovery at Kamloops, ferrierite has been observed in nearly 30 localities. The rare deposit near Lovelock, Nevada, discovered by P.E. Galli in 1965, was formed through hydration reactions in a sequence of rhyolitic pyroclastic rocks [3].

2.2 Structure of ferrierite

The X-ray crystal structure of ferrierite was solved by Vaughan and Kerr [4]. Ferrierite has generally *Immm* symmetry for the framework atoms, but a monoclinic structure has also been determined. The topology of the *Immm* framework can be described in terms of a 5-1 secondary building unit (Figure 1.1), which is characteristic of the mordenite family of zeolites (mordenite, ferrierite, bikitaitie, epistilbite, dachiardite) and several synthetic zeolites [4]. Synthetic ferrierite is a member of the high-silica, medium-pore zeolite family, and contains two-dimensional network of ten-membered ring (10-MR) and eight-membered ring (8-MR) intersecting channels, as shown in Figure 2.1.

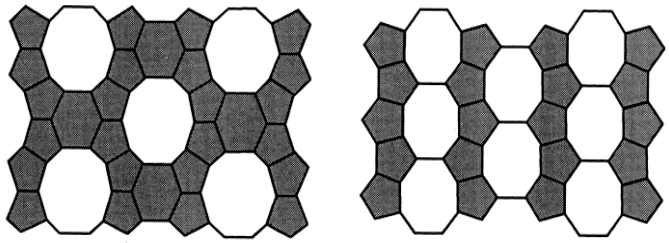

(a) (b)

Figure 2.1 Ferrierite crystal structure: (a) 10-MR channels viewed along (001) (b) 8-MR channels viewed along (010) [5].

The building units of ferrierite contain four unique tetrahedral T-sites, which in a purely siliceous material are occupied by Si. The Al occupation at all the four T-sites is, however, less probable in synthetic ferrierite since the Si/Al is typically in the range 8.33 – 17.86 [6]. Ferrierite has a stable structure and hence constitutes a promising material for fundamental and applied studies [7]. The position and relative intensity of the diffraction peaks are shown in Figure 2.2 [8].

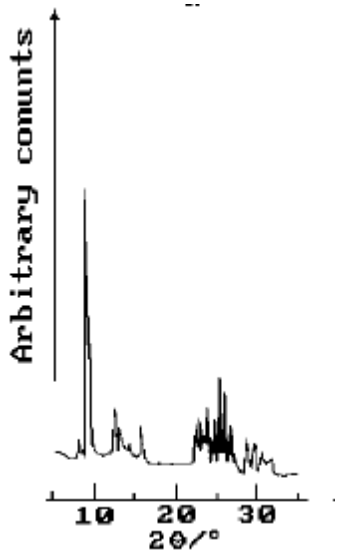

Figure 2.2 XRD pattern of siliceous ferrierite [8].

The intensity of the peak at 9.5^{o} 2θ of siliceous ferrierite is extremely high. This is due to the optimum orientation of the single crystals of the zeolite on the XRD test plate. In this case the (200) and (400) reflection planes were parallel to the surface of the sample discs [8].

2.3 Synthesis of ferrierite

Ferrierite is a naturally occurring aluminosilicate zeolite that can be synthesised in both pure silica and aluminosilicate forms using inorganic (e.g. K^+, Na^+) or organic bases (e.g. pyrrolidine) [9]. Its siliceous form ferrierite can be prepared by both aqueous and non-aqueous routes (e.g. from dried aluminosilicate gels) [10]. Aluminosilicate zeolites synthesis involves mixing together Si and Al species, metal cations, organic molecules and water, which are then treated hydrothermally. Thereafter, the mixture is converted into a microporous crystalline aluminosilicate [11]. The effects of structure-directing agents SDAs and silica sources are discussed in Sections 2.3.1 and 2.3.2 below.

2.3.1 Effect of structure-directing agents

A number of structure-directing agents, SDAs, such as diethanolamine [10], piperidine [12], pyridine [13], cyclohexylamine, pyrrolidine [14], and many other organic amines have been used in the synthesis of ferrierite. ZSM-5 and ferrierite have been prepared from amorphous alkaline SiO_2/Al_2O_3 gel by treating the dried gel at high temperatures in an atmosphere of water vapour and gaseous ethylenediamine (EDA) and triethylamine (TEA) [15]. This method is called vapour-phase transport (VPT) [15]. Matsukata and co-workers [16] carried out three runs to elucidate the roles of amines in the crystallisation of ferrierite using the VPT method. The XRD patterns of the synthesised materials are shown in Figure 2.3.

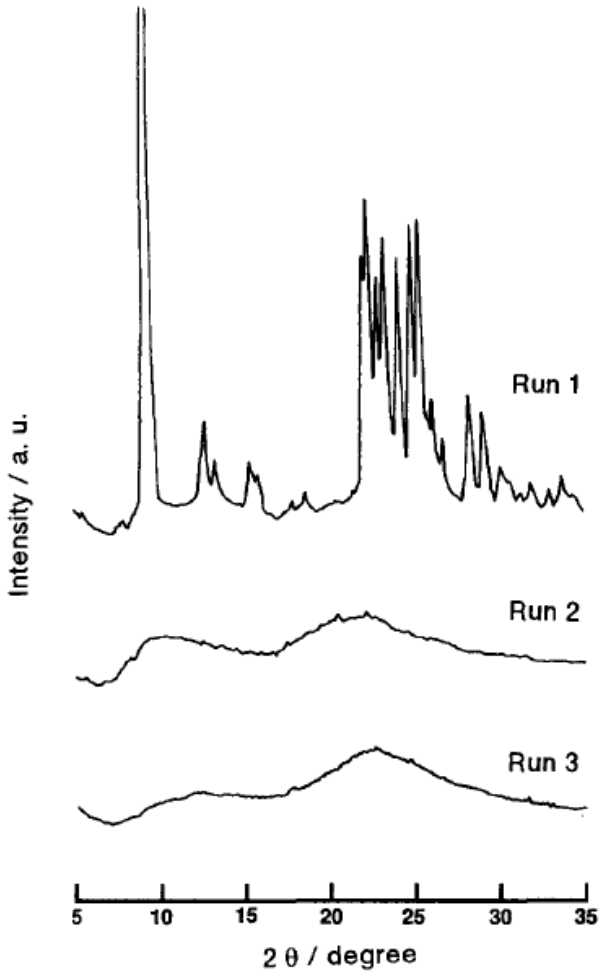

Figure 2.3 XRD patterns of solids obtained by the VPT method (Run 1: EDA / 5.3 TEA / 2.5 H_2O, Run 2: 2.5 EDA / 0 TEA /H_2O, Run 3: 0 EDA / 2.1 TEA / H_2O) [16].

No crystallisation occurred in runs 2 and 3, that is in the EDA-water and TEA-water systems, respectively. On the other hand, run 1 gave fully crystallised ferrierite, indicating that co-existence of EDA and TEA is required for the formation of ferrierite, i.e., EDA and/or TEA acted as structure-directing agents. Flake-like crystals were formed after 3 days, disappeared after 8.5 days and needle-like crystals were formed instead. Development of flake-like morphology and its disappearance corresponded to increasing intensities of reflection peaks for ferrierite and their decrease, respectively [16]. The synthesis of ferrierite from gels of variable composition using EDA or pyrrolidine as a template has also been reported [17]. Ferrierite was the only crystalline phase observed throughout the entire crystallisation field when EDA was the SDA, and mordenite appeared as a crystalline impurity when pyrrolidine was used as the SDA [18]. Ferrierite was also co-produced with Theta-1, ZSM-5, mordenite, and cristobalite zeolites when diethanolamine and water were used at

various SiO_2/Al_2O_3 ratios [19]. By varying the nature of the alkylamine template, it was possible to change the shape of the ferrierite crystals obtained as shown in Figure 2.4 [20]. An important point to conclude is that some templates do not produce only the targeted ferrierite, but produce other zeolite phases as impurities.

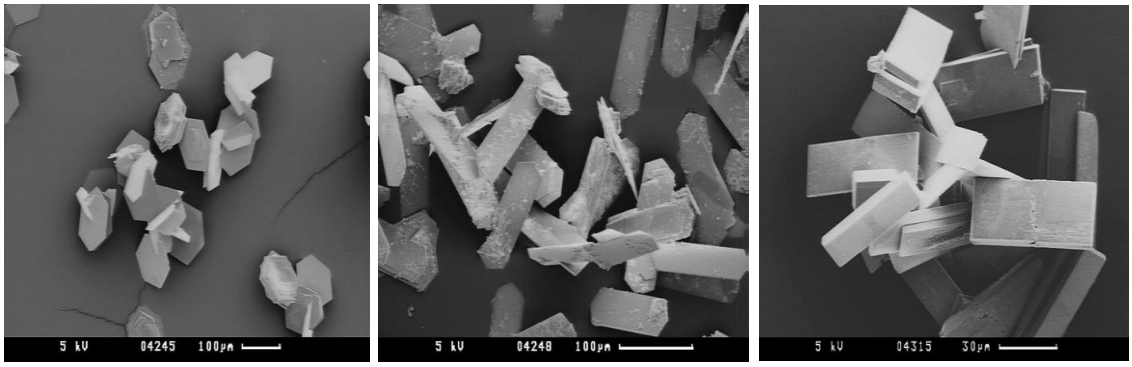

(a) (b) (c)

Figure 2.4 Scanning electron micrographs of ferrierite synthesised using: (a) *n*-propylamine, (b) *n*-butylamine and (c) *n*-pentylamine [20].

Increasing the number of carbon atoms in the amine template changed the crystal shapes. With *n*-propylamine, crystals with hexagonal-flat-prismatic morphology were obtained, Figure 2.4 (a). The crystals obtained in the synthesis with *n*-butylamine had stretched hexagonal-flat-prismatic morphology, Figure 2.4 (b), whereas the crystals obtained with *n*-pentylamine showed rectangular flat prismatic morphology, Figure 2.4 (c) [20]. It was also possible to synthesise ferrierite without SDAs. The zeolite compared well with the ferrierite samples synthesised in the conventional manner using organic templates [21]. A high-silica content ferrierite was synthesised by recrystallisation of Al-containing magadiite in an air-dry state or as an aqueous suspension with piperidine as SDA [12]. The morphology of ferrierite recrystallised from the Al-containing magadiite in aqueous medium resulted in aggregates characterised by parallel arrangement of individual plate-like crystallites. In contrast, ferrierite conventionally synthesised by crystallisation of a gel-like Al_2O_3/SiO_2 source with piperidine as the template in aqueous medium exhibited characteristic agglomerates of plate-like irregular serrated crystallites [12].

Another ferrierite synthesis method involving a mixture of two SDAs, in this case the 1-benzyl-1-methylpyrrolidinium cation (*bmp*) and quinuclidinium (*Qui*) or

tetramethylammonium (TMA) cations, in the absence of inorganic cations and in fluoride media. When the *bmp* was used as the only SDA, a mixture of four different species (mordenite, ferrierite, α-quartz and unidentified mixture of phases) was obtained as shown in Figure 2.5 [22].

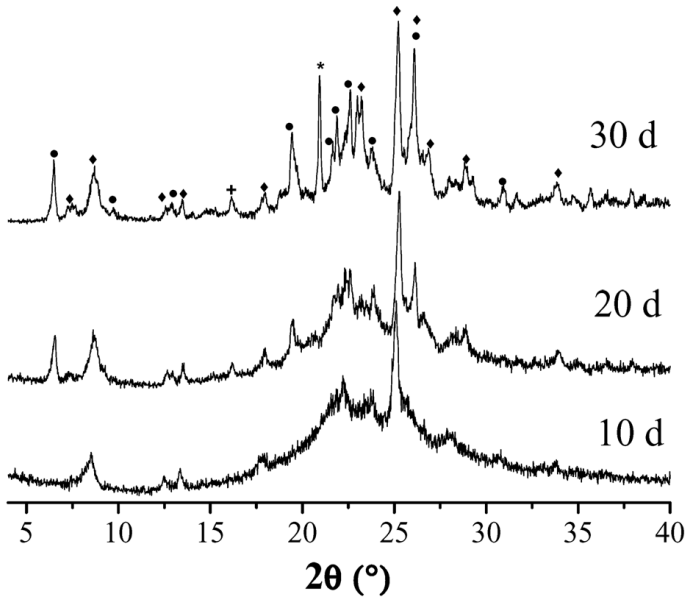

Figure 2.5 XRD patterns of samples synthesised using *Qui-bmp* as co-templates obtained at 150 °C after 10, 20 and 30 days. Symbols indicate the phases present in the products: mordenite (●), ferrierite (◆), α-quartz (*), unidentified phase (+) [22].

After 10 days of heating at 150 °C, the product showed a pattern with resemblance to that of a ferrierite structure characterised by very broad diffraction peaks and a high background base line, thus indicating poor crystallinity of the sample. Prolonging the heating to 20 days led to the appearance of competing phases. The X-ray diffraction pattern exhibited the diffractions of the ferrierite structure, plus the characteristic diffractions of mordenite. The sample heated at 150 °C for 30 days showed XRD pattern similar to the one synthesised for 20 days, but a more defined diffraction pattern with an additional very sharp reflection at 2θ ~ 20.9°, assigned to quartz [22]. The ferrierite crystallised over shorter heating times when TMA was used as a co-template was stable to prolonged hydrothermal treatment. In contrast, when the *Qui* was used as a co-template, mordenite competed with ferrierite at long crystallisation times [23]. Garcia *et al*. [24] also reported the use of the *bmp* cation together with TEA as co-SDA. The use of these two SDAs resulted in the crystallisation of ferrierite-layered materials with a large interlayer spacing. These ferrierites were stable and did not show a decrease in the interlayer distance.

Consequently, a progressive condensation of the ferrierite layers over the extended synthesis time is indicated, as opposed to the synthesis using the *Qui* as co-SDA.

2.3.2 Influence of the silica source

It is well known that different SiO_2 sources can affect the formation of the silicate, which plays an important role in zeolite synthesis [25]. Important parameters describing the process of zeolite crystallisation, such as the nucleation and crystallisation rates, depend on the dissolution of the silica precursors. The fragile silicate intermediates released during the process of silica source dissolution, are influenced by the nature of the silica used [26]. In addition, different SiO_2 sources, which differ in particle radius, can considerably affect zeolite crystallisation rates. Furthermore, the impurities introduced by the SiO_2 source can also change the properties of the final products, such as crystal size, morphology, chemical composition and catalytic properties [24]. Some SiO_2 sources reported in the syntheses of ferrierite are listed in Table 2.1.

Table 2.1: Silica sources used to synthesise ferrierite

SiO_2 source	**Gel composition**	**Period**	**Temperature (^oC)**	**References**
Sodium silicate	20 Na_2O : 6.6 pyrrolidine : 66 SiO_2 : Al_2O_3 : 0.47 AOT : 1600 H_2O	40 - 60 h	140 - 160	[29, 30]
	20 Na_2O : Al_2O_3 : 37 pyrrolidine : 66 SiO_2 : 1460 H_2O	50 h	180	[28]
	20 Na_2O : 9.45 pyrrolidine : 66 SiO_2 : Al_2O_3 : 6:3 H_2SO_4 : 0:12 Tween-X : 1600 H_2O	35 h	160	[18]
	24 SiO_2 : Al_2O_3 : 12 Na_2O : 470 H_2O : 0.77 H_2SO_4	5 days	180	[17]
TEOS	0.06 Co-SDA : 0.48 ROH : 0.48 HF : 0.03 Al_2O_3 : 0.94 SiO_2 : 4.30 - 4.70 H_2O (ROH = *bmp* or pyrrolidine)	10 - 83 days	135	[24]
Aerosil 200	97 SiO_2 : Al_2O_3 : 117 pyrrolidine : 27:5 Na_2O : 495 H_2O	62 h	175	[31]
Ludox AS-40	2.6 K_2O : 1.2 Na_2O : Al_20_3 : 60 SiO_2 : 32 DEA : 1200 H_2O (OH/SiO_2 = 0.08)		150	[19]
Ludox AS-30	1.85 Na_2O : Al_2O_3 : 20 SiO_2 : 592 H_2O : 19.7 pyrrolidine	8 - 480 h	150 - 225	[1]
Silica sol	0.5 THF : 0.215 Na_2O : SiO_2 : 0.05 Al_2O_3 : 20 H_2O.	8 - 12 days	200	[10, 27]

The synthesis of ferrierite involving variations of the SiO_2/Al_2O_3 molar ratio was investigated over the range of 10 - 25 at constant temperature of 177 ^oC using Ludox AS-30 as the silica source [1]. Figure 2.6 illustrates a very important parameter to be considered in the synthesis of ferrierite, namely, the nature of the SiO_2 precursor.

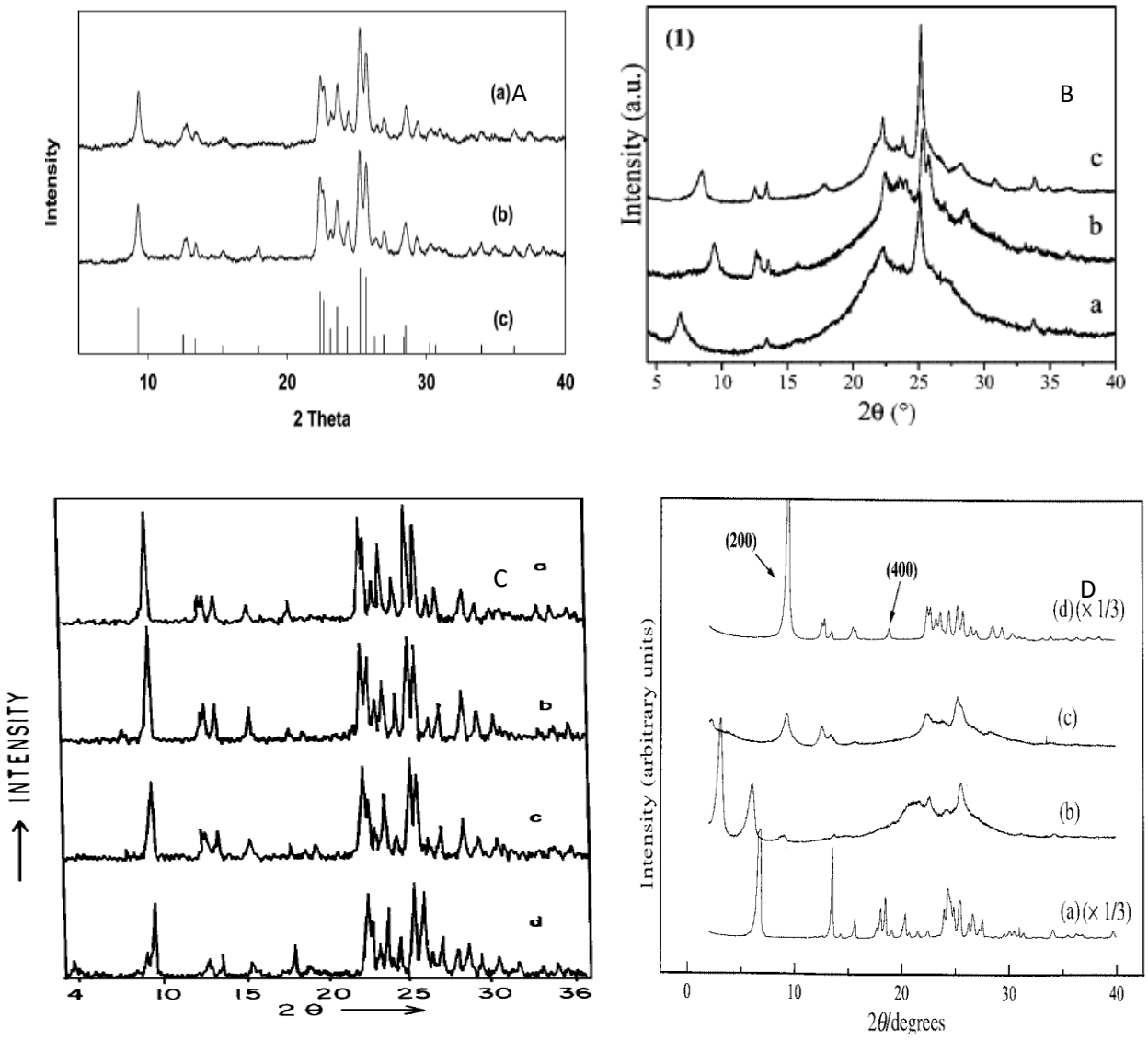

Figure 2.6 XRD patterns of ferrierite synthesised using different SiO_2 sources, A: Ludox AS-30 [1], B: TEOS [24], C: water-glass [28] and D: Aerosil 200 [31] as silica sources.

The letters in the figure (a, b, c, and d) represent changes in the synthesis parameters by each individual author varied. However, the main focus here is the influence of the SiO_2 source. It can be seen from Figure 2.6 that the quality of ferrierite depends on the identity of the SiO_2 source used in the synthesis. The crystallinity of the zeolite, which is related to the number and intensity of the XRD

peaks, seems to be excellent when the synthesis is carried out using water-glass, Ludox AS-30 and Aerosil 200 as SiO_2 sources. Little or no amorphous matter is observed with these sources. On the other hand, TEOS produced a poorly crystallised sample containing significant amount of amorphous material, as evidenced by a broad feature in the range 17 – 30^o 2θ. In summary, the collection of XRD patterns in Figure 2.6 demonstrates the variation of structural features of ferrierite obtained by different researchers using different SiO_2 sources for the hydrothermal synthesis of this zeolite. This collection motivated in the synthesis of ferrierites carried out in this work (Chapters 3 and 4). The inferiority of the ferrierite synthesised using TEOS as the SiO_2 source in this dissertation agrees well with Figure 2.6 B (as demonstrated further below).

2.4 Acidity of zeolites (including ferrierite)

The activity and selectivity patterns of a particular acidic zeolite for different catalytic reactions are recognised to depend upon the combination of several factors, for example, the number and distribution of acid sites in the framework [1]. Controlling the distribution of framework Al atoms, hence that of the acid sites, is a much sought-for objective, as it would have a strong impact on catalytic activity and selectivity [32]. Fourier transform infrared spectroscopy (FTIR) and NH_3-TPD allow for the quantitative determination of the amount and strength of acid sites [1]. Belhekar *et al.* [33] studied the acidity variations in Fe-ferrierite and Al-ferrierite, which were prepared by a single and by three different routes, respectively. The FTIR spectra in the O-H stretching region of the ferrierite samples outgassed at 400 ^{o}C are shown in Figure 2.7 [32].

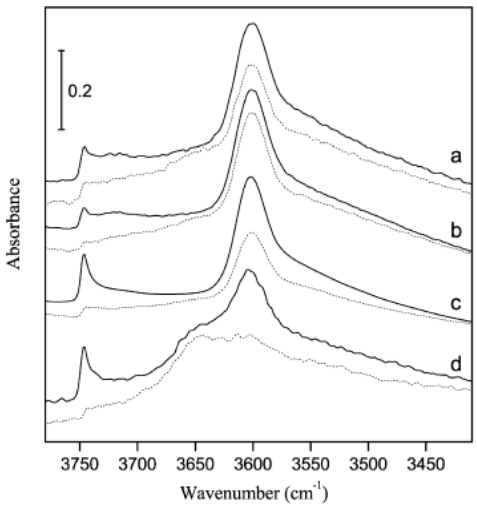

Figure 2.7 FTIR spectra of ferrierite in the O-H stretching region [32].

Full lines in the figure indicates the outgassing of ferrierite samples at 400 ^{o}C, whereas dotted lines show adsorption of pyridine by contact with the amine vapour at 150 ^{o}C for 4 h. Letters a, b, c and d on the figure represent adsorption of pyridine after 4 h, 7, 10 and 20 days, respectively. The ferrierite samples exhibit an intense asymmetric band at 3601 cm^{-1}, which corresponds to Brønsted acid sites, and a weak shoulder at 3550 cm^{-1}, characteristic of bridging hydroxyl groups (Si-OH-Al), as well as a weaker band at 3747 cm^{-1}, corresponding to terminal silanols [32].

Canizares and Carrero [34] studied H-ferrierite and alkaline earth metal-exchanged form of ferrierite by NH_3-TPD. The TPD profiles are shown in Figure 2.8.

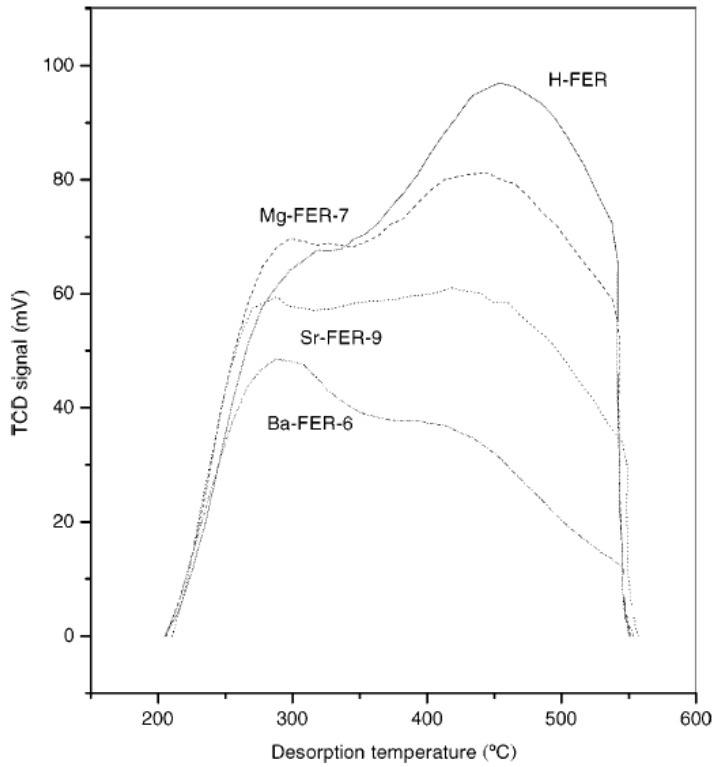

Figure 2.8 NH_3-TPD of H-ferrierite and ferrierite exchanged with alkaline earth metals [34].

Desorption of ammonia with increasing temperature, showed two peaks at 270 and 460 ^oC for the H form of ferrierite. These peaks were assigned to ammonia eluted from weak and strong acid sites, respectively. When H-ferrierite was ion-exchanged with alkaline earth metal aqueous solutions, the intensity of the strong acidity peak was found to decrease with increasing alkaline earth metal content. However, the weak acidity peak somewhat increases, and both peaks shift towards lower temperatures. In other words, the presence of Mg^{2+}, Sr^{2+} and Ba^{2+} ions in cationic positions of ferrierite (instead of protons) produced an increase in the weak/strong acid sites ratio, lower acid strength and a decrease in the total number of acid sites. These observations are accounted for by the changes observed in the NH_3-TPD profiles in Figure 2.8 [34].

2.5 Catalysis by ferrierite

Renewable resources are becoming increasingly important for producing a variety of fine and bulk chemicals. Terpene feedstocks are some of these raw materials. Of these, the *alfa* and the *beta* isomers of pinene are used to manufacture a number of products for the pharmaceutical and chemical industries [35]. The isomerisation of *α*-

pinene, catalysed by acid centres, is of industrial significance. It gives bicyclic products, exemplified by camphene, and monocyclic products such as limonene and p-cymene, as shown in Figure 2.9 [36].

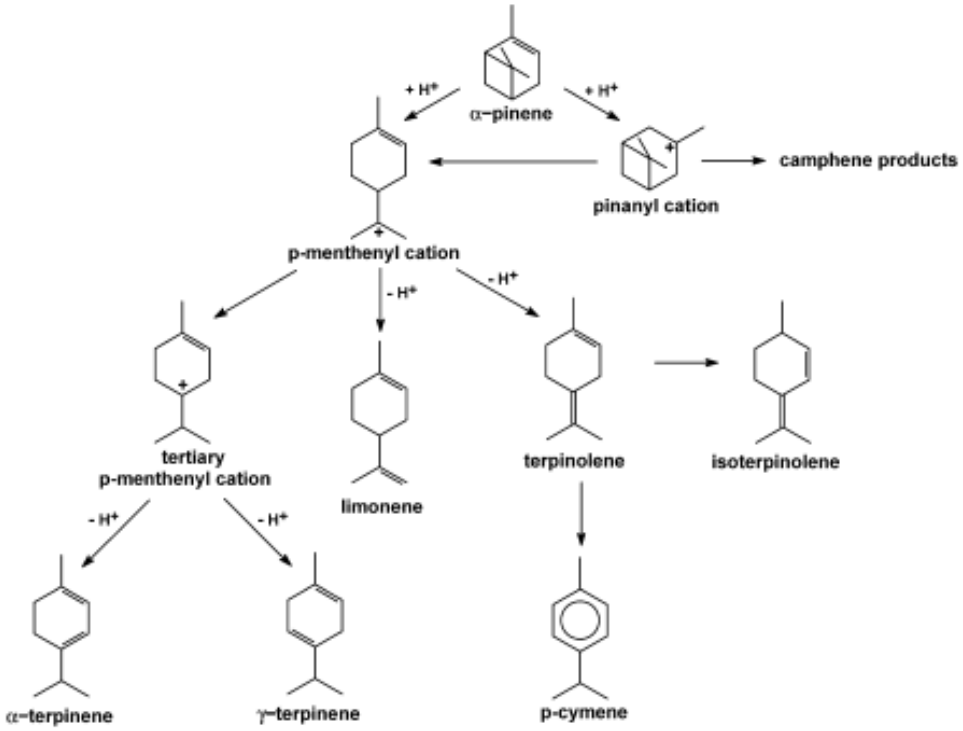

Figure 2.9 Mechanism of the *α*-pinene isomerisation [36].

Camphene is an intermediate compound for producing isoborneol, isobornyl acetate and camphor. Relatively mild dealumination of ferrierite with HCl produced a catalyst that yielded 97 % conversion of *α*-pinene, compared to 72 % of the parent hydrogen form of ferrierite. The ferrierite selectivity toward camphene and limonene was affected by the dealumination level. A greater selectivity toward limonene was observed at the expense of camphene formation with increasing Si/Al ratio of the catalyst due to the increased number of Brønsted acid sites created by dealumination [36].

Isoalkenes are used in oil refining as reactants for fuel components, such as *tert*-amyl methyl ether (TAME), methyl *tert*-butyl ether (MTBE), ethyl t*ert*-butyl ether (ETBE) and isooctane. MTBE is the octane-enhancer of choice to replace tetraethyl lead in reformulated gasoline. Currently, for the production of MTBE isobutene is predominantly obtained from catalytic steam cracking fractions [37]. Isoalkenes can be produced from *n*-alkenes in alkene skeletal isomerisation processes. Skeletal

isomerisation of *n*-butenes has been considered as an alternative for increasing the production of isobutene [38]. The skeletal isomerisation of butenes is a difficult reaction to catalyse. Present catalysts include phosphoric acid, metal halides, Al_2O_3, halogenated Al_2O_3, and aluminosilicates. Zeolites have gained interest as environmentally-friendly catalysts for these processes [32, 38]. Medium pore zeolites with pore diameters in the range 4 - 5.5 Å were found to be active for skeletal isomerisation of linear butenes to isobutene [39]. Among these zeolites, ferrierite has been found to be an excellent catalyst for skeletal isomerisation of *n*-alkenes to *iso*-alkenes [40], e.g., isomerisation of *n*-butene to isobutene [41]. The high selectivity isobutene production, during isomerisation of *n*-butene, is reached after some time on stream. This happens when a carbonaceous deposit is formed, since it suppresses undesirable side reactions [46]. Ferrierite in the potassium form does not show activity in the *n*-butene skeletal isomerisation. The addition of tungsten and boron to the potassium ferrierite promotes the isobutene production, even without changing the profile of the acid strength distribution [47].

Zinc-modified ferrierite showed high selectivity in the cyclisation of EDA and propylene glycol to 2-methyl pyrazine. The cyclisation is a key step for the synthesis of 2-amido pyrazine, a well-known anti-tuberculosis drug [44]. Pyrazine and its derivatives are also useful intermediates for flavouring materials, other drugs and agrochemicals. They are prepared by dehydration-cyclisation and/or partial dehydrogenation of EDA and propylene glycol [44].

2.6 Heavy metals

There has been growing concern over the diverse effects of heavy metals found in water on humans and aquatic ecosystems. Heavy metals in wastewater originate from industries such as mining, metallurgy, machine manufacturing, chemical, electronics and as well as municipal sewage [45]. Many heavy metals and their compounds are toxic, and some are subjected to bio-magnification [46]. In recent years, emissions associated with production involving metals have decreased in many countries due to new legislation, improved cleaning methods and altered industrial activities [47].

2.6.1 The metal contaminant levels of heavy metals

Due to the discharge of large amounts of metal-contaminated wastewater from chemical-intensive industries, heavy metals, such as Cd, Cr, Cu, Ni, As, Pb, and Zn are the most hazardous. Because of their high solubility in water, they can be ingested by living organisms. Once they enter the food chain, heavy metals may accumulate in the human body. If the metals are ingested beyond the permitted concentration, i.e., the metal contaminant level (MCL), they can cause serious health disorders as summarised in Table 2.2 [48].

Table 2.2: The MCL standards for the most hazardous heavy metals [48]

Heavy metal	Toxicities	MCL (mg/L)
Arsenic	Skin manifestations, visceral cancers, vascular disease	0.050
Cadmium	Kidney damage, renal disorder, human carcinogen	0.010
Chromium	Headache, diarrhoea, nausea, vomiting, carcinogenic	0.050
Copper	Liver damage, Wilson's disease, insomnia	0.25
Nickel	Dermatitis, nausea, chronic asthma, coughing, human, carcinogen	0.20
Zinc	Depression, lethargy, neurological signs and increased thirst	0.80
Lead	Damage the foetal brain, diseases of the kidney, circulatory system, nervous system	0.0060
Mercury	Rheumatoid arthritis, and diseases of the kidneys, circulatory system, nervous system	0.000030

The World Health Organization (WHO) recommended 1.5 ppm as the maximum acceptable concentration of Cu in drinking water on account of its toxicity [49]. Therefore, it is necessary to treat Cu-contaminated wastewater prior to discharge into the environment [50].

2.6.2 Methods for the removal of heavy metals

Heavy metal removal from inorganic effluents can be achieved by conventional treatment processes, such as chemical precipitation, ion-exchange, and electrochemical removal [51]. Some of these processes have significant disadvantages, for example, incomplete removal, high energy requirements, production and disposal of toxic sludge, as well as high capital and operational costs

[52]. The ion-exchange method is feasible when an exchanger has a high selectivity for the metal to be removed and concentrations of competing ions are low [53]. Chemical precipitation is the most often used method for the removal of heavy metals [54].

Applications of the precipitation method evolved from the need for phosphorus removal from primary wastewater effluents to curb eutrophication of receiving waters. Current applications of chemical-enhanced primary treatment (CEPT) serve to enhance further treatment through improved removal of suspended solids, and phosphorus during treatment [53]. Studies have shown that CEPT is also effective to capture metals from municipal wastewater [55]. However, it is important to note that the presence of chelating agents, such as ethylenediaminetetraacetic acid, in wastewater can inhibit the metals capture process [56]. For economic and technical reason, the most often adopted method is neutral chemical precipitation. But it has been proved that the following problems are present in neutral precipitation [51]:

(i) Heavy metal-contaminated wastewater is generally acidic, which should not be discharge into, e.g. rivers, until neutral treatment. This is achieved by controlling its pH using the neutral precipitation method,

(ii) When amphoteric metals, such as zinc, lead, tin, aluminium, etc. coexist in wastewater, and the pH is raised, the amphoteric metals appear have the tendency of re-dissolving. It is therefore important to control the pH value strictly and carry out fractional precipitation,

(iii) Some metal ions can form very stable complexes with halogen, cyanogen roots, humic substance, etc. These compounds are very difficult to remove by the method of neutral precipitation, thus it is necessary to carry out wastewater pre-treatment, and

(iv) Precipitation of hydroxide produced by heavy metal ions in the alkaline medium will strip again along with the lowering of the pH, which causes secondary pollution.

From an economy and efficiency point of view, adsorption is regarded as the most promising and widely used method among all methods of heavy metal removal [57]. Adsorption depends on a number of parameters, such as physical and chemical properties of the adsorbent and the adsorbate, temperature, pH, concentration,

pressure, etc. Therefore, determination of the adsorption mechanism and the optimum operation conditions are generally a difficult task [58]. Some of the adsorbents used are discussed in Section 2.6.3 below.

2.6.3 Adsorbents used for the removal of heavy metals

Several adsorbents including activated carbon, chitosan, zeolites, clay, moss peat and fly ash, have been investigated for the removal of heavy metals from waste water [59]. Since its first introduction for heavy metal removal, activated carbon is undoubtedly the most popular and widely used adsorbent for wastewater treatment applications throughout the world. In spite of its prolific use, high quality activated carbon remains an expensive material. Activated carbon also requires complexing agents to improve its performance for the removal of inorganic matters. This situation makes it no longer attractive for use in small-scale industries [60].

Chitosan has largely been employed as a non-toxic flocculent in the treatment of organic polluted wastewater, and as a chelating agent for the removal of toxic heavy metals from industrial wastewater [61]. This is due to its excellent metal-binding capacities and its low cost as compared to activated carbon [62]. Countries like Thailand, Japan and China use fishery wastes such as shrimp, lobster and crab shells to produce chitosan. These waste materials could be obtained for free from local fishery industries. Since such waste is abundantly available, chitosan may be produced at low cost [63].

Clay is another potential alternative to activated carbon [60]. Clays exhibit large surface areas and are capable of adsorbing cationic, and anionic metal species. These materials are also able to participate in cationic and anionic exchange processes. Their sorption capacities, cation and anion exchange properties and binding energies vary widely [64].

Among the different minerals which possess adsorbent properties, zeolites appear to be a promising class of materials to remove heavy metals from wastewater. The advantage of zeolites over other adsorbents, apart from their lower cost, is their ion

selectivity [65]. Several researchers have studied the removal of heavy metals by natural zeolites in wastewater treatment [56]. Alvarez-Ayuso *et al.* [66] studied the sorption behaviour of Cr^{3+}, Ni^{2+}, Zn^{2+}, Cu^{2+}, and Cd^{2+} ions by natural clinoptilolite and synthetic NaP1 zeolites. They found that the sorption capacity of synthetic NaP1 zeolite was 10 times greater than that of the natural zeolite. Qiu and Zeng [67] studied the removal of Ni^{2+}, Zn^{2+}, Cu^{2+}, Pb^{2+} and Co^{2+} using cancrinite zeolite synthesised using fly ash. It was found that cancrinite zeolite had a higher maximum exchange level than natural zeolites (clinoptilolite and scolecite), synthetic zeolites (zeolite NaP1, NaY, zeolite A) and ion exchange resins (IRN77, SKN 1, Ca-alginate based resin). The higher maximum exchange level of cancrinite was attributed to the low Si/Al ratio and its pore size.

Motsi *et al.* [68] studied the effect of concentration, counter ion interactions and effects of particle size on the adsorption of Fe^{3+}, Cu^{2+}, Mn^{2+} and Zn^{2+} by natural clinoptilolite. Removal of heavy metal ions was not only due to ion exchange, but also due to precipitation of metal hydroxides from the solution. The rate of adsorption was directly proportional to the pH value of the solution. Adsorption of Fe^{3+}, Cu^{2+}, Mn^{2+} and Zn^{2} by clinoptilolite decreased in more acidic solutions, due to hydrogen ion competition. Motsi *et al.* [69] further studied the kinetics of Fe^{3+}, Cu^{2+}, Mn^{2+} and Zn^{2+} uptake from single component solutions by natural zeolite (clinoptilolite) and the results are shown in Figure 2.10.

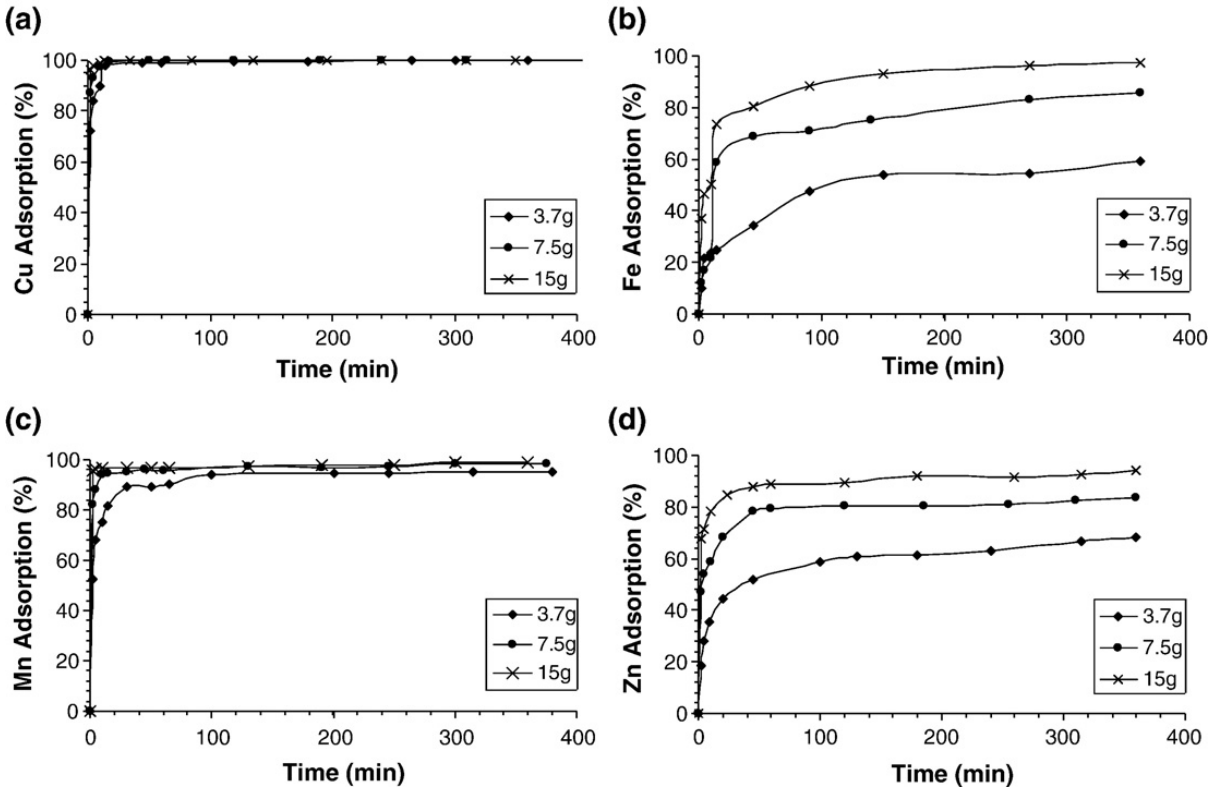

Figure 2.10 Kinetics of heavy metal ion adsorption by clinoptilolite from single-component solutions (grain size: 1 - 3 mm, 100 ml of solution, pH 3.5): (a) Cu, (b) Fe, (c) Mn and (d) Zn [69].

The results show that the adsorption is a heterogeneous process with an initial rapid adsorption rate, followed by a slower rate. This is particularly noticeable for the Fe^{3+} and Zn^{2+} cations, which adsorb more slowly as seen in Figures 2.10 (b) and (d). In the first 40 min adsorption sites are available, the cations interact easily with the sites and hence a high rate of adsorption is observed. The initial stage of fast adsorption corresponded to ion exchange in micro-pores on the surface of the zeolites grains [69]. Furthermore, the driving force for adsorption, which was the concentration difference between the bulk solution and the solid-liquid interface, is initially very high and also result in a higher adsorption rate. However, after the initial period, slower adsorption is due to slower diffusion of cations into the interior channels of, the cations subsequently occupy the exchangeable positions within the crystal structure of the zeolite. In this case it was suggested that ion-exchange takes place between the exchangeable cations (Ca^{2+}, Na^{+} and K^{+}) within the zeolite crystal structure and heavy metal ions (Fe^{3+}, Cu^{2+}, Mn^{2+} and Zn^{2+}) [69].

Panayotova [70] conducted a series of experiments using Bulgarian natural zeolite and its modified forms for the removal of several metal ions such as Ni^{2+}, Cu^{2+}, Cd^{2+}, Zn^{2+} and Pb^{2+}. Natural and NaOH-modified, NaCl-modified, HCl-modified and CH_3COONa-modified zeolites were tested in the adsorption of Ni^{2+}. For raw zeolite, the uptake process obeyed the first order irreversible kinetics. This showed that the ion exchange was the basic mechanism of the metal uptake by the zeolite. The zeolite modification with CH_3COONa and NaCl increased Ni^{2+} adsorption by 25-30 %. For Cu^{2+} removal, the uptake by zeolite from wastewater proved to be as effective as precipitation of copper hydroxide. The presence of Ca^{2+} and Mg^{2+} did not significantly influence the uptake of Cu^{2+}. The zeolite modified with CH_3COONa, NaCl and NaOH exhibited higher Cu^{2+} uptake ability.

2.6.4 Adsorption capacities of zeolites

Several zeolites were investigated for the removal of Cu^{2+} in aqueous solutions under different conditions. Table 2.3 summarises the adsorption capacities of different zeolites as studied by different authors.

Table 2.3: Adsorption capacities of different zeolites

Zeolite	pH	Initial concentration (mg/l)	Adsorption Capacity (mg/g)	References
Clinoptilolite	5.5	300	11	[72]
	5	0 – 0.60	0.13	[77]
	4.5	20 - 400	0.54	[70]
NaX	6	25	7	[73]
NaY	5	100	-	[74]
13X	3.5 – 4.5	190	-	[75]
Iranian natural zeolite	5	1	-	[76]
Zeolite 4A	5	0 – 0.60	0.39	[77]
	3 - 4	50 - 100	22 – 72	[56]
Faujasite X	5	0 – 0.60	0.35	[77]
Faujasite Y	5	0 – 0.60	0.22	[77]
Na-P1	5	0 – 0.60	0.29	[77]
Mordenite	5	0 – 0.60	0.16	[77]
Zeolite A	3	200	38	[78]
Zeolite X	3	200	29	[78]

The adsorption of Cu^{2+} from water is influenced by parameters, such as the initial concentration of metal ions in solution, mass of zeolite, pH of the contact solution and contact time [71].

2.7 References

[1] Z. Gogebakan, H. Yucel, A. Culfaz, Crystallization field and rate study for the synthesis of ferrierite, Industrial & Engineering Chemistry Research 46 (2007) 2006 – 2012.

[2] B.M England, J. Ostwald, Ferrierite: An Australian occurrence, Mineralogical Magazine 42 (1978) 385 – 389.

[3] S.B. Rice, K.G. Parke, D.E.W. Vaughan, Chemical controls on ferrierite crystallization during digenesis of silicic pyroclastic rocks near Lovelock, Nevada, American Mineralogist 77 (1992) 314 – 328.

[4] S.B. Rice, Transmission electron microscope observations of planar defects in ferrierite from Kamloops Lake, British Columbia, American Mineralogist 80 (1995) 930 – 936.

[5] N. Yamamoto, T. Okubo, Ionic conductivity of single-crystal ferrierite, Microporous and Mesoporous Materials 40 (2000) 283 – 288.

[6] N. Venkatathri, A comparison study on synthesis and characterization of FER type molecular sieves, Bulletin of the Catalysis Society of India 5 (2006) 101 – 109.

[7] R. Rachwalik, Z. Olejniczak, B. Sulikowski, Dealumination of ferrierite type zeolite: Physicochemical and catalytic properties, Catalysis Today 101 (2005) 147 – 154.

[8] Y. Long, M. Ma, Y. Sun, H. Jiang, Synthesis, ion-exchange, structural characterization and adsorption of K, Na-FER type zeolite, Journal of Inclusion Phenomena and Macrocyclic Chemistry 37 (2000) 103 – 120.

[9] R.J. Darton, R.E. Morris, High resolution ^{29}Si MAS NMR study of the thermal behaviour of the aluminosilicate zeolites ferrierite, Solid State Science 6 (2006) 342 – 345.

[10] G. Guo, Y. Sun, Y. Long, Synthesis of FER type zeolite with tetrahydrofuran as the template, Chemical Communications (2000) 1893 – 1894.

[11] E. Terres, Influence of the synthesis parameters on textural and structural properties of MCM-41 mesoporous material, Microporous and Mesoporous Materials 431 (1996) 111 – 116.

[12] G. Pal-Borbely, H.K. Beyer, Y. Kiyozumi, F. Mizukami, Synthesis and characterization of ferrieirite made by recrystallization of an aluminium-containing hydrated magadiite, Microporous and Mesoporous Materials 22 (1998) 57 – 68.

[13] S.J. Weigel, J. C. Gabriel, E.G. Puebla, A.M. Bravo, N.J. Henson, L.M. Bull, A.K. Cheetham, Structure-directing effects in zeolite synthesis: A single-crystal X-ray diffraction, ^{29}Si MAS NMR, and computational study of the competitive formation of siliceous ferrierite and dodecasil-3C (ZSM-39), Journal of American Chemical Society 118 (1996) 2427 – 2435.

[14] S. Shevade, R.K. Ahedi, A.N. Kotasthane, Synthesis and characterization of ferrisilicate analogs of ferrierite (Fe-FER) zeolites, Catalysis Letters 49 (1997) 69 – 75.

[15] T. Matsufuji, N. Nishiyama, K. Ueyama, M. Matsukata, Crystallization of ferrierite (FER) on a porous alumina support by a vapor-phase transport method, Microporous and Mesoporous Materials 32 (1999) 159 – 168.

[16] M. Matsukata, N. Nishiyama, K. Ueyama, Crystallization of FER and MFI zeolites by a vapour-phase transport method, Microporous Materials 7 (1996) 109 – 117.

[17] T. Matsufuji, S. Nakagawa, N. Nishiyama, M. Matsukata, K. Ueyama, Synthesis and permeation studies of ferrierite/alumina composite membranes, Microporous and Mesoporous Materials 38 (2000) 43 – 50.

[18] R.B. Khomane, B.D. Kulkarni, R.K Ahedi, Synthesis and characterization of ferrierite-type zeolite in the presence of nonionic surfactants, Journal of Colloid and Interface Science 236 (2001**)** 208 – 213.

[19] N.R. Forbes, L.V.C. Rees, The synthesis of ferrierite, ZSM-5 and Theta-1 in the presence of diethanolamine: Experimental, Zeolites 15 (1995) 444 – 451.

[20] R.A. Rakoczy, Y. Traa, P. Kortunov, S. Vasenkov, J. Karger, J. Weitkamp, Synthesis of large crystals of all-silica zeolite ferrierite, Microporous and Mesoporous Materials 104 (2007) 179 – 184.

[21] A. Rakoczy, M. Breuninger, M. Hunger, Y. Traa, J. Weitkamp, Template-free synthesis of zeolite ferrierite and characterization of its acid sites, Chemical Engineering & Technology 25 (2002) 273 – 275.

[22] A.B. Pinar, L. Gomez-Hortiguela, J. Perez-Pariente, Cooperative structure directing role of the cage-forming tetramethylammonium cation and the bulkier benzylmethylpyrrolidinium in the synthesis of zeolite ferrierite, Chemistry of Materials 19 (2007) 5617 – 5626.

[23] A.B. Pinar, R. Garcia, J. Perez-Pariente, Synthesis of ferrierite from gels containing a mixture of two templates, Collection of Czechoslovak Chemical Communications 72 (2007) 666 – 678.

[24] R. Garcia, L. Gómez-Hortigüela, I. Díaz, E. Sastre, and J. Pérez-Pariente, Synthesis of materials containing ferrierite layers using quinuclidine and 1-benzyl-1-methylpyrrolidine as structure-directing agents. An experimental and computational study, Chemistry of Materials 20 (2008) 1099 – 1107.

[25] S. Mintova, V. Valtchev, Effect of the silica source on the formation of nanosized silicalite-1: an in situ dynamic light scattering study, Microporous and Mesoporous Materials 55 (2002) 171 – 179.

[26] J. Yu, Synthesis of zeolites, Studies in Surface Science and Catalysis 168 (2007) 39 – 104.

[27] X. Cheng, J. Wang, J. Guo, H. He, Y. Long, FER zeolite crystallized in THF-Na_2O-SiO_2-Al_2O_3-H_2O reactant system containing catalytic amount of organic additives, Microporous and Mesoporous Materials 119 (2009) 60 – 67.

[28] R.J. Ahedi, A.N. Kotasthane, Studies in the crystallization of ferrierite (FER) type zeolites in presence of promoting medium, Journal of Porous Materials 4 (1997) 171 – 179.

[29] R. Anand, R.B. Khomane, B.S. Rao, B.D. Kulkarni, Vapor phase Beckmann rearrangement of cyclohexanone oxime over different ferrierite zeolite catalysts, Catalysis Letters 78 (2002) 189 – 194.

[30] R.J. Ahedi, A.N. Kotasthane, B.S. Rao, A. Manna, B.D. Kulkarni, Synthesis of ferrierite-type zeolite in the presence of a catalytic amount of pyrrolidine and sodium bis(2-ethyhlhexyl) sulfosuccinate, Journal of Colloid and Interface Science 236 (2001) 47 – 51.

[31] A. Corma, U. Diaz, M.E. Domine, V. Fornes, Ti-ferrierite and TiITQ-6: synthesis and catalytic activity for the epoxidation of olefins with H_2O_2, Chemical Communications (2000) 137 – 138.

[32] A.B. Pinar, C. Marquez-Alvarez, M. Grande-Casas, J. Perez-Pariente, Template-controlled acidity and catalytic activity of ferrierite crystals, Journal of Catalysis 263 (2009**)** 258 – 265.

[33] A.A. Belhekar, R.K. Ahedi, S. Kuriyavar, S.S. Shevade, B.S. Rao, R. Anand, Z. Tvaruzkov, Effect of acid sites of Al- and Fe-ferrierite on m-xylene isomerization, Catalysis Communications 4 (2003) 295 – 302.

[34] P. Canizares, A. Carrero, Comparative study of the catalytic properties of ferrierite zeolite exchanged with alkaline earth metals in the skeletal isomerization of *n*-butene, Catalysis Letters 64 (2000) 239 – 246.

[35] A.L. Cánepa, C.M. Chanquía, G.A. Eimer, S.G. Casuscelli, Oxidation of olefins employing mesoporous molecular sieves modified with copper, Applied Catalysis A: General 462– 463 (2013) 8 – 14.

[36] R. Rachwalik, Z. Olejniczak, J. Jiao, J. Huang, M. Hunger, B. Sulikowski, Isomerisation of α-pinene over dealuminated ferrierite-type zeolites, Journal of Catalysis 252 (2007) 161 – 170.

[37] A.C. Buttler, C.P. Nicolaides, Catalytic skeletal isomerization of linear butenes to isobutene, Catalysis Today 18 (1993) 443 – 471.

[38] T.J. Keskitalo, K.J.T. Lipiainen, A.O.I. Krause, Kinetic modelling of coke oxidation of a ferrierite catalyst, Industrial & Engineering Chemistry Research 45 (2006) 6458 – 6467.

[39] C. Wattanakit, S. Nokbin, B. Boekfa, P. Pantu, J. Limtrakul, Skeletal isomerization of 1-butene over ferrierite zeolite: A quantum chemical analysis of structures and reaction mechanisms, Journal of Physical Chemistry 116 (2012) 5654 – 5663.

[40] S. Bordiga, G.T. Palomino, C. Paze, A. Zecchima, Vibrational spectroscopy of H_2, N_2, CO and NO adsorbed on H, Li, Na, K-exchanged ferrierite, Microporous and Mesoporous Materials 34 (2000) 67 – 80.

[41] R.J. Pellet, D.G. Casey, H.M. Huang, R.V. Kessler, E.J. Kuhlman, C.L. O'Young, J.R. Ugolini, R.A. Sawicki, Isomerization of *n*-butene to isobutene by ferrierite and modified ferrierite catalysts, Journal of Catalysis 157 (1995) 423 – 435.

[42] W.Q. Xu, Y.G. Yin, S.L. Suib, J.C. Edwards, C.L. O'Young, Modification of non-template synthesized ferrierite/ZSM-35 for *n*-butene skeletal isomerization to isobutylene, Journal of Catalysis 163 (1996) 232 – 244.

[43] I.L. Coronati, G.M. Font, N.E. Fontana, C.A. Querini, R.A. Comeli, Linear butene skeletal isomerization over boron-promoted ferrierite, Catalysis Today 133–135 (2008) 63 – 68.

[44] R. Anand, B.S. Rao, Synthesis of 2-methyl pyrazine over zinc-modified ferrierite (FER) catalysts, Catalysis Communications 3 (2002) 29 – 35.

[45] J.L. Gardea-Torresday, L. Tang, J.M. Salvador, Copper adsorption by esterified and unesterified fractions of sphagnum peat moss and its different humic substances, Journal of Hazardous Materials 48 (1996**)** 191 – 206.

[46] M. Karvelas, A. Katsoyiannis, C. Samara, Occurrence and fate of heavy metals in the wastewater treatment process, Chemosphere 53 (2003) 1201 – 1210.

[47] S. Babel, T.A. Kurniawan, Cr(VI) removal from synthetic wastewater using coconut shell charcoal and commercial activated carbon modified with oxidising agents and/or chitosan, Chemosphere 54 (2004) 951 – 967.

[48] M.A. Barakat, New trends in removing heavy metals from industrial wastewater, Arabian Journal of Chemistry 4 (2011) 361 – 377.

[49] WHO, Guidelines for drinking-water quality 4th Edition (2011) 340.

[50] O.S. Amuda, I.A. Amoo, K.O. Ipinmoroti, O.O. Ajayi, Coagulation/flocculation process in the removal of trace metals present in industrial wastewater, Journal of Applied Sciences and Environmental Management 10 (2006) 159 – 162.

[51] A.K. Meena, G.K. Mishra , P.K. Rai , Chitra Rajagopal, P.N. Nagar, Removal of heavy metal ions from aqueous solutions using carbon aerogel as an adsorbent, Journal of Hazardous Materials B122 (2005) 161 – 170.

[52] K.S. Hui, C.Y.H. Chao, S.C. Kot, Removal of mixed heavy metals ions in wastewater by zeolite 4A and residual products from recycled coal fly ash, Journal of Hazardous Materials B127 (2009) 89 – 101.

[53] P.D. Johnson, P. Girinathannair, K.N. Ohlinger, S. Ritchie, L. Teuber, J. Kirby, Enhanced removal of heavy metals in primary treatment using coagulation and flocculation, Water Environment Research 80 (2008) 472 – 479.

[54] B.J. Watten, P.L. Sibrell, M.F. Schwartz, Acid neutralization within limestone sand reactors receiving coal mine drainage, Environmental Pollution 137 (2003) 295 – 304.

[55] A.C. Ridge, D.L. Sedlak, Effect of ferric chloride addition on the removal of Cu and Zn complexes with EDTA during municipal wastewater treatment, Water Research 38 (2004) 921–934.

[56] X. Querol, N. Moreno, J.C. Umana, R. Juan, S. Hernandez, C. Fernandez-Pereira, C. Ayora, M. Janssen, J. Garcia-Martinez, A. Linares-Solano, D. Carzola-Amoros, Application of zeolite material synthesised from fly ash to the decontamination of wastewater and fuel gas, Journal of Chemical Technology and Biotechnology 77 (2002) 292 – 298.

[57] S. Mehdizadeh, S. Sadjadi, S.J. Ahmadi, M. Outokesh, Removal of heavy metals from aqueous solution using platinum nanopartcles/Zeolite-4A, Journal of Environmental Health Science & Engineering 12 (2014) 1 – 7.

[58] M. Uysal, I. Ar, Removal of Cr(VI) from industrial wastewaters by adsorption Part I: Determination of optimum conditions, Journal of Hazardous Materials 149 (2007) 482 – 491.

[59] E. Katsou, S. Malamis, K.J. Haralambous Industrial wastewater pre-treatment for heavy metal reduction by employing a sorbent-assisted ultrafiltration system, Chemosphere 82 (2011) 557 – 564.

[60] S. Babel, T.A. Kurniawan, Low-cost adsorbents for heavy metals uptake from contaminated water: A review, Journal of Hazardous Materials 97 (2003) 219 – 243.

[61] V. Mohanasrinivasan, M. Mishra, J.S. Paliwal, S.K. Singh, E. Selvarajan, V. Suganthi, C.S.Devi, Studies on heavy metal removal efficiency and antibacterial activity of chitosan prepared from shrimp shell waste, Biotechnology 4 (2014) 167 – 175.

[62] K.J. Adarsh, G. Madhu, A comparative study on metal adsorption, International Journal of Innovative Research in Science, Engineering and Technology 3 (2014) 9609 – 9617.

[63] S. Nomanbhay, K. Palanisamy, Removal of heavy metal from industrial wastewater using chitosan coated oil palm shell charcoal, Electronic Journal of Biotechnology 8 (2005) 43 – 53.

[64] C. Rosales-Landeros, C. E. Barrera-Díaz, B. Bilyeu, V. V. Guerrero, F. U. Nunez, A review on Cr(VI) adsorption using inorganic materials, American Journal of Analytical Chemistry 4 (2013) 8 – 16.

[65] H.R. Tashauoei, H.M. Attar, M.M. Amin, M. Kamali, M. Nikaeen, M.V. Dastjerdi, Removal of cadmium and humic acid from aqueous solutions using surface modified nanozeolite A, International Journal of Environmental Science and Technology 7 (2010) 497 – 508.

[66] E. Alvarez-Ayuso, A. Garcia-Sanchez, X. Querol, Purification of metal electroplating waste waters using zeolites, Water Research 37 (2003) 4855 – 4862.

[67] W. Qiu, Y. Zheng, Removal of lead, copper, nickel, cobalt, and zinc from water by a cancrinite-type zeolite synthesized from fly ash, Chemical Engineering Journal 145 (2009) 483 – 488.

[68] T. Motsi, N.A. Rowson, M.J.H. Simmons, Kinetic studies of the removal of heavy metals from acid mine drainage by natural zeolite, International Journal of Mineral Processing 101 (2011) 42 – 49.

[69] T. Motsi, N.A. Rowson, M.J.H. Simmons, Adsorption of heavy metals from acid mine drainage by natural zeolite, International Journal of Mineral Processing 92 (2009) 42 – 48.

[70] M. Panayotova, Kinetics and thermodynamics of removal nickel ions from wastewater by use of natural and modified zeolite, Fresenius Environmental Bulletin 10 (2001) 267 – 272.

[71] L.M. Cozmuta, A.M. Cozmuta, A. Peter, C. Nicula, E.B. Nsimba, H. Tutu, the influence of pH on the adsorption of lead by Na-clinoptilolite: Kinetic and equilibrium studies, Water SA 38 (2012) 269 – 278.

[72] N. Dizadji, M. Rashtchi, S. Dehpouri, N. Nouri, Experimental investigation of adsorption of copper from aqueous solution using vermiculite and clinoptilolite, International Journal of Environmental Research 7 (2013) 887 – 894.

[73] P. Pandey, S.S. Sambi, S.K. Sharma, S. Singh, Batch adsorption studies for the removal of Cu(II) ions from zeolite NaX from aqueous stream, Proceedings of the world congress of Engineering and Computer Science 1 (2009) San Francisco, USA.

[74] A. Krobba, D. Nibou, S. Amokrane, H. Mekatel, Adsorption of copper(II) onto molecular sieves NaY, Desalination and Water Treatment 37 (2012) 31 – 37.

[75] T. Mishra, S.K. Tiwari, Studies on sorption properties of zeolite derived from Indian Fly ash, Journal of Hazardous Materials B137 (2006) 299 – 303.

[76] H. Merrikhpour, M. Jalali, Comparative and competitive adsorption of cadmium, copper, nickel, and lead ions by Iranian natural zeolite, Clean Technologies and Environmental Policy 15 (2013) 303 – 316.

[77] P. Kabwadza-Corner, M.W. Munthali, E. Johan, N. Matsue, Copper study of copper adsorptivity and selectively toward zeolites, American Journal of Analytical Chemistry 5 (2014) 395 – 405.

[78] C. Wang, J. Li, X. Sun, L. Wang, X. Sun, Evaluation of zeolites synthesised from fly ash as potential adsorbents for wastewater containing heavy metals, Journal of Environmental Sciences 21 (2009) 127 – 136.

CHAPTER THREE

EXPERIMENTAL

3.1 Introduction

In this Chapter, the materials, preparation methods and characterisation techniques used to synthesise and characterise ferrierite zeolites using different silica sources are described. The characterisation techniques used were X-ray powder diffraction (XRD), scanning electron microscopy (SEM), ammonia temperature-programmed desorption (NH_3-TPD) and Brunauer-Emmett-Teller (BET) surface area measurements. The heavy metal removal (Cu^{2+}) experimental procedure is also described. The measurement of the Cu^{2+} uptake by zeolites was done with the help of atomic adsorption spectrometry (AAS).

3.2 Synthesis of ferrierite

3.2.1 Reagents

The following reagents were acquired from Sigma-Aldrich: tetraethyl orthosilicate (TEOS, 98 %), aluminium sulphate octadecahydrate ($Al_2(SO_4)_3.18H_2O$, 98 %), pyrrolidine (99 %), colloidal silica (Ludox LS-30, 30 % SiO_2, 70 % H_2O) and water-glass (26.5 % SiO_2, 10.6 % Na_2O, 62.9 % H_2O). Sodium hydroxide (NaOH, 99 %), ammonium nitrate (NH_4NO_3, 98 %), sulphuric acid (H_2SO_4, 98 %), hydrochloric acid (HCl, 32 %) and copper sulphate pentahydrate ($CuSO_4.5H_2O$, 98 %) were purchased from Rochelle Chemicals and Aerosil 200 from Degussa.

3.2.2 Procedure

The synthesis was carried out using procedure reported by Anand and Rao [1]. Ferrierite zeolite was synthesised using the initial gel composition of:

$$20\ Na_2O : Al_2O_3 : 37\ \text{pyrrolidine} : 66.5\ SiO_2 : 6.3\ H_2SO_4 : 1460\ H_2O.$$

The gel was prepared by mixing four different solutions (A, B, C and D). The SiO_2 sources used in this study were TEOS, water-glass, Ludox LS-30 and Aerosil 200. Solution A was prepared by mixing 13.26 g NaOH and 25.00 g distilled water. Solution B was prepared by adding appropriate amount of the SiO_2 source in 25.00 g of distilled water. The mixture was stirred for 30 min using an overhead stirrer. To this mixture a template (16.70 g pyrrolidine) was added. This was followed by addition of solution C, which was prepared by dissolving 4.27 g $Al_2(SO_4)_3.18H_2O$ in 25.00 g distilled water. Solution D (prepared by mixing 3.96 g of H_2SO_4 and 10.00 g distilled water) was added to the mixture. Finally, 45.32 g of distilled water was added and the gel (pH ±11) was stirred vigorously for 24 h, followed by hydrothermal treatment in a 300 ml home-made stainless steel autoclave without stirring at 160 ^oC for 72 h. Other versions of the synthesis with TEOS involved HCl-hydrolysis prior to the gel preparation step, and also pre-mixing with water-glass. In the HCl-hydrolysis step, a solution of 69.60 g TEOS in 25.00 g distilled water was stirred with 10.25 ml of an aqueous solution of HCl (0.30 M) at 90 °C for 4 h. For pre-mixing, mole composition of 1 : 1 and 1 : 3 (TEOS : water-glass) were used.

The as-synthesised ferrierite samples were thoroughly washed with distilled water, using a Buchner funnel of 14.0 cm in diameter, fitted with glass microfiber filter paper (Whatman GF/C) of 12.5 cm in diameter. They were washed until free from sulphate as detected by addition of barium chloride solution to the filtrates (the presence of white precipitates showed the presence of sulphate ions). All the ferrierite materials were dried at 100 ^oC for 24 h using an oven (Labotech Ecotherm). The dried materials were then calcined at 500 ^oC for 18 h to remove the template (pyrrolidine), using a furnace (Carbolite type S30 fitted with a 2AU ESF Eurotherm). During calcination, the temperature was increased from room temperature in steps of 50 ^oC at 15 min intervals until it reached 500 ^oC.

The Na-forms of the synthetic zeolites produced above were ion-exchanged with 1 M NH_4NO_3 in the ratio of 1 g zeolite : 25 ml NH_4NO_3 solution. The suspension, contained in a beaker, was gently stirred for 1 h using an overhead stirrer. The NH_4^+ solution was then decanted and a fresh solution added. The ion exchange procedure was repeated three times. The NH_4^+-form of the zeolite was then washed with distilled water until filtrates were free from nitrates. This was done by adding iron sulphate and concentrated sulphuric acid into the filtrate (a brown ring formation

showed the presence of nitrate ions). The NH_4^+-forms of the zeolites were converted to H^+-forms by calcination at 500 ^oC for 18 h.

3.3 Physicochemical characterisation of ferrierite zeolites

This section describes the characterisation of the prepared materials by XRD, SEM, NH_3-TPD and BET. The experimental procedures using these techniques are explained.

3.3.1 X-ray powder diffraction

The XRD patterns of the sodium ferrierites were obtained on a Bruker AXS D8, equipped with a primary beam Göbel mirror, a radial Soller slit and a Vanatec-1 detector, using Cu-K_α radiation (40 kV, 40 mA). About two spatulas of each zeolite were finely ground with a mortar and pestle. The ground zeolite was packed on the sample holder and pressed sufficiently. The sample holder was loaded into the diffractometer and the diffractometer switched on to allow the X-rays to strike the sample at different angles. Each zeolite was analysed for 30 min. The relative % XRD crystallinity of the materials was calculated using the sum of intensities of the characteristic peaks and equation 3.1 [2].

$$\textit{Relative \% XRD crystallinity} = \frac{sum\ of\ intensities\ of\ characteristic\ peaks\ (sample)}{sum\ of\ intensities\ of\ characteristic\ peaks\ (reference)} \times\ 100\% \qquad (3.1)$$

The ferrierite derived from water-glass had the highest sum of the characteristic peaks and was used (i.e., 100 % crystalline) as the reference. The peak listing is indicated on Appendices A1 to A7. The crystallite size was calculated using the Scherrer equation (3.2) [3]:

$$\tau = \frac{K\lambda}{\beta cos\theta} \qquad (3.2)$$

where τ is the crystallite size of the ordered (crystalline) domains, which may be smaller or equal to the grain size; K is a dimensionless shape factor, with a value close to unity. The shape factor has a typical value of about 0.9, but varies with the actual shape of the crystallite; λ is the X-ray wavelength; β is the line broadening at

half the maximum intensity, after subtracting the instrument line broadening, in radians and θ is the Bragg angle. The most intense peak at $2\theta = 9^{o}$ was used to calculate the crystallite size.

3.3.2 Scanning electron microscopy

A 40.0 mm × 20.4 mm aluminium stub was covered with 12 mm double sided carbon tape (S-05082-AB, SPI Supplies, USA). Carbon tape was also attached to transparency paper, which was subsequently cut into small (12 mm x 3 mm) pieces to strengthen the carbon tape. These pieces were dipped into the sample resulting in small quantities (about 0.1 mg) of powder or small lumps (< 3 mm^3) attaching to the carbon tape. Several (6 - 8) of these small carbon tape pieces containing different samples were placed on the double sided carbon tape that was attached to the aluminium stub. Excess powder was removed by using a single blast of compressed dry nitrogen gas. The samples were then coated with gold under argon gas using an Emitech K550X sputter coater (Ashford, England). They were viewed on a scanning electron microscope; JEOL JSM-5800LV (JEOL, Tokyo, Japan). The samples were imaged at 5 kV and at the lowest beam current that would achieve the optimum resolution of a specific magnification. The low beam intensity was used as a precaution to avoid sample damage.

3.3.3 Ammonia temperature-programmed desorption

The NH_3-TPD was performed in an in-house constructed apparatus, equipped with a thermal conductivity detector (TCD) to study the acid strength distribution of selected materials. Experiments were performed as follows:

The (0.20 g) sample was degassed in helium gas at a flow rate of 60 ml/min. The sample was heated to 500 ^{o}C, and cooled to 100 ^{o}C for 10 min. The helium gas was left flowing, and a mixture of NH_3 in He gas (4 % NH_3, balance He) was adsorbed on the zeolite for 1 h at 100 ^{o}C. The mixture of NH_3 and He gas was replaced by He gas to remove the weakly-adsorbed NH_3 on the surface of the zeolite for 15 min. Further

NH_3-esorption was carried out in He at a flow rate of 60 ml/min by heating the sample from 100 ^oC to 700 ^oC at a heating rate of 10 ^oC/min. Both, the weakly and strongly adsorbed NH_3 were quantified by TCD.

3.3.4 Brunauer-Emmett-Teller surface area measurements

The BET surface areas of synthesised zeolites were measured using a Quantachrome Nova 1000 series instrument. About 0.10 g of zeolite was degassed (using nitrogen gas) under vacuum at 400 ^oC overnight. After the degassing process, the zeolite was loaded on the analysis station for measuring of the isotherms. The BET surface areas were determined at a P/P_o between 0.05 and 0.35. The results were analysed using the Nova data reduction software provided with the instrument. The surface areas were determined from ten point BET plots.

3.4 Adsorption of Cu^{2+} from aqueous solutions

An appropriate amount of zeolite (adsorbent) was added to an aqueous solution containing some concentration of Cu^{2+} in a 250 ml Erlenmeyer flask. The mixture was stirred using a Heidolph MR 3001 K magnetic stirrer. At the end of stirring, the suspension was filtered through a Whatman No. 42 filter paper (100 cm in diameter), and the filtrate was analysed for Cu^{2+} using a Varian Spectra 110 AAS. The following AAS parameters were used throughout the analyses:

(i) Light source: Copper hollow cathode lamp,
(ii) Flame type: Air-acetylene flame,
(iii) Wavelength: 327.4 nm,
(iv) Lamp current: 4.0 mA, and
(v) Slit width: 0.5 nm

A 100 ppm stock solution of Cu^{2+} was prepared by dissolving 0.39 g $CuSO_4$. $5H_2O$ in 1000 ml distilled water using a volumetric flask. In order to prepare the calibration curve, four standard solutions with concentrations of 2.0 ppm, 4.0 ppm, 6.0 ppm and 8.0.ppm were prepared from the 100 ppm stock solution. The resulting calibration curve was used to quantify the amount of Cu^{2+} in the adsorption experiments. The

following parameters were investigated for their influence on the metal uptake by different zeolites:

(i) *Initial pH of the Cu^{2+} solution*: The effect of the initial pH on the equilibrium uptake of Cu^{2+} was analysed over a pH range from 2 to 7. The pH was adjusted using 0.10 M NaOH and/or 0.10 M HCl and measured by a BOECO PT-380 pH meter. Ferrierite (0.10 g) was mixed with 50 ml of a metal ion solution of a fixed concentration (8.00 ppm) and stirred for 24 h,

(ii) *Initial concentration of Cu^{2+}*: The influence of the initial concentration on the removal of the copper ions was investigated by mixing 0.10 g of ferrierite and 50 ml of a metal ion solution with a concentration of 2.00, 4.00, 6.00, 8.00 or 10.00 ppm at pH 5,

(iii) *Contact time*: The effect of contact time [period of contact between the adsorbent (ferrierite zeolite) and the adsorbate (Cu^{2+} solution)] on the removal of the copper ions was investigated. Ferrierite (0.10 g) was mixed with 50 ml of an adsorbate solution of a fixed concentration (8.00 ppm) at pH 5, and stirred for contact times ranging from 30 min to 180 min.

(iv) *Adsorbent dose (in g of zeolite per L of solution)*: The influence of the dose on the removal of copper ions was carried out by mixing 0.10, 0.20, 0.30, 0.40, 0.50 and 0.60 g adsorbent with 50 ml of a metal ion solution of concentration 8.00 ppm at an initial pH 5.

The percent metal ion removal (R) was calculated by using equation (3.3):

$$R = (C_i - C_e)/C_i \times 100\ \% \qquad (3.3)$$

where C_i and C_e are the initial and equilibrium concentrations (ppm) of Cu^{2+} in the solution, respectively. The amount of each Cu^{2+} ion adsorbed at equilibrium by sorbent, qe (mg/g), was calculated using equation (3.4):

$$q_e = V(C_i - C_e)/M \qquad (3.4)$$

3.5 References

[1] R. Anand, B.S. Rao, Synthesis of 2-methyl pyrazine over zinc-modified ferrierite (FER) catalysts, Catalysis Communications 3 (2002) 29 – 35.

[2] S.S. Rayalu, J.S. Udhoji, S.U. Meshram, R.R. Naidu, S. Devotta, Estimation of crystallinity in fly ash-based zeolite-A using XRD and IR spectroscopy, Current Science 89 (2005) 2147 – 2151.

[3] A. Monshi, M.R. Foroughi, M.R. Monshi, Modified Scherrer equation to estimate more accurately nano-crystallite size using XRD, World Journal of Nano Science and Engineering 2 (2012) 154 – 160.

CHAPTER FOUR

RESULTS AND DISCUSSION

4.1 Introduction

In this chapter, the results of ferrierite synthesised using different silica sources under the same conditions are presented and discussed. For ease of reference, the codenames in Table 4.1 have been used to relate the zeolitic products to the silica precursors from which they were synthesised.

Table 4.1: Codenames of zeolitic products

Zeolitic codename	**SiO_2 precursor**
FER-TS	TEOS
FER-WG	Water-glass (water-glass)
FER-LS	Ludox LS-30
FER-A200	Aerosil 200

The influence of each of these silica precursors on the structural, acidic and textural properties of the final zeolite was investigated using XRD, SEM, NH_3-TPD and BET surface area measurements. The physicochemical properties of the materials were not only affected by the nature of the SiO_2 source, but also by some other synthesis manipulations, such as acid-hydrolysis and water-glass addition when TEOS was used as the primary silica source. The resulting Na-forms of the zeolites, as well as their H-forms, were tested for efficiency in the removal of Cu^{2+} ions from aqueous solutions.

4.2 Characterisation of the ferrierites

Only the Na-form ferrierites characterisation results are presented in this section.

4.2.1 X-ray powder diffraction

The XRD results are presented in the form of XRD patterns, relative % XRD crystallinities and crystallite sizes. The characteristic diffraction peaks of ferrierite are at $2\theta = 9^{o}$ and $22^{o} \leq 2\theta \geq 26^{o}$ [1].

Figure 4.1 shows the XRD patterns of the zeolitic materials synthesised using different SiO_2 sources.

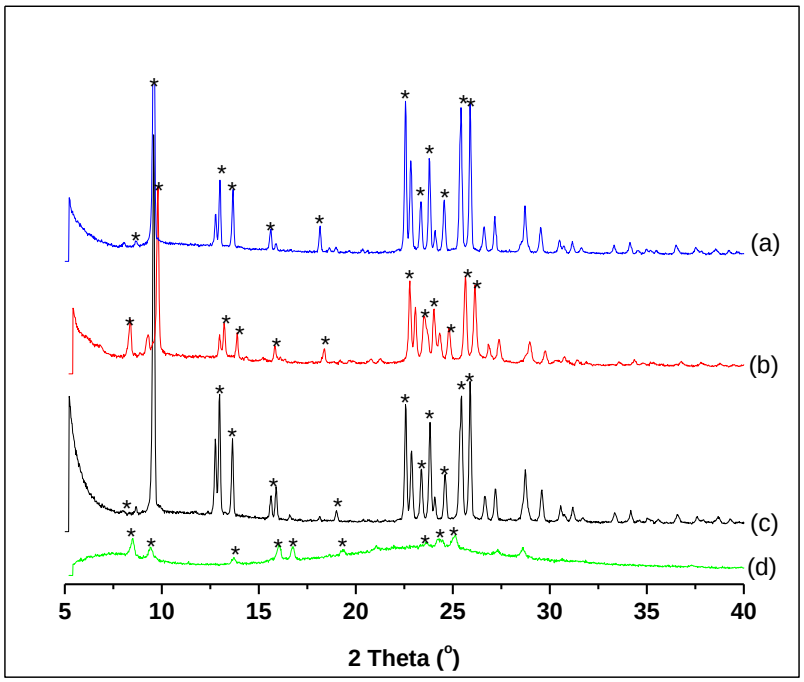

Figure 4.1 XRD patterns for (a) FER-LS, (b) FER-A200, (c) FER-WG and (d) FER-TS. The asteriks (*) show the characteristic peaks of ferrierite.

The XRD patterns in Figure 4.1 shows that the three SiO_2 sources, viz., water-glass, Ludox LS-30 and Aerosil 200 produced highly crystalline zeolite phases as judged from the number of peaks and their intensities. On the other hand, TEOS as a silica source produced ferrierite with the most inferior structural quality. This observation suggests that the inorganic silica sources, and particularly the liquid-phase ones (water-glass and Ludox LS-30), favoured the crystallisation of ferrierite more than the organic silica source (TEOS). The origin of this difference may lie in the aqueous

solution chemistry of these silica sources, wherein the organic TEOS has partial solubility in water, thus leading to different crystallisation rates and mechanisms.

It is clear from the figure that TEOS is the worst SiO_2 precursor for the synthesis of ferrierite under these conditions. An amorphous material was produced when ferrierite was synthesised using unhydrolysed TEOS as the sole SiO_2 source. This was also reported in the literature [8, 9] as presented in Section 2.3.2. All other SiO_2 precursors produced zeolites with similar XRD patterns, suggesting that similar materials were formed. The observed difference in the peak intensities signifies the difference in the relative crystallinities. The asteriks in the figure show the characteristic peaks of ferrierite, by analogy with the XRD patterns described elsewhere [1, 2]. The peaks of FER-WG are sharper than those associated with FER-LS and FER-A200. The XRD patterns of FER-LS and FER-WG show similar features to those of materials prepared using Ludox AS-40 and water-glass reported in the literature [2 - 7], suggesting successful synthesis of ferrierite in the present study (compare also Figure 2.6 Chapter 2). A comparison with the XRD patterns reported in the literature shows that the samples are related to the family of layered precursors of ferrierite, for example the one denoted PREFER by Garcia *et al*. [8]. From Figure 4.1, it can be seen that the quality (in terms of crystallinity) of ferrierite varies as a function of the SiO_2 precursor in the order FER-WG > FER-LS > FER-A200 > FER-TS.

To further investigate the influence of the silica source on the quality of ferrierite, the worst-performing SiO_2 source (TEOS) was mixed with different amounts of the best-performing source (water-glass) prior to gel preparation. The produced zeolites exhibited XRD features shown in Figure 4.2 below.

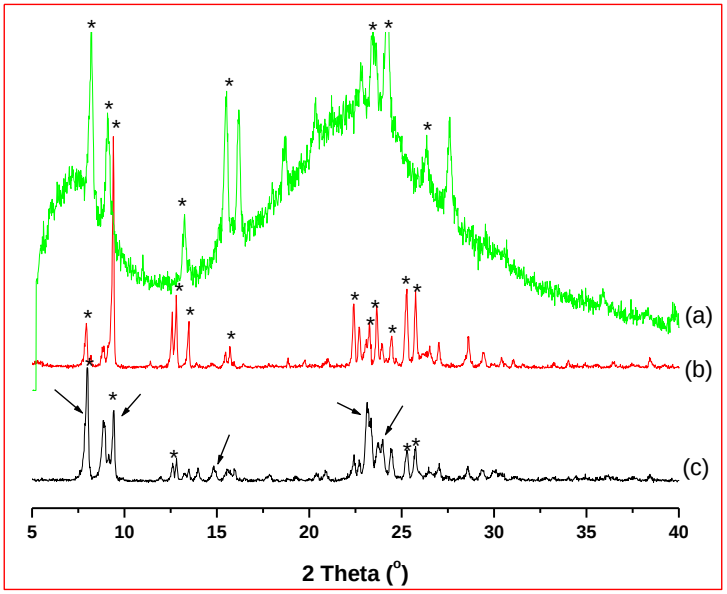

Figure 4.2 XRD patterns of ferrierite showing the influence of water-glass addition to TEOS: (a) FER-TS, (b) FER-TS/WG (1 : 1) and, (c) FER-TS/WG (1 : 3). The arrows indicate the presence of ZSM-5.

As already seen in Figure 4.1, TEOS is an inferior silica source for the synthesis of ferrierite under these conditions. As shown in Figure 4.2 (b) and (c), mixing SiO_2 sources lead to a great improvement in the quality of the material produced compared to using TEOS alone [Figure 4.2 (a)]. It is believed that the alkaline water-glass assists in the hydrolysis of TEOS to silicic acid, which is able to undergo condensation and polymerisation to SiO_2 or to be incorporated into the zeolite structure. An equimolar mixture of TEOS and water-glass produced ferrierite as the only phase, as shown in Figure 4.2 (b). However, the peak at 8^o 2θ is more intense than the peak that appears at 8^o 2θ for FER-WG as presented in Figure 4.1 (c). The intensity of the peak at 8^o 2θ was also described by Kim *et al*. [4]. The mixture with a mole ratio of 1 : 3 (TEOS/water-glass) produced a mixture of two phases, viz. ferrierite and ZSM-5. The ZSM-5 zeolite peaks are indicated by arrows in Figure 4.2 (c), as deduced from a comparison with literature [10, 11]. In conclusion, equimolar mixture of TEOS and water-glass gave an improved ferrierite material compared to TEOS as sole the SiO_2 source.

Another synthesis manipulation involved the prior acid hydrolysis of TEOS before preparation of the gel. The XRD patterns for the materials produced are shown in Figure 4.3.

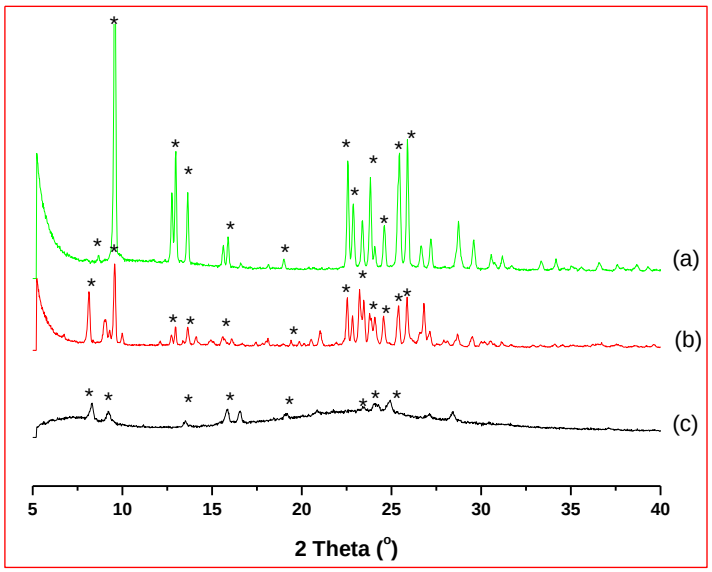

Figure 4.3 XRD patterns for (a) FER-WG, (b) HCl-hydrolysed TEOS and (c) unhydrolysed TEOS.

Figure 4.3 shows that the quality of ferrierite synthesised using TEOS as silica source can be improved by prior acid-hydrolysis of TEOS. The synthesis of ferrierite without prior acid-hydrolysis of TEOS produced an amorphous material as shown by the broad XRD feature in the range 18 - 30^{o} 2θ, with very little of the crystalline phase being present (i.e. fewer Bragg diffraction peaks). This is due to the poor solubility of TEOS in water because of the organic substituents present in its structure. Pre-hydrolysis of TEOS with HCl, led to a highly crystalline phase of ferrierite [Figure 4.3 (b)]. This is attributed to the formation of silicic acid, which is accompanied by the condensation of adjacent silanol groups to generate Si-O-Si linkages [12].

The relative crystallinities of the materials as influenced by the silica source used are shown in Table 4.2 (calculated by Equation 3.1).

Table 4.2: Relative XRD crystallinity of synthesised ferrierite zeolites		
Sample	**SiO_2 precursor**	**Relative XRD Crystallinity (%)**
FER-WG	Water-glass	100
FER-LS	Ludox LS-30	97
FER-A200	Aerosil 200	88
Unhydrolysed FER-TS	TEOS	15
HCl-hydrolysed FER-TS	Pre-hydrolysed TEOS	41
FER-TS/WG	TEOS + water-glass (1 : 1)	4
FER-TS/3WG	TEOS + water-glass (1 : 3)	4

The percentage crystallinities of the materials are 100, 97, 88 and 15 % for FER-WG, FER-LS, FER-A200 and FER-TS, respectively. The poor crystallinity of the FER-TS is evidenced by a high background and broad feature in the range 18 - 30^o 2θ of the XRD pattern of this material. When TEOS is acid-hydrolysed, the crystallinity increases from 15 to 41 %. This is due to the fact that TEOS reacts readily in aqueous solution under the stimulation of an acid [13]. Surprisingly, the mixture of water-glass and TEOS produced materials with percentage crystallinity of 4, irrespective of the component ratios.

The crystallite sizes of the materials were calculated by Equation 3.2 and are listed in Table 4.3.

Table 4.3: Crystallite sizes of the synthesised ferrierite zeolites	
Sample	**Crystallite size (nm)**
FER-WG	80
FER-LS	88
FER-A200	80
Unhydrolysed TEOS	79
HCl-hydrolysed TEOS	80
FER-TS/WG	113
FER-TS/3WG	79

The crystallite sizes of five zeolites (FER-WG, FER-A200, ferrierite from unhydrolysed TEOS, ferrierite from acid-hydrolysed TEOS and FER-(TS/3WG) are of a similar size. Interestingly, ferrierite synthesised using an equimolar mixture of water-glass and TEOS as the SiO_2 source has a larger crystallite size.

4.2.2 Scanning electron microscopy

The results of SEM are expressed in terms of micrographs and morphology. Figure 4.4 shows the micrographs (with 7500X magnification) for FER-TS, FER-WG, FER-A200, and FER-LS.

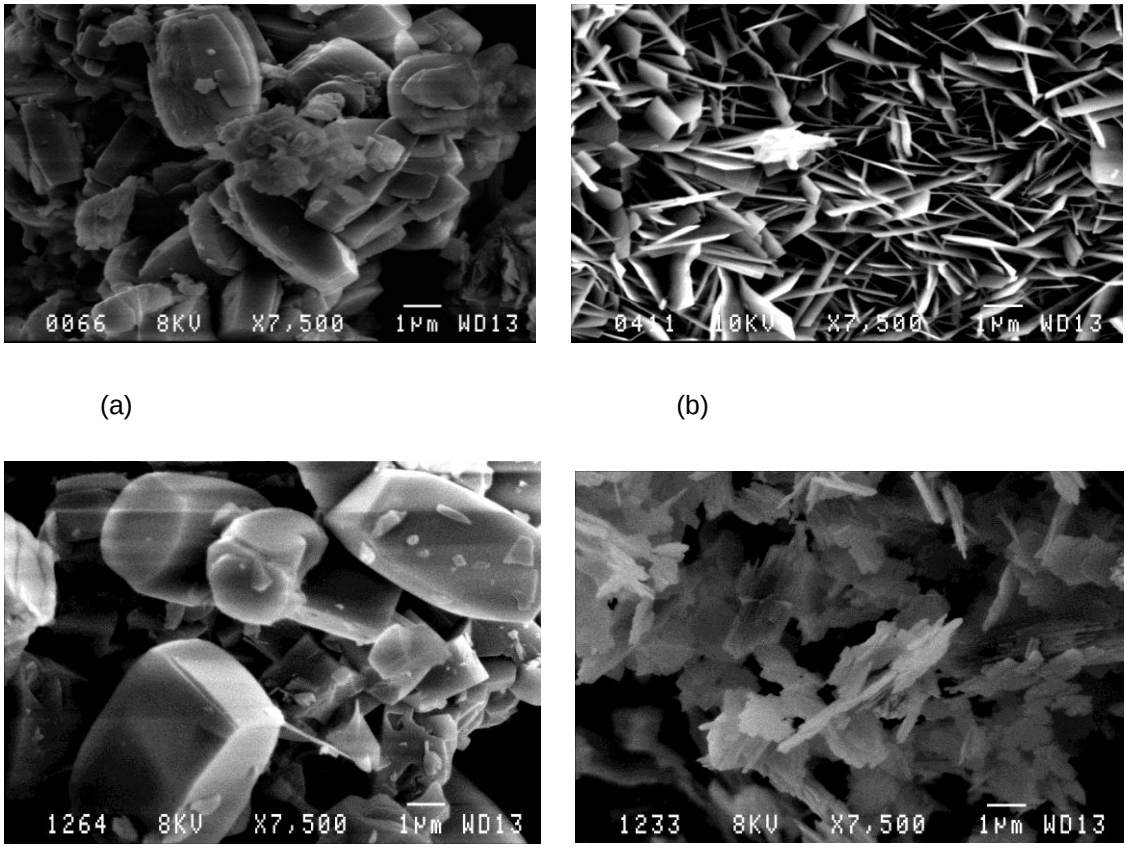

(a) (b)

(c) (d)

Figure 4.4 SEM micrographs for (a) FER-TS, (b) FER-WG, (c) FER-A200, and (d) FER-LS.

The morphologies of the ferrierite crystals indicate that they are influenced by the identity of the SiO_2 source used. The micrograph of FER-TS shows hexagonal-type morphology and aggregates of smaller particles, as shown in Figure 4.4 (a). These smaller particles, appearing as impurities on the micrograph, support the low crystallinity of FER-TS found by XRD [Figure 4.1 (d)]. The scanning electron micrograph of FER-WG shows thin sheets and a flake-like morphology [Figure 4.4 (b)]. The SEM image of the FER-A200 zeolite shows octagonal prismatic and hexagonal type morphologies as shown in Figure 4.4 (c). A thin-plate-like morphology is observed for FER-LS [Figure 4.4 (d)]. This is a more common morphology for natural ferrierite [12]. There is no amorphous phase observed in the images of FER-WG and FER-LS, which is in agreement with XRD (compare Table 4.2).

Figure 4.5 compares the SEM images of ferrierite synthesised using unhydrolysed and pre-HCl-hydrolysed TEOS

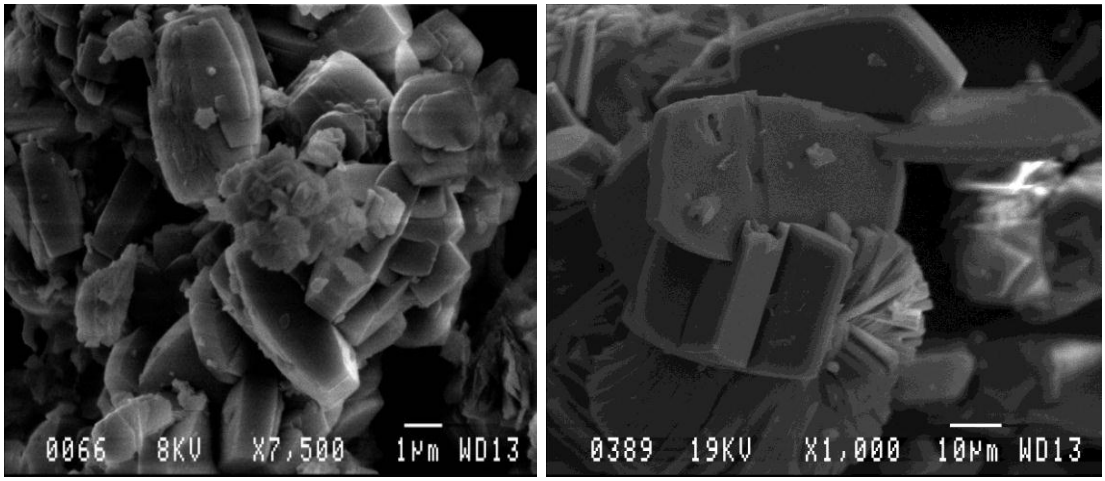

(a) (b)

Figure 4.5 SEM micrographs of ferrierite synthesised using: (a) unhydrolysed TEOS and (b) acid-hydrolysed TEOS.

The micrographs in this case show hexagonal-type morphology and appear to be stacked together when TEOS was pre-hydrolysed [Figure 4.5 (b)]. Amorphous phases (appearing as clusters) are not observed in (b), as compared to the sample prepared with unhydrolysed TEOS, Figure 4.5 (a).

In Figure 4.6, the micrographs of the ferrierite zeolites synthesised using a mixture of TEOS and water-glass as the SiO_2 source are shown.

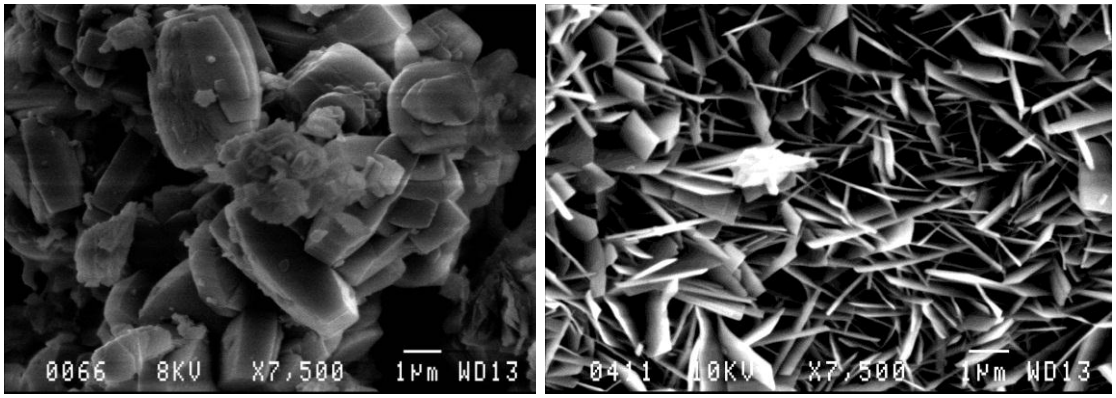

(a) (b)

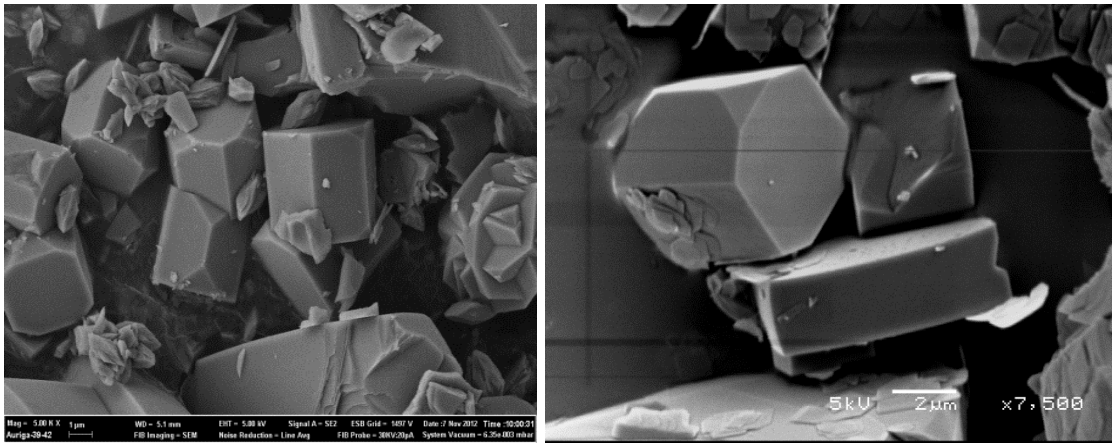

(c) (d)

Figure 4.6 SEM micrographs of (a) FER-TS, (b) FER-WG (c) FER-TS/WG (1 : 1) and, (d) FER-TS/WG (1 : 3).

Striking changes in morphology accompanying the addition of two different amounts of water-glass to TEOS prior to the preparation of the ferrierite synthesis gel are observed. The morphology of ferrierites synthesised from gels that are mixtures of TEOS and water-glass is octagonal prismatic with triangular faces along certain edges [Figures 4.6 (c) and (d)]. For comparison, the micrographs of FER-TS and FER-WG are shown in Figure 4.6 (a) and (b), respectively. This change in morphology (shape) induced by the addition of water-glass seems to support the observations made by XRD features observed in Figure 4.2.

4.2.3 Ammonia temperature-programmed desorption

The NH_3-TPD desorption profiles illustrates the distribution of acid site strength of the zeolites. Each peak in the TPD profile corresponds to acid sites of a certain strength, depending on the desorption temperature. These acid sites can be classified as weak, intermediate and strong. Figure 4.7 shows the ammonia desorption profiles of representative ferrierite materials synthesised in this work.

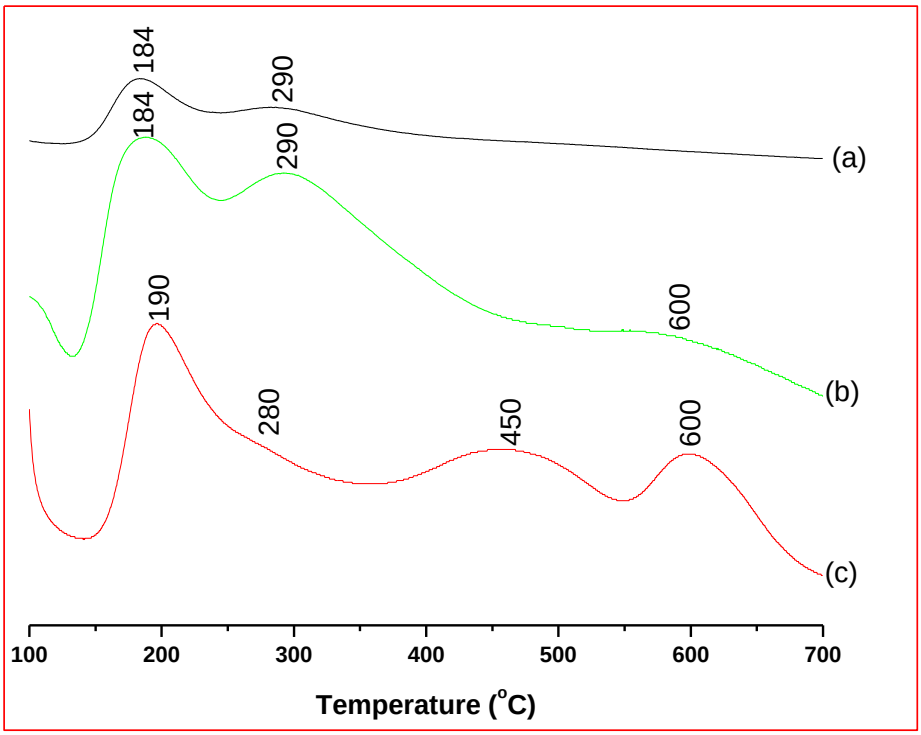

Figure 4.7 NH_3-TPD profiles of ferrierites: (a) HCl-hydrolysed TEOS, (b) unhydrolysed TEOS, and (c) FER-LS.

There are two broad peaks at 184 ^oC and 290 ^oC of ferrierites synthesised using HCl-hydrolysed and unhydrolysed TEOS [Figure 4.7 (a) and (b)], but ferrierite produced from unhydrolysed TEOS has an extra peak at 600 ^oC. The FER-LS also has three desorption peaks, one at low temperature 190 ^oC and two at high temperatures, 450 ^oC and 600 ^oC, as shown in Figure 4.7 (c). The desorption peaks at low temperatures < 300 ^oC correspond to the weak- and medium-strength acid sites, whereas peaks at high temperatures (above 350 ^oC) correspond to strong acidity [14 - 16]. According to Peixoto *et al*. [17], desorption peaks at low

temperature can be correlated to Lewis acid sites and desorption peaks at high temperature to Brønsted acid sites. At low temperatures, ammonia is physically adsorbed to ferrierite, while it is chemically adsorbed at high temperatures [18]. The NH_3-TPD profile of ferrierite synthesised using unhydrolysed TEOS is similar to the profile of FER-LS [Figure 4.7 (c)], even though a less crystalline material is produced when TEOS is used as the SiO_2 source. In order of increasing acidity, these zeolites can be arranged as FER-LS < unhydrolysed FER-TS < acid-hydrolysed FER-TS.

4.2.4 Brunauer-Emmett-Teller surface area measurements

The BET surface areas of chosen ferrierite materials synthesised in this work and from literature are shown in Table 4.4.

Table 4.4: BET surface areas of synthesised ferrierite zeolites

Sample	Specific surface area (m^2/g)	Specific surface area (m^2/g) from literature
FER-TS	6	-
FER-LS	300	490 [19]
FER-A200	320	60 [20]
FER-WG	325	335 [21]

The surface areas are different for samples prepared from different silica sources. The FER-TS has the lowest surface area of all samples (6 m^2/g). This is attributed to impurities present on the material as evidenced by the XRD pattern and SEM micrograph of the material (Figures 4.1 (d) and 4.4 (a)). No BET surface area for ferrierite synthesised using TEOS has been reported in the literature. Ferrierite synthesised using water-glass has higher surface area (325 m^2/g) than the materials synthesised using TEOS, Ludox LS-30 and Aerosil 200 as silica sources. However, the surface areas of ferrierites synthesised using water-glass and Ludox LS-30 are low, compared to same materials synthesised using the same SiO_2 sources as reported by others researchers. This is not the case with ferrierite synthesised using Aerosil 200, which has a high surface area than its counter-part. The surface area follows the order: FER-WG > FER-A200 > FER-LS > FER-TS. There seems to be a correlation between the XRD data and the BET surface area, lower crystallinity materials have lower surface areas as seen on Figure 4.1.

4.3 Adsorption of Cu^{2+} from aqueous solution by ferrierite zeolite

This section describes the adsorption of copper ions (Cu^{2+}) from water by ferrierite zeolites in their Na- and H-forms. Each measurement was performed in triplicate. The raw data obtained from AAS measurements, including the calibration curves, are found in Appendix B. The value of R was calculated using Equation 3.3.

4.3.1 Effect of initial pH on the adsorption of Cu^{2+} by Na-ferrierite

The pH is one of the most important factors influencing the solution chemistry of the heavy metals. The solution chemistry includes hydrolysis, complexation by organic and/or inorganic ligands, redox reactions and precipitation [22]. The effect of pH on the adsorption of Cu^{2+} by Na-ferrierite zeolites synthesised under identical conditions, but using different SiO_2 sources are shown in Figure 4.8.

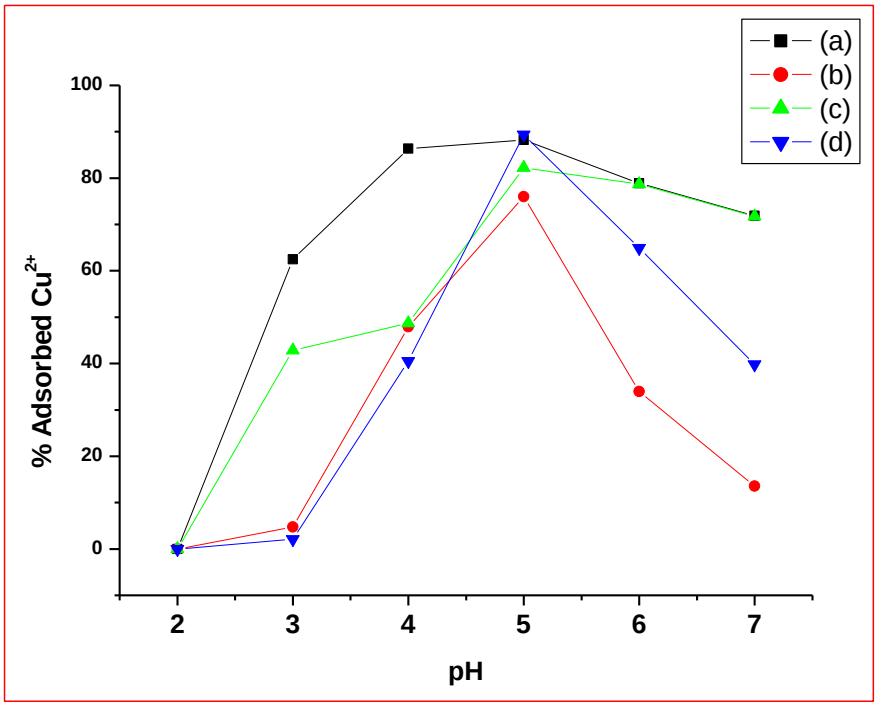

Figure 4.8 Effect of pH on Cu^{2+} adsorption by Na-ferrierite: (a) FER-TS, (b) FER-WG, (c) FER-LS and, (d) FER-A200 (Experimental condition: 0.100 g dose, contact time 24 h and initial concentration of 8 ppm).

The adsorption of Cu^{2+} from aqueous solution by Na-form zeolites is low at lower pH, increases with increasing pH up to 5, and thereafter decreases. This decrease can be attributed to the higher concentration and higher mobility of H^+ ions present in the solution. The zeolites favour the preferential adsorption of H^+ ions compared to the Cu^{2+} ions [23]. It would be plausible to suggest that at lower pH values, the surface of the adsorbent is surrounded by hydronium ions, thereby preventing the Cu^{2+} ions from approaching the binding sites of the zeolite. At higher H^+ concentration, the adsorbent surface becomes more positively charged such that the attraction between the zeolite and the metal ions is reduced. In contrast, as the pH increases, a more negatively charged surface of the ferrierite become available and then facilitating greater copper removal [24].

The percentage removals of Cu^{2+} by the materials at pH 5 are 89, 88, 82 and 76 for FER-A200, FER-TS, FER-LS and FER-WG, respectively. Metal uptake does not reach 100% with the materials studied within the pH range investigated. This might be due to the competition between H^+ and the zeolite adsorption sites for metal ions [23]. The rapid increase in metal uptake from pH 4 to pH 5 by FER-WG can be attributed to the replacement of exchangeable cations at the exchangeable sites (i.e. Na^+ with Cu^{2+} cations in the aqueous solution) [25 - 29]. At higher pH values (i.e. pH 6 and pH 7) there is a decrease in the adsorption capacity of Cu^{2+} by ferrierites. Previous studies have attributed this observation to precipitation of copper hydroxide. At pH 6 there are three species present in solution, namely Cu^{2+} in very small quantities, $Cu(OH)^+$ and $Cu(OH)_2$ in large quantities [25]. The three species are adsorbed at the surface of the adsorbent through the functional groups present on the adsorbent, or by hydrogen bonding [23].

The ranking of the SiO_2 sources according to the metal uptake efficiency of ferrierite is: FER-TS > FER-LS > FER-WG > FER-A200 in the pH range 2 to 5. This superior performance of FER-TS is unexpected on the basis of its poor physicochemical properties (XRD, SEM and BET). This good performance might be due to the dimensions of the material. The FER-WG is expected to have a high metal uptake since it is the most crystalline material and has the highest BET surface area. This unexpected relationship between the surface area and Cu^{2+} uptake has been observed by other researchers using other zeolites.

The optimum pH is found to be pH 5 for all materials investigated. The results obtained from the effect of pH on the adsorption capacity of ferrierites indicate that the major factors which affect the Cu^{2+} adsorption pH are the competition of H^{+} ions with Cu^{2+} for zeolite adsorption sites ions at low pH (under pH 4), ion-exchange (pH 5) and precipitation of some Cu hydroxide onto ferrierite (pH 6 and 7).

4.3.2 Metal uptake efficiency by Na-ferrierites as a function of contact time

The metal uptake efficiency by Na-ferrierite as a function of contact time was studied on initial Cu^{2+} concentration of 8 ppm at pH 5 and room temperature. The results are shown in Figure 4.9.

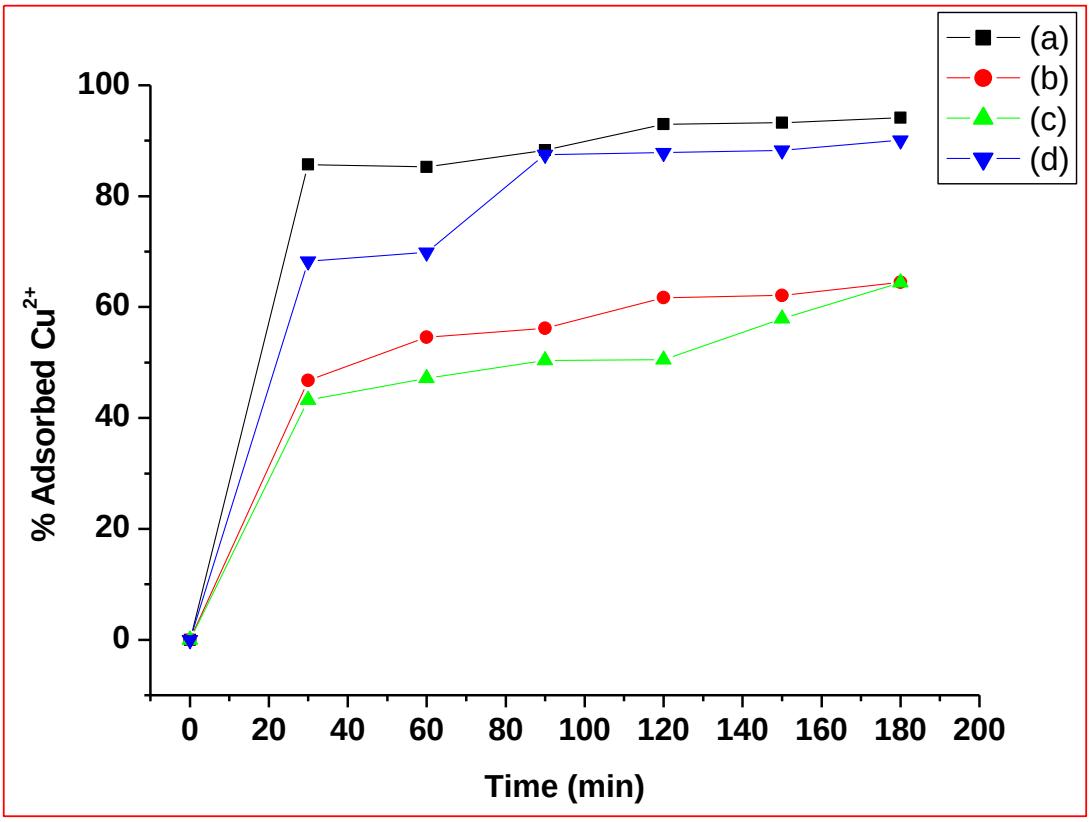

Figure 4.9 Metal uptake efficiencies as a function of contact time by Na-form: (a) FER-A200, (b) FER-LS, (c) FER-WG and, (d) FER-TS (Experimental condition: 0.100 g dose, pH 5 and initial concentration of 8 ppm).

The adsorption of Cu^{2+} by zeolites increases as the contact time increases as shown in the figure above. A contact time of about 90 min is sufficient to achieve equilibrium

and the adsorption did not change significantly with further increase of the contact time. The FER-A200 zeolite performs better than the other materials. The maximum metal uptakes for the materials are ranked according to SiO_2 sources as follows: Aerosil 200 > TEOS > Ludox LS-30 > water-glass.

4.3.3 Adsorption of Cu^{2+} by Na-ferrierite as a function of zeolite dose

Influence of Na-ferrierite dose (g/L) on Cu^{2+} adsorption is shown in Figure 4.10.

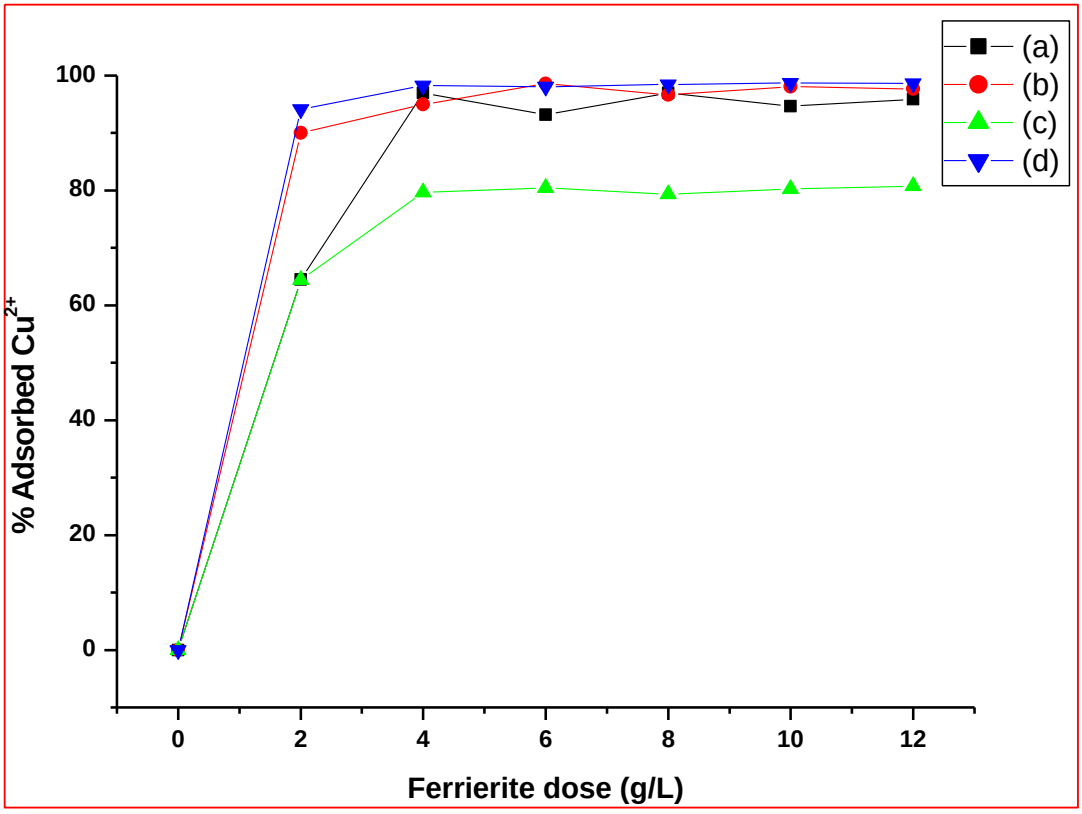

Figure 4.10 Adsorption of Cu^{2+} by Na-ferrierite as a function of zeolite dose: (a) FER-LS, (b) FER-TS (c) FER-WG and, (d) FER-A200 (Experimental condition: pH 5, contact time 3 h and initial concentration of 8 ppm).

The increase in adsorbent dose from 2.0 to 4.0 g/L resulted in an increase in the adsorption of Cu^{2+} ions. This is because of the availability of more binding sites for the complexation of the metal ions. A further increase in adsorbent dose, above 4.0 g/L, does not cause any significant improvement in adsorption. This is due to the binding of almost all ions to the adsorbent and/or the establishment of an equilibrium

between the ions bound to the adsorbent and those remaining un-adsorbed in the solution [22, 26]. It also is worth noting that the metal uptake improves for all materials investigated as the dose increases. The Cu^{2+} adsorption reached a maximum of 99, 98, 97 and 81 % for FER-A200, FER-TS, FER-LS and FER-WG, respectively. In conclusion, the metal uptake for each zeolite increases initially and reaches equilibrium at a dose of 4 g/L. It is to noted that the performance of FER-A200, FER-TS, FER-LS is similar in the dose range of > 4.0 g/L, which is higher than the performance of FER-WG.

4.3.4 Influence of the initial concentration of Cu^{2+} on the adsorption of Cu^{2+} by Na-ferrierites

Figure 4.11 shows the influence of the initial Cu^{2+} concentration on the Cu^{2+} adsorption by Na-ferrierite zeolites.

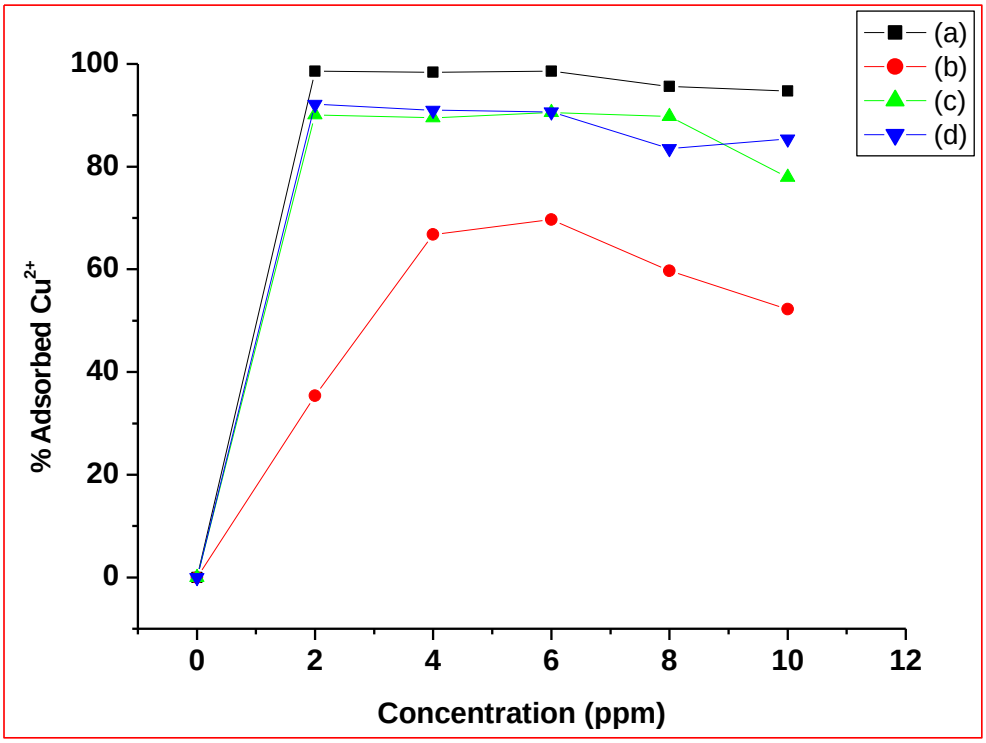

Figure 4.11 Influence of initial concentration on adsorption of Cu^{2+} by Na-form zeolites: (a) FER-A200, (b) FER-WG, (c) FER-LS and, (d) FER-TS (Experimental condition: 0.100 g dose, contact time 3 h and pH 5).

As already seen in Figures 4.9 and 4.10, also Figure 4.11 suggests that the use of water-glass as a SiO_2 precursor produces an inferior adsorbent material compared to the other three SiO_2 sources. There is a slight decrease in Cu^{2+} uptake onto FER-A200, FER-LS and FER-TS as the initial concentration increases. This is attributed to the fact that the availability of metal ions in the aqueous solution exceeds the available binding sites of the materials [27]. However, this is not the case for the adsorption of Cu^{2+} by FER-WG, which shows a different trend as shown in Figure 4.11 (b). At low initial concentrations (i.e. 2 and 6 ppm), there is an increase in the percentage removal of Cu^{2+}. As the initial concentration is raised further, the adsorption of the metal ions reaches a maximum of 74 % at 6 ppm. Then there is a decrease in metal uptake as the concentration increases to 8 and 10 ppm.

4.3.5 Effect of the initial pH on the adsorption of Cu^{2+} by H-ferrierites

The adsorption of Cu^{2+} by ferrierites in the hydrogen form was studied to compare it with the Na-forms. Figure 4.12 shows the effect of the pH on adsorption of Cu^{2+} by ferrierites in the hydrogen form.

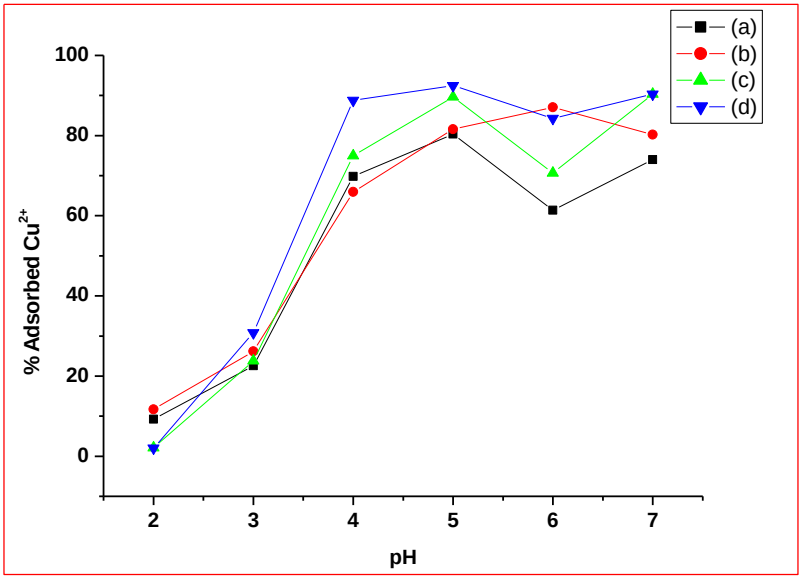

Figure 4.12 Effect of pH on Cu^{2+} adsorption by H-form: (a) FER-A200, (b) FER-TS, (c) FER-LS and, (d) FER-WG (Experimental condition: 0.100 g dose, contact time 24 h and initial concentration of 8 ppm).

The adsorption of Cu^{2+} ions by H-ferrierites increases as the pH increases from pH 2 up to pH 5. This is the same trend followed by the Na-ferrierites (Figure 4.8). However, the maximum percentage removal of Cu^{2+} attained at pH 5 for the H-forms is higher than that of Na-form. The metal uptake as a function of pH for the materials is ranked as follows: FER-WG > FER-LS > FER-TS > FER-A200. The FER-TS has the highest percentage removal at pH 6 and this might be due to precipitation of copper [25]. Hence, the optimum pH adsorption of Cu^{2+} by H-ferrierites is taken as pH 5.

4.3.6 Influence of initial concentration on adsorption of Cu^{2+} by H-ferrierite

The experimental results of the removal of Cu^{2+} on H-ferrierite as a function of the initial Cu^{2+} concentration are presented in Figure 4.13.

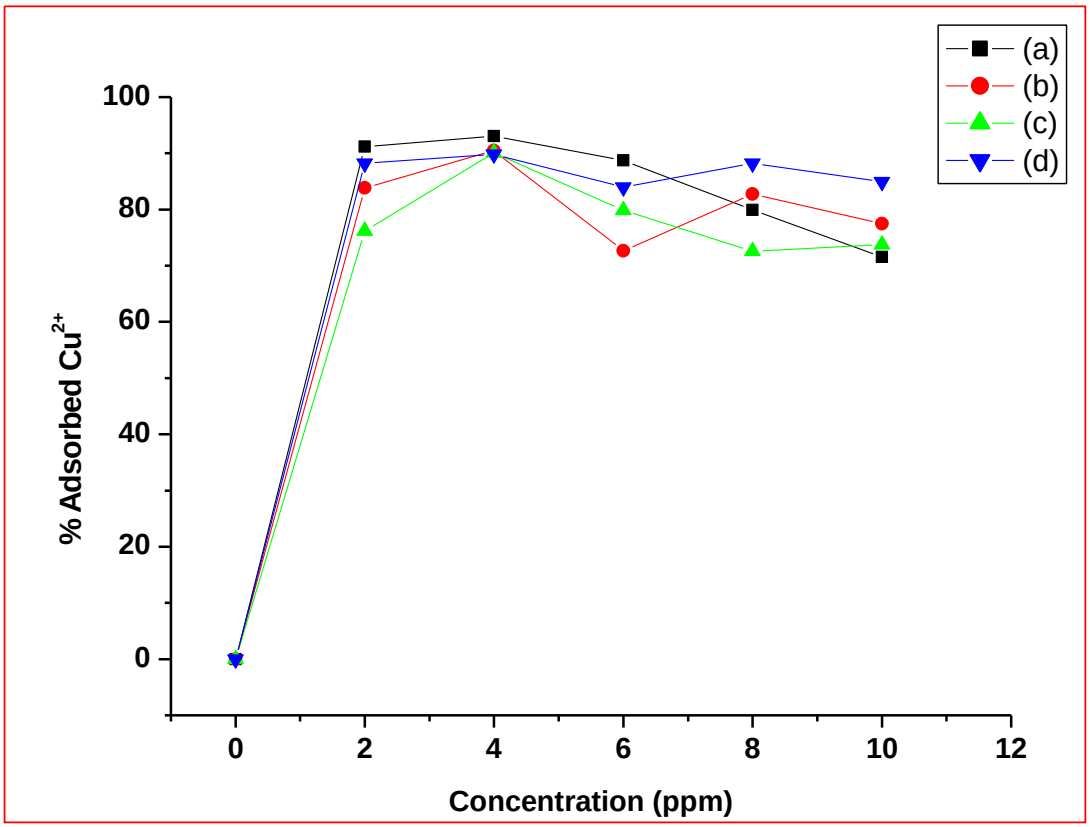

Figure 4.13 Influence of initial concentration on adsorption of Cu^{2+} by H-form: (a) FER-A200, (b) FER-TS, (c) FER-LS and, (d) FER-WG. (Experimental condition: 0.100 g dose, contact time 3 h and pH 5).

The Cu^{2+} adsorption increases as the initial concentration increases from 2 ppm to 4 ppm. As the initial concentration increases further from 4 ppm to 10 ppm, the adsorption decreases for FER-A200 and FER-LS. The metal uptake for materials synthesised using water-glass and TEOS as silica sources increases when the concentration is raised from 6 to 8 ppm. It decreases again as the concentration is increased from 8 to 10 ppm. The H-form zeolites follow the general trend of the Na-form zeolites with respect to metal uptake when the initial concentration is investigated. However, the H-FER-WG zeolite has a higher affinity for metal ions than its Na-form (compare Section 4.3.4).

4.3.7 The adsorption of Cu^{2+} by H-ferrierites as a function of contact time

The effect of contact time on the adsorption of Cu^{2+} by H-ferrierites is shown in Figure 4.14.

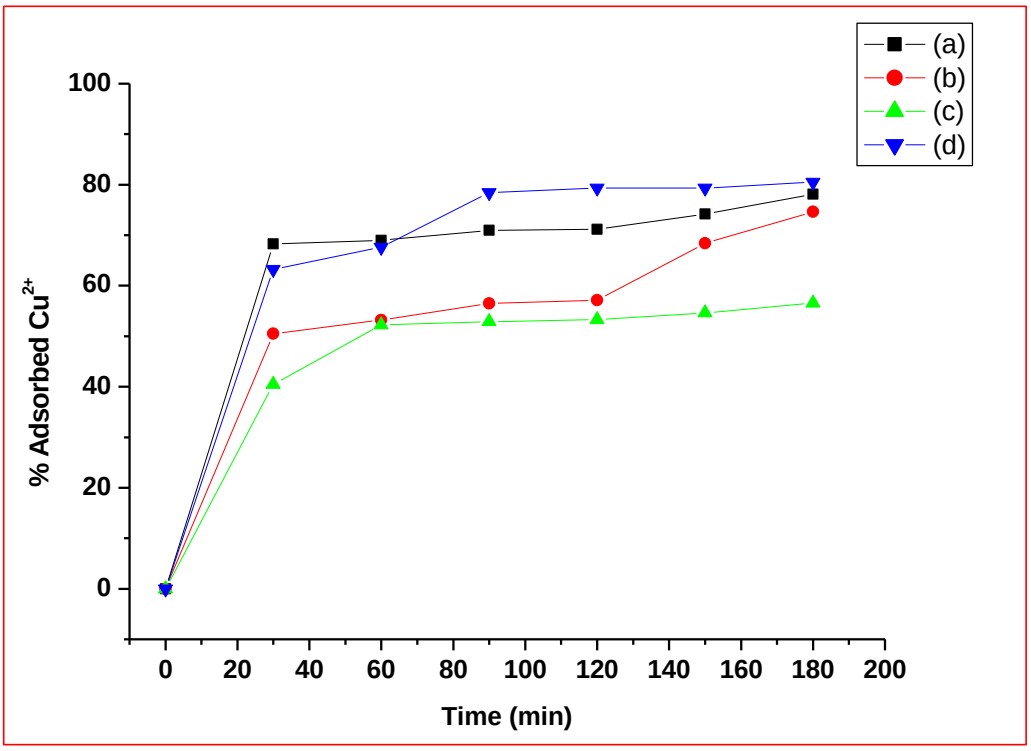

Figure 4.14 Metal uptake efficiencies as a function of contact time by H-ferrierite: (a) FER-A200, (b) FER-TS, (c) FER-LS and, (d) FER-WG (Experimental condition: 0.100 g dose, pH 5 and initial concentration of 8 ppm).

The zeolites show increasing metal uptake for contact times below 90 min. Beyond 90 min some zeolites did not show any further increase in adsorption. Equilibrium adsorption is attained within ≥ 90 min of contact time for FER-WG and FER-LS. The adsorption increases further as the contact time increases beyond 90 min for FER-TS and FER-A200. It is clear from the results that the contact time required for metal uptake by the materials is dependent on the nature of the SiO_2 source used. None of these zeolites attained 100 % Cu^{2+} adsorption. The Cu^{2+} adsorption by H-ferrierites is low as compared to Na-form ferrierites, except for FER-WG which has a high metal uptake in H-form than Na-form (compare Figure 4.9).

4.3.8 Influence of H-ferrierite dose on adsorption of Cu^{2+}

The effect of H-ferrierite dose on Cu^{2+} adsorption is presented in Figure 4.15.

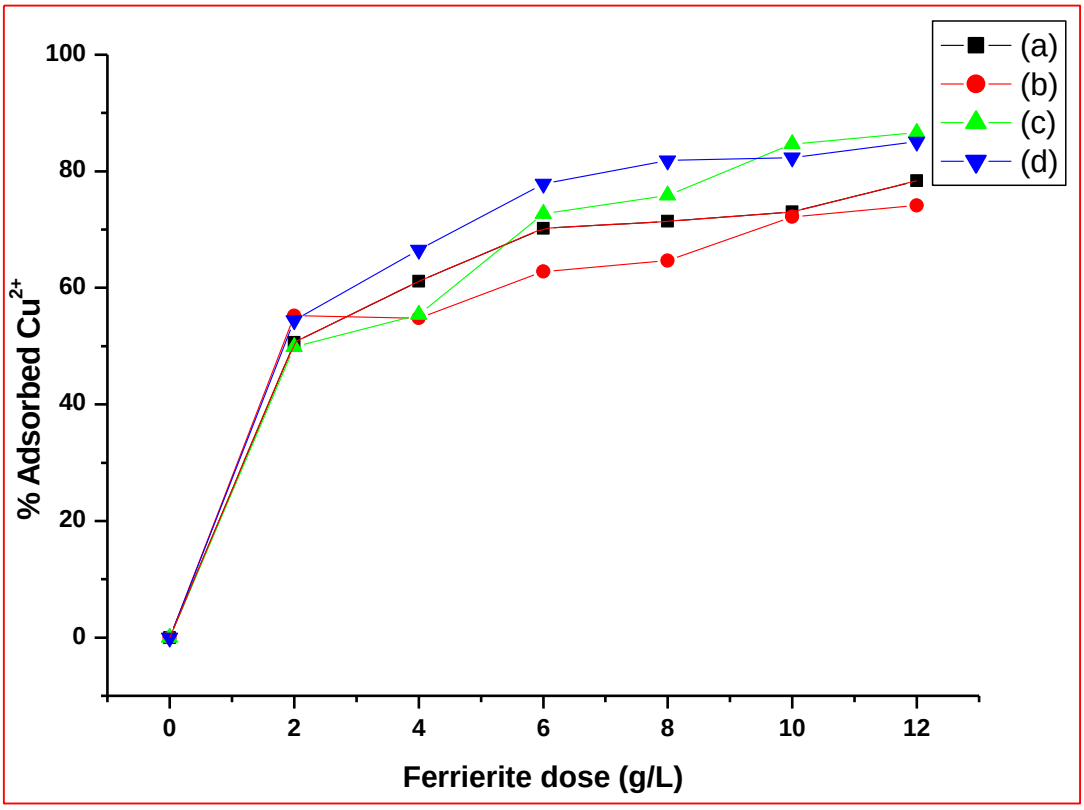

Figure 4.15 Adsorption of Cu^{2+} by H-ferrierite as a function of zeolite dose: (a) FER-A200, (b) FER-LS, (c) FER-TS and, (d) FER-WG (Experimental condition: pH 5, contact time 3 h and initial concentration of 8 ppm).

The percentage adsorption increases rapidly with increase in the amount of adsorbent. This is to be expected because, for a fixed initial solute concentration, increasing adsorbent amount provides greater surface area or increased number of adsorption sites [28 - 30]. However, this is not the case with the Na-form of these materials, which reached a plateau at an adsorbent dose of 4 g/L, as shown in Figure 4.10. In conclusion, the uptake of metal ions depends appreciably on the amount/dose of ferrierite.

4.3.9 Adsorption capacities of Na- and H-ferrierites: A comparison

The adsorption capacities (calculated by Equation 3.4) at pH 5 of ferrierite materials obtained using different silica sources are tabulated below.

Table 4.5 Adsorption capacities of ferrierites

Silica source	**Adsorption capacities (q_e, mg/g)**	
	Na-ferrierite	**H-ferrierite**
Aerosil 200	3.574	3.215
Water-glass	3.039	3.699
TEOS	3.528	3.264
Ludox LS-30	3.288	3.586

It can be seen from Table 4.5 that regardless of the silica source used in the synthesis of ferrierite, and regardless of the form (Na- or H-) of these materials, their adsorption capacities remained in the range 3.0 – 3.7 mg/g. This range of Cu^{2+} adsorption capacities supersedes that of other zeolitic adsorbents that have been investigated in the literature (see Table 2.3). Therefore, the zeolite ferrierite has promising potential for use in the removal of copper and other heavy metals from metal-laden water.

4.4 References

[1] Y. Long, M. Ma, Y. Sun, H. Jiang, Synthesis, ion-exchange, structural characterization and adsorption of K, Na-FER type zeolite, Journal of Inclusion Phenomena and Macrocyclic Chemistry 37 (2000) 103 – 120.

[2] R.K. Ahedi, A.N. Kotasthane, Studies in the crystallization of ferrierite type zeolites in presence of promoting medium, Journal of Porous Materials 4 (1997) 171 – 179.

[3] H. Choo, S.B. Hong, L. Kevan, Comparative ESR and catalytic studies of ethylene dimerization on Pd(II)-exchanged clinoptilolite, mordenite, ferrierite and SUZ-4, Journal of Physical Chemistry 105 (2001) 7730 – 7738.

[4] T.J. Kim, W.S. Ahn, S.B. Hong, Synthesis of zeolite ferrierite in the absence of inorganic cations, Microporous Materials 7 (1996) 35 – 40.

[5] P. Canizares, A. Carrero, P. Sánchez, Isomerization of *n*-butene over ferrierite zeolite modified by silicon tetrachloride treatment, Applied Catalysis A: General (2000) 93 – 105.

[6] L. Jianquan, L. Guanghuan, L. Juying, A novel method for the preparation of ferrierite zeolite, Catalysis Letters 20 (1993) 345 – 348.

[7] R.B. Khomane, B.D. Kulkarni, R.K. Ahedi, Synthesis and characterization of ferrierite-type zeolite in the presence of nonionic surfactants, Journal of Colloid and Interface Science 236 (2001) 208 – 213.

[8] R. Garcia, L. Gómez-Hortigüela, I. Díaz, E. Sastre, and J. Pérez-Pariente, Synthesis of materials containing ferrierite layers using quinuclidine and 1-benzyl-1-methylpyrrolidine as structure-directing agents: An experimental and computational study, Chemistry of Materials 20 (2008) 1099 – 1107.

[9] C. Marquez-Alvarez, A.B. Pinar, R. Garcıa, M. Grande-Casas, J. Perez-Pariente, Influence of Al distribution and defects concentration of ferrierite catalysts synthesised from Na-free gels in the skeletal isomerisation of *n*-butene, Topics in Catalysis (2008) 226 – 286.

[10] www.iza-structure.org/databases 22/10/2014.

[11] Z. Gogebakan, H. Yucel, A. Culfaz, Crystallization field and rate study for the synthesis of ferrierite, Industrial & Engineering Chemistry Research 46 (2007) 2006 – 2012.

[12] Y.J. Wu , X.Q. Ren, Y.D. Lu, J. Wang, Facile synthesis of small crystal ZSM-5 zeolite by acid-catalyzed hydrolysis of tetraethyl orthosilicate, Science in China Series B: Chemistry 52 (2009) 549 – 551.

[13] W.M. Jones, D.B. Fischbach, Novel processing of silica hydrosols and gels, Journal of Non-Crystalline Solids 101 (1988) 123 – 126.

[14] Y. Shang, P. Yang, M. Jia, W. Zhang, T. Wu, Modification of MCM-22 zeolites with silylation agents: Acid properties and catalytic performance for the skeletal isomerization, Journal of Catalysis (2008) 907 – 912.

[15] E. Kilic, L. Yilmaz, HZSM-5 and H-ferrierite acidity modification by silylation and their activities in n-butene isomerization, International Journal of Chemical Reactor Engineering 8 (2010) 1 – 19.

[16] J.H. Flores, M.I.P. da Silva, Acid properties of the hybrid catalyst CuO–ZnO or CuO–ZnO–Al_2O_3/H-ferrierite: An infrared study, Colloids and Surfaces A: Physicochemical and Engineering Aspects 322 (2008) 113 – 123.

[17] D.P.B. Peixoto, S.M.C. de Menezes, M.I.P. da Silva, Influence of different processes of dealumination on acid properties of an H-ferrierite zeolite, Materials Letters 57 (2003) 3933 – 3942.

[18] G. Bagnasco, Improving the selectivity of NH_3-TPD measurements, Journal of Catalysis 159 (1996) 249 – 252.

[19] W. Xu, Y. Yin, S.L. Suib, J.C. Edwards, C. Young, *n*-Butene skeletal isomerization to isobutylene on shape selective catalysts: Ferrierite/ZSM-35, Journal of Physical Chemistry 99 (1995) 9443 – 9451.

[20] R. Anand, R.B. Khomane, B.S. Rao, B.D. Kulkarni, Vapor phase Beckmann rearrangement of cyclohexanone oxime over different ferrierite zeolite catalysts, Catalysis Letters 78 (2002) 189 – 194.

[21] A. Corma, U. Diaz, M.E. Domine, V. Fornes, Ti-ferrierite and TiITQ-6: synthesis and catalytic activity for the epoxidation of olefins with H_2O_2, Chemical Communications (2000) 137 – 138.

[22] A. Ozer, D. Ozer, A. Ozer, The adsorption of copper(II) ions on to dehydrated wheat bran (DWB) : Determination of the equilibrium and thermodynamic parameters, Process Biochemistry 39 (2004) 2183 – 2191.

[23] S. Deng, Y. Ting, Characterization of PEI-modified biomass and biosorption of Cu(II), Pb(II) and Ni(II), Water Research 39 (2005) 2167 – 2177.

[24] K.S. Hui, C.Y.H. Chao, S.C. Kot, Removal of mixed heavy metals ions in wastewater by zeolite 4A and residual products from recycled coal fly ash, Journal of Hazardous Materials B127 (2009) 89 – 101.

[25] T.S. Anirudhan, S. Jalajamony, S.S. Sreekumari, Adsorptive removal of Cu^{2+} ions from aqueous media onto 4-ethyl thiosemicarbazide intercalated organophilic calcined hydrotalcite, Journal of Chemical and Engineering Data 28 (2013) 24 – 31.

[26] N.D. Tumin, A.L. Chan, Z. Gawain, S.A. Rashid, Adsorption of copper from aqueous solution by Elias Guineensis activated carbon, Journal of Engineering Science and Technology 2 (2008) 180 – 189.

[27] P.N. Dave, N. Subrahmanyam, S. Sharma, Kinetics and thermodynamics of copper ions removal from aqueous solutions by use of activated charcoal, Indian Journal of Chemical Technology 16 (2009) 234 – 239.

[28] K.G. Bhattacharya, S.S. Gupta, Adsorptive accumulation of Cd(II), Co(II), Cu(II), Pb(II), and Ni(II) from water on montmorillonite: Influence of acid activation, Journal of Colloid and Interface Science 310 (2007) 411 – 424.

[29] K.G. Bhattacharya, S.S. Gupta, Removal of Cu(II) by natural and acid-activated clays: An insight of adsorption isotherm, kinetic and thermodynamics, Desalination 272 (2011) 66 – 75.

[30] D. Hritcu, G. Dodi, M.I. Popa, Heavy metal ions adsorption on chitosan-magnetite microspheres, International Review of Chemical Engineering 4 (2012) 364 – 368.

CHAPTER FIVE

SUMMARY, CONCLUSIONS AND RECOMMENDATIONS

5.1 Summary

In this study, ferrierite zeolites were synthesised using four silica sources, namely, TEOS, Aerosil 200, Ludox LS-30 and water-glass under identical conditions. Additional experiments for the synthesis using TEOS involved acid-hydrolysis prior to the gel preparation step, and also pre-mixing with water-glass. The crystallinities and crystallite sizes of the synthesised materials were determined using X-ray powder diffraction (XRD). The morphologies of the products were studied by SEM. Nitrogen adsorption measurements were performed to determine the BET surface areas of the materials. The temperature-programmed desorption (NH_3-TPD) of ammonia was performed in order to determine the acid strength distribution on selected materials. The prepared materials were used for the removal of copper ions from simulated wastewater by a batch method. The effects of initial pH, initial Cu^{2+} concentration, contact time and ferrierite dose were investigated.

Water-glass, Ludox LS-30, Aerosil 200 produced ferrierites with similar XRD patterns, differing only in peak intensities. Ferrierite prepared from water-glass had the highest crystallinity of all prepared samples. An amorphous phase was dominant when ferrierite was synthesised from TEOS. The order of crystallinity of the materials depending on the SiO_2 source was: water-glass > Ludox LS-30 > Aerosil 200 > tetraethyl orthosilicate. The inorganic silica sources produced ferrierite materials with higher relative XRD crystallinities and BET surface areas than the organic silica source (TEOS). This tendency may be associated with the miscibility of the silica sources with water in during gel formation.

The physicochemical properties of the materials were not only affected by the nature of the SiO_2 source, but also by acid-hydrolysis and water-glass addition when TEOS was used as the silica source. The XRD patterns, morphologies (SEM) and BET

surface areas were significantly changed by the addition of water-glass to TEOS in the gel preparation stage of the synthesis.

The morphologies of all ferrierite materials indicated that they were influenced by the type of the SiO_2 source used. Ferrierite zeolites derived from water-glass consisted of thin sheets (flake-like images), whereas Ludox LS-30 based materials had a thin plate-like morphology. The acid site distributions deduced from NH_3-TPD profiles showed two peaks corresponding to weak acid sites at temperature below 300 ^oC for all three materials investigated (FER-LS, ferrierites synthesised using unhydrolysed and acid-hydrolysed TEOS). The ferrierite materials synthesised using unhydrolysed TEOS and Ludox LS-30 as SiO_2 sources showed also strong acid sites at temperature above 550 ^oC.

The removal of Cu^{2+} from synthetic aqueous solutions using the ferrierites synthesised from water-glass, Aerosil 200, Ludox LS-30 and TEOS was explored. The Na-form of ferrierite synthesised from Aerosil 200 had the best adsorption capacity for Cu^{2+}. The Na-form of ferrierite derived from water-glass was the poorest Cu^{2+} adsorbent over the whole parameter range (pH, contact time, adsorbent dose and initial metal ion concentration), even though it was the most crystalline material of all. However, it showed superiority for Cu^{2+} removal in its H-form, whereas H-ferrierite derived from Ludox LS-30 was the worst adsorbent material. The results obtained suggest that the use of ferrierite zeolites for the removal of Cu^{2+} ions from effluents contaminated with heavy metal might become useful in wastewater treatment.

5.2 Conclusions

The synthesis of ferrierite depends on the type of SiO_2 used. This was shown by the XRD patterns of the synthesised materials, which were different with each SiO_2 used. Ferrierite synthesised using water-glass as the silica source was the most crystalline material, whereas an amorphous phase was produced when TEOS material was used. However, acid-hydrolysis of TEOS and pre-mixing of TEOS with water-glass improved the crystallinity of the materials produced. Novel crystal shapes, comprising octagonal prisms with additional triangular phases, were observed in ferrierite samples prepared by the use of TEOS/water-glass mixture as

silica source. These morphologies have never been reported in the literature. The synthesised materials showed acid site distribution of similar nature, with two desorption peaks below 300 ^{o}C. The BET surface area of ferrierite synthesised using TEOS low. This was due to the amorphous nature of the material produced.

Ferrierite has demonstrated potential as an adsorbent for Cu^{2+} ions removal in aqueous media. Importantly, the adsorption capacities for Cu^{2+} was found insensitive to the acid form or sodium form as shown in Table 4.5. Based on this study, ferrierite synthesised using Aerosil 200 as a silica source is suitable for the removal of Cu^{2+} ions from wastewater. This silica source produced ferrierite with 88 % crystallinity and 320 m^2/g BET surface area. It performed best in Cu^{2+} ions removal under variables investigated, i.e., pH, contact time, adsorbent dose and initial concentration. About 4.0 $g_{zeolite}/L_{solution}$ of the material was used and 94 % of Cu^{2+} ions were adsorbed within 180 min of contact time.

5.3 Recommendations

Future investigations will be required to improve the % XRD crystallinity to 100 % of ferrierite derived from Aerosil 200 as SiO_2 source. This may be achieved by either varying the silica to alumina ratio, temperature or synthesis time. Further investigations will be to study the effects of particle sizes and silica to alumina ratio in the removal of copper ions from aqueous solution.

APPENDICES

Appendix A

Table A1: XRD data showing peak positions and intensities of unhydrolysed FER-TS	
Peak position	**Intensity**
9.577	510
22.582	1135
22.881	1116
23.822	1143
24.593	1045
25.448	818
25.897	792
Sum	6559
% Crystallinity	15

Table A2: XRD data showing peak positions and intensities of hydrolysed FER-TS	
PEAK POSITION	**Intensity**
9.603	3598
22.539	2169
22.828	1424
23.229	2493
23.451	2069
23.784	1519
25.407	1831
25.874	2185
Sum	17288
% Crystallinity	41

Table A3: XRD data showing peak positions and intensities of FER-WG	
Peak position	**Intensity**
9.581	15101
22.584	4649
22.873	3072
23.384	2381
23.829	4157
24.607	2184
25.451	5162
25.896	5720
Sum	42426
% Crystallinity	100

Table A4: XRD data showing peak positions and intensities of FER-LS	
Peak position	**Intensity**
9.581	11160
22.562	6100
22.851	3705
23.362	2272
23.806	3800
24.562	2348
25.429	5848
25.896	6007
Sum	41240
% Crystallinity	97

Table A5: XRD data showing peak positions and intensities of FER-A200	
Peak position (2θ)	**Intensity**
9.581	9868
22.539	5339
22.828	3761
23.740	2583
23.784	3415
24.562	2413
25.407	5048
25.198	4713
Sum	37140
% Crystallinity	88

Table A6: XRD data showing peak positions and intensities of FER-(TS + WG)	
Peak position (2θ)	**Intensity**
9.581	906
22.539	151
22.828	37
23.740	38
23.784	102
24.562	26
25.407	313
25.198	310
Sum	1883
% Crystallinity	4

Table A7: XRD data showing peak positions and intensities of FER-(TS + 3WG)	
Peak position (2θ)	**Intensity**
9.581	484
22.539	164
22.828	42
23.740	213
23.784	219
24.562	161
25.407	199
25.198	169
Sum	1651
% Crystallinity	4

Appendix B

Table B1: Calibration standards	
Standard (ppm)	**Absorbance**
0.0	0.0000
2.0	0.1829
4.0	0.3585
6.0	0.5106
8.0	0.6750

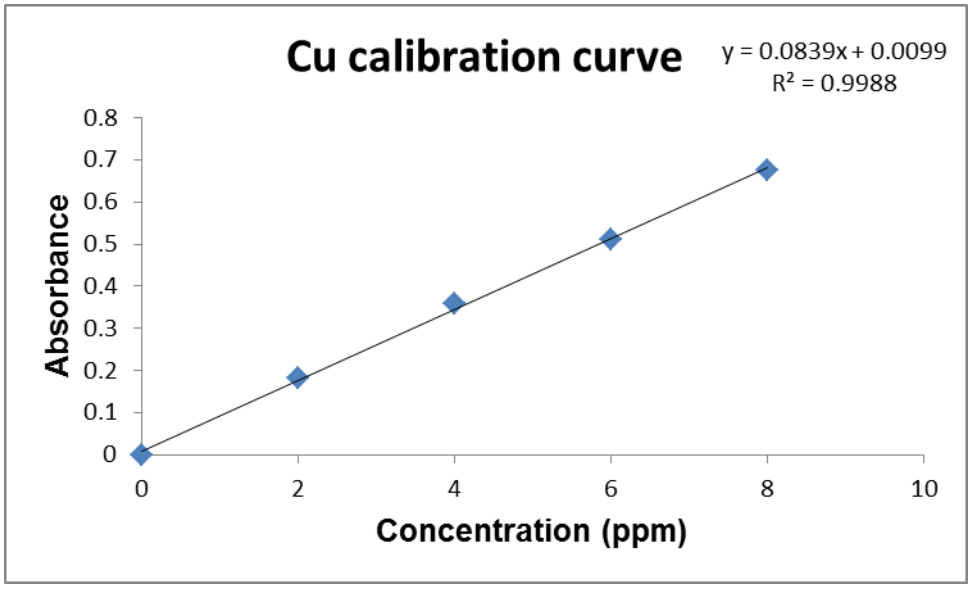

Figure B1 Calibration curve for the determination of copper in water.

Table B2: Effect of pH on Cu^{2+} adsorption by Na-FER-A200 zeolite					
pH	**C_e**	**Absorbance**	**C_i - C_e (ppm)**	**q_e (mg/g)**	**R (%)**
2	Over	0.8141	-	-	-
3	7.832	0.6046	0.168	0.084	2.10
4	4.756	0.3827	3.244	1.622	40.55
5	0.851	0.0691	7.149	3.574	89.36
6	2.806	0.2283	5.194	2.597	64.93
7	4.813	0.3870	3.187	1.594	39.84

Table B3: Effect of pH on Cu^{2+} adsorption by Na-FER-WG					
pH	**C_e**	**Absorbance**	**C_i - C_e (ppm)**	**q_e (mg/g)**	**R (%)**
2	Over	0.6270	-	-	-
3	7.620	0.5945	0.380	0.190	4.75
4	4.165	0.3291	3.835	1.918	47.94
5	1.922	0.1522	6.078	3.039	75.98
6	5.284	0.4164	2.716	1.358	33.95
7	6.915	0.5480	1.085	0.542	13.56

Table B4: Effect of pH on Cu^{2+} adsorption by Na-FER-TEOS					
pH	**C_e**	**Absorbance**	**C_i - C_e (ppm)**	**q_e (mg/g)**	**R (%)**
2	over	0.8900	-	-	-
3	3.001	0.2617	4.999	2.500	62.49
4	1.094	0.0891	6.906	3.453	86.33
5	0.943	0.0768	7.057	3.528	88.21
6	1.691	0.1380	6.309	3.154	78.86
7	2.248	0.1836	5.752	2.876	71.90

Table B5: Effect of pH on Cu^{2+} adsorption by Na-FER-LS					
pH	**C_e**	**Absorbance**	**C_i - C_e (ppm)**	**q_e (mg/g)**	**R (%)**
2	Over	0.8445	-	-	-
3	4.573	0.3936	3.427	1.864	42.84
4	4.103	0.0666	3.897	1.948	48.71
5	1.423	0.0230	6.577	3.288	82.21
6	1.706	0.0276	6.294	3.147	78.68
7	2.260	0.1936	5.740	2.870	71.75

Table B6: Metal uptake efficiency by Na-FER-LS as a function of contact time					
Time (h)	**C_e**	**Absorbance**	**C_i - C_e (ppm)**	**q_e (mg/g)**	**R (%)**
30	4.260	0.3778	3.74	1.870	46.75
60	3.635	0.3248	4.365	2.183	54.56
90	3.508	0.3139	4.492	2.246	56.15
120	3.062	0.2753	4.938	2.469	61.70
150	3.035	0.2730	4.965	2.483	62.06
180	2.847	0.2565	5.153	2.577	64.47

Table B7: Metal uptake efficiency by Na-FER-WG as a function of contact time					
TIme (h)	**C_e**	**Absorbance**	**C_i - C_e (ppm)**	**q_e (mg/g)**	**R (%)**
30	4.538	0.4011	3.462	1.731	43.23
60	4.226	0.3750	3.774	1.887	47.18
90	3.969	0.3533	4.031	2.016	50.39
120	3.958	0.3524	4.042	2.021	50.52
150	3.370	0.3020	4.63	2.315	57.88
180	2.847	0.2568	5.153	2.577	64.41

Table B8: Metal uptake efficiency by Na-FER-TS as a function of contact time					
Time (h)	**C_e**	**Absorbance**	**C_i - C_e (ppm)**	**q_e (mg/g)**	**R (%)**
30	2.539	0.1888	5.461	2.731	68.26
60	2.408	0.1788	5.592	2.796	69.90
90	1.000	0.0731	7.000	3.500	87.50
120	0.975	0.0712	7.025	3.513	87.81
150	0.937	0.0685	7.063	3.532	88.29
180	0.792	0.0577	7.208	3.604	90.10

Table B9: Metal uptake efficiency by Na-FER-A200 as a function of contact time					
Time (h)	**C_e**	**Absorbance**	**C_i - C_e (ppm)**	**q_e (mg/g)**	**R (%)**
30	1.41	0.1045	6.859	3.430	85.73
60	0.940	0.0860	7.060	3.530	85.25
90	0.939	0.0859	7.061	3.530	88.26
120	0.561	0.0514	7.439	3.720	92.98
150	0.543	0.0497	7.457	3.729	93.21
180	0.468	0.0392	7.532	3.766	94.15

Table B10: Adsorption of Cu^{2+} by Na-FER-A200 as a function of zeolite dose					
Dose (g/L)	**C_e (ppm)**	**Absorbance**	**C_i - C_e (ppm)**	**q_e (mg/g)**	**% R**
2	0.468	0.0392	7.532	3.766	94.15
4	0.141	0.0117	7.859	3.930	98.24
6	0.157	0.0130	7.843	3.922	98.04
8	0.125	0.0103	7.875	3.938	98.44
10	0.105	0.0086	7.895	3.948	98.69
12	0.142	0.0118	7.858	3.929	98.65

Table B11: Adsorption of Cu^{2+} by Na-FER-WG as a function of zeolite dose					
Dose (g/L)	**C_e (ppm)**	**Absorbance**	**C_i - C_e (ppm)**	**q_e (mg/g)**	**% R**
2	2.847	0.2565	5.153	2.577	64.41
4	1.627	0.1332	6.373	3.412	79.66
6	1.566	0.1276	6.434	3.470	80.42
8	1.651	0.1350	6.349	3.174	79.36
10	1.578	0.1308	6.422	3.211	80.28
12	1.537	0.1276	6.463	3.232	80.79

Table B12: Adsorption of Cu^{2+} by Na-FER-TS as a function of zeolite dose					
Dose (g)	**C_e (ppm)**	**Absorbance**	**C_i - C_e (ppm)**	**q_e (mg/g)**	**% R**
2	0.792	0.0577	7.208	3.604	90.10
4	0.400	0.0381	7.600	3.800	95.00
6	0.274	0.0226	7.726	3.863	96.58
8	0.269	0.0222	7.731	3.866	96.64
10	0.156	0.0129	7.844	3.922	98.05
12	0.185	0.0153	7.815	3.908	97.69

Table B13: Adsorption of Cu2+ by Na-FER-LS as a function of zeolite dose					
Dose (g)	**C_e (ppm)**	**Absorbance**	**C_i – C_e (ppm)**	**q_e (mg/g)**	**% R**
2	2.847	0.2565	5.153	2.577	64.47
4	0.241	0.0196	7.759	3.880	96.99
6	0.544	0.0445	7.456	3.728	93.20
8	0.242	0.0197	7.758	3.879	96.98
10	0.428	0.0350	7.572	3.786	94.65
12	0.331	0.0270	7.669	3.834	95.86

Table B14: Influence of initial concentration on adsorption of Cu^{2+} by Na-FER-A200					
Initial concentration	**C_e (ppm)**	**Absorbance**	**$C_i - C_e$ (ppm)**	**q_e (mg/g)**	**% R**
2	0.063	0.0035	1.937	0.968	98.60
4	0.028	0.0015	3.972	1.986	98.42
6	0.085	0.0047	5.915	2.958	98.58
8	0.352	0.0195	7.648	3.824	95.60
10	0.525	0.0290	9.475	4.738	94.75

Table B15: Influence of initial concentration on adsorption of Cu^{2+} by Na-FER-LS					
Initial concentration	**C_e (ppm)**	**Absorbance**	**$C_i - C_e$ (ppm)**	**q_e (mg/g)**	**% R**
2	0.198	0.0109	1.802	0.901	90.10
4	0.421	0.0232	3.579	1.790	89.48
6	0.567	0.0314	5.433	2.716	90.55
8	0.819	0.0455	7.181	3.591	89.76
10	2.208	0.1248	7.792	3.896	77.92

Table B16: Influence of initial concentration on adsorption of Cu^{2+} by Na-FER-WG					
Initial concentration	**C_e (ppm)**	**Absorbance**	**$C_i - C_e$ (ppm)**	**q_e (mg/g)**	**% R**
2	1.293	0.0723	0.707	0.354	35.35
4	1.329	0.0743	2.671	1.334	66.78
6	1.818	0.1021	4.182	2.091	69.70
8	3.224	0.1842	4.776	2.388	59.70
10	4.779	0.2765	5.221	2.611	52.21

Table B17: Influence of initial concentration on adsorption of Cu^{2+} by Na-FER-TS					
Initial concentration	**C_e (ppm)**	**Absorbance**	**$C_i - C_e$ (ppm)**	**q_e (mg/g)**	**% R**
2	0.157	0.0086	1.843	0.922	92.15
4	0.361	0.0199	3.639	1.820	90.98
6	0.560	0.0310	5.440	2.720	90.67
8	1.316	0.736	6.684	3.342	83.55
10	1.458	0.0816	8.542	4.271	85.42

Table B18: Effect of pH on adsorption of Cu^{2+} by H-FER-WG					
pH	**C_e**	**Absorbance**	**$C_i - C_e$**	**q_e (mg/g)**	**% R**
2	7.839	0.7349	0.1610	0.0805	2.01
3	5.535	0.5317	2.465	1.232	30.81
4	0.894	0.0858	7.106	3.553	88.83
5	0.602	0.0576	7.398	3.699	92.48
6	1.258	0.1211	6.742	3.371	84.28
7	0.773	0.0741	7.227	3.614	90.34

Table B19: Effect of pH on adsorption of Cu^{2+} by H-FER-A200					
pH	**C_e**	**Absorbance**	**$C_i - C_e$**	**q_e (mg/g)**	**% R**
2	7.259	0.6856	0.741	0.3705	9.26
3	6.194	0.5917	1.806	0.9030	22.58
4	2.417	0.2340	5.583	2.7915	69.79
5	1.571	0.1515	6.429	3.2145	80.36
6	3.097	0.3001	4.903	2.4515	61.39
7	2.082	0.2013	5.918	2.9590	73.98

Table B20: Effect of pH on adsorption of Cu^{2+} by H-FER-TS					
pH	**C_e**	**Absorbance**	**$C_i - C_e$**	**q_e (mg/g)**	**% R**
2	7.064	0.6687	0.936	0.4680	11.70
3	5.905	0.5656	2.095	1.0480	26.19
4	2.725	0.2640	5.275	2.6375	65.94
5	1.472	0.1419	6.528	3.2640	81.60
6	1.035	0.0994	6.965	3.4825	87.06
7	1.581	0.1524	6.419	3.2095	80.24

Table B21: Effect of pH on adsorption of Cu^{2+} by H-FER-LS					
pH	**C_e**	**Absorbance**	**$C_i - C_e$**	**q_e (mg/g)**	**% R**
2	7.832	0.7343	0.168	0.084	2.100
3	6.094	0.5827	1.906	0.953	23.82
4	2.001	0.1934	5.999	3.000	74.99
5	0.829	0.0795	7.171	3.586	89.64
6	2.346	0.2271	5.654	2.827	70.68
7	0.773	0.0741	7.227	3.614	90.34

Table B22: Influence of initial concentration on adsorption of Cu^{2+} by H-FER-WG					
Initial concentration	**C_e**	**Absorbance**	**$C_i - C_e$**	**q_e (mg/g)**	**% R**
2	0.235	0.0223	1.765	0.8825	88.25
4	0.407	0.0387	3.593	1.7965	89.82
6	0.962	0.0919	5.038	2.5190	83.97
8	0.941	0.0898	7.059	3.5295	88.24
10	1.509	0.1446	8.491	4.2455	84.91

Table B23: Influence of initial concentration on adsorption of Cu^{2+} by H-FER-A200					
Initial concentration	**C_e**	**Absorbance**	**$C_i - C_e$**	**q_e (mg/g)**	**% R**
2	0.176	0.0167	1.824	0.912	91.20
4	0.278	0.0264	3.722	1.861	93.05
6	0.677	0.0645	5.323	2.662	88.72
8	1.609	0.1543	6.391	3.196	79.89
10	2.847	0.2734	7.153	3.576	71.53

Table B24: Influence of initial concentration on adsorption of Cu^{2+} by H-FER-TS					
Initial concentration	**C_e**	**Absorbance**	**$C_i - C_e$**	**q_e (mg/g)**	**% R**
2	0.323	0.0307	1.677	0.8385	83.85
4	0.382	0.0363	3.618	1.809	90.45
6	1.664	0.1595	4.336	2.168	72.67
8	1.380	0.1321	6.620	3.310	82.75
10	2.250	0.2160	7.750	3.875	77.50

Table B25: Influence of initial concentration on adsorption of Cu^{2+} by H-FER-LS					
Initial concentration	**C_e**	**Absorbance**	**$C_i - C_e$**	**q_e (mg/g)**	**% R**
2	0.476	0.0453	1.524	0.762	76.20
4	0.396	0.0375	3.604	1.802	90.10
6	1.208	0.1156	4.792	2.396	79.87
8	2.196	0.2108	5.804	2.902	72.55
10	2.625	0.2522	7.375	3.688	73.75

Table B26: The adsorption of Cu2+ by H-FER-WG as a function of contact time					
Time (min)	**C_e**	**Absorbance**	**$C_i - C_e$**	**q_e (mg/g)**	**% R**
30	2.941	0.1710	5.059	2.530	63.24
60	2.588	0.1504	5.412	2.706	67.65
90	1.723	0.0999	6.277	3.138	78.46
120	1.651	0.0945	6.349	3.174	79.36
150	1.653	0.0958	6.347	3.174	79.34
180	1.562	0.0905	6.438	3.219	80.48

Table B27: The adsorption of Cu^{2+} by H-FER-A200 as a function of contact time					
Time (min)	**C_e**	**Absorbance**	**$C_i - C_e$**	**q_e (mg/g)**	**% R**
30	2.539	0.1475	5.461	2.731	68.26
60	2.482	0.1442	5.518	2.759	68.98
90	2.323	0.1350	5.677	2.838	70.96
120	2.306	0.1340	5.694	2.847	71.18
150	2.062	0.1197	5.938	2.969	74.22
180	1.750	0.1014	6.250	3.125	78.12

Table B28: The adsorption of Cu^{2+} by H-FER-TS as a function of contact time					
Time (min)	**C_e**	**Absorbance**	**$C_i - C_e$**	**q_e (mg/g)**	**% R**
30	3.958	0.2297	4.042	2.021	50.52
60	3.744	0.2174	4.256	2.128	53.20
90	3.479	0.2022	4.521	2.261	56.51
120	3.428	0.1992	4.572	2.286	57.15
150	2.529	0.1470	5.471	2.736	68.39
180	2.030	0.1178	5.970	2.985	74.62

Table B29: The adsorption of Cu^{2+} by H-FER-LS as a function of contact time					
Time (min)	**C_e**	**Absorbance**	**$C_i - C_e$**	**q_e (mg/g)**	**% R**
30	4.765	0.2755	3.235	1.618	40.44
60	3.820	0.2218	4.180	2.090	52.25
90	3.771	0.2190	4.229	2.114	52.86
120	3.740	0.2172	4.260	2.130	53.25
150	3.629	0.2108	4.371	2.186	54.64
180	3.475	0.2019	4.525	2.262	56.56

Table B30: Effect of dose on adsorption of Cu^{2+} by H-FER-WG					
Dose (g/L)	**C_e**	**Absorbance**	**$C_i - C_e$**	**q_e (mg/g)**	**% R**
2	3.643	0.1692	4.357	2.178	54.46
4	2.677	0.1247	5.323	2.662	66.54
6	1.772	0.0826	6.228	3.114	77.85
8	1.454	0.0677	6.546	3.273	81.82
10	1.411	0.0657	6.589	3.294	82.36
12	1.197	0.0557	6.803	3.402	85.04

Table B31: Effect of dose on adsorption of Cu^{2+} by H-FER-A200					
Dose (g/L)	C_e	**Absorbance**	$C_i - C_e$	q_e (mg/g)	% R
2	3.948	0.1831	4.052	2.026	50.65
4	3.108	0.1446	4.892	2.446	61.15
6	2.383	0.110	5.617	2.808	70.21
8	2.287	0.1066	5.713	2.858	71.41
10	2.158	0.1006	5.842	2.921	73.02
12	1.729	0.0806	6.271	3.136	78.39

Table B32: Effect of dose on adsorption of Cu^{2+} by H-FER-LS					
Dose (g/L)	**C_e**	**Absorbance**	**$C_i - C_e$**	**q_e (mg/g)**	**% R**
2	3.583	0.1665	4.417	2.208	55.21
4	3.613	0.1678	4.387	2.194	54.84
6	2.978	0.1386	5.022	2.511	62.78
8	2.826	0.1316	5.174	2.587	64.68
10	2.223	0.1036	5.777	2.888	72.21
12	2.069	0.0964	5.931	2.966	74.14

Table B33: Effect of dose on adsorption of Cu^{2+} by H-FER-TS					
Dose (g/L)	**C_e**	**Absorbance**	**$C_i - C_e$**	**q_e (mg/g)**	**% R**
2	4.011	0.1859	3.989	1.994	49.86
4	3.568	0.1657	4.432	2.216	55.40
6	2.184	0.1018	5.816	2.908	72.70
8	1.932	0.0900	6.068	3.034	75.85
10	1.224	0.0570	6.776	3.388	84.70
12	1.070	0.0498	6.930	3.465	86.62